Conclusions

Conclusions

1) En la present Tesi Doctoral s'ha desenvolupat el nou mètode DELOS® de cristal·lització amb fluids comprimits, en el qual s'aprofita el comportament com a co-solvent dels fluids comprimits sobre sistemes "solut/dissolvent orgànic/fluid comprimit" a alta pressió.
2) S'ha demostrat que la força promotora de la cristal·lització en el nou procés DELOS® és el gran, ràpid i extremadament homogeni descens de temperatura experimentat per una dissolució del solut a cristal·litzar en un dissolvent convencional expandit amb un fluid comprimit (p.ex. CO_2), quan es sotmet a despressurització.
3) S'ha demostrat que el descens de temperatura en un procés DELOS® està causat per l'evaporació del fluid comprimit del sistema "solut/dissolvent orgànic/fluid comprimit", que es troba en una sola fase líquida, o dissolució expandida, durant la seva despressurització.
4) El processament de materials moleculars de naturalesa variada per mitjà del mètode DELOS® realitzat en el present treball, ha permès demostrar que el valor de sobresaturació màxim assolit durant aquest procés de cristal·lització, ΔC_{max}, i la corresponent velocitat de nucleació, els quals governen en gran mesura la mida de partícula dels materials cristal·lins finals, poden ser modulats, en el procés DELOS®, mitjançant el contingut en CO_2 de la dissolució expandida, X_W, i la concentració de la dissolució inicial, β_I. Aquests estudis també han permès demostrar que el procés DELOS® és un procés adequat per a l'obtenció de sòlids cristal·lins constituïts per una sola fase polimòrfica, que en alguns casos pot ser metastable.
5) En el present treball, s'ha desenvolupat un nou procés de preparació de nanosuspensions a partir de dissolucions expandides amb CO_2, que s'ha anomenat DELOS-SUSP, i que es basa en el procés de cristal·lització DELOS®.

En el present treball s'han realitzat estudis, a nivell molecular, dels fenòmens de solvatació en dissolucions expandides amb CO_2, com les que s'empren en el procés DELOS®. Aquests estudis han permès extreure les següents conclusions:

6) Mitjançant la utilització d'espectroscòpia d'IR a alta pressió, anàlisi per LSER de modes vibracionals i càlculs ab initio, s'ha demostrat que el diferent comportament de solubilitat del paracetamol en acetona i etanol expandits amb CO_2, amb la variació del contingut en

CO_2, és degut a la major pertorbació que causa l'augment de CO_2 sobre la interacció dipol-dipol entre el grup carbonil del paracetamol i l'acetona, en relació a la pertorbació que sofreix la interacció de tipus enllaç d'hidrogen entre el grup carbonil del paracetamol i l'etanol.

7) Mitjançant estudis d'IR a alta pressió sobre el sistema "metenamina/etanol/CO_2" en una sola fase líquida, s'ha caracteritzat per primera vegada en dissolvents expandits amb CO_2, la regió cibotàctica del solut a partir de l'estudi de modes vibracionals de molècules de dissolvent presents en aquesta regió. Aquests estudis han permès concloure que l'augment de la solubilitat de la metenamina en etanol expandit amb CO_2, en més d'un ordre de magnitud en relació al CO_2 pur, i en un 30% en relació a l'etanol pur, està directament relacionat amb l'organització de les molècules de dissolvent en dues capes de solvatació al voltant de la metenamina. S'ha deduït l'existència d'una primera capa constituïda per molècules d'etanol que no es veu afectada, en quan a composició, quan el contingut en CO_2 del sistema augmenta, i l'existència d'una segona capa ocupada inicialment per molècules d'etanol, les quals són progressivament substituïdes per molècules de CO_2 a mesura que la concentració de CO_2 augmenta. D'aquesta organització de la regió cibotàctica se'n dedueix que la formació de clusters metenamina-ethanol-CO_2, amb interaccions cooperatives metenamina-etanol i etanol-CO_2, és la responsable de l'efecte sinèrgic que s'observa en la solubilitat de la metenamina en etanol expandit amb CO_2.

Annex 1 - Part Experimental

Annex 1 - Part Experimental

A. Instrumentació utilitzada en la realització dels experiments DELOS®

La configuració instrumental dissenyada per a la realització d'experiments DELOS® que es troba esquematitzada en la Figura 13 del Capítol 1, ha estat adaptada a dos equipaments instrumentals de diferent escala que es troben en el Laboratori de Fluids Supercrítics de MATGAS. A continuació es descriuen aquests dos equipaments, als quals ens referirem, respectivament, com a equipament d'alta pressió a escala de laboratori i com a planta pilot d'altes pressions i altes temperatures.

Equipament d'alta pressió a escala de laboratori

L'equip a escala de laboratori que s'ha utilitzat per a realitzar els experiments de cristal·lització descrits en el present treball s'esquematitza en la Figura A1. Aquest equip té com a element principal un autoclau o reactor R de 300 mL de capacitat per a treballar a altes pressions (P_{max}=25 MPa). Aquest autoclau (Autoclave Engineers, Erie, USA) consisteix en un recipient encamisat que pot ser connectat a un bany de recirculació termostatitzat. L'agitació en R es realitza per mitjà d'un agitador d'acoblament magnètic (Autoclave Engineers, Erie, USA). El CO_2 líquid provinent d'una bateria de 4 cilindres és bombejat a l'interior de R a través d'una bomba d'alta pressió (DOSAPRO MILTON ROY, Pont-Saint-Pierre, France). El CO_2 d'entrada a la bomba es refreda mitjançant el seu contacte amb un líquid refredat per l'acció d'un compressor. El cabal d'addició de CO_2 es mesura amb un caudalímetre màssic de coriolis C1 (KROHNE, Duisburg, Alemanya). Una línia independent connectada a dos cilindres de N_2 comprimit permet l'addició d'aquest gas a R. La pressió a l'interior de R es mesura amb un transductor de pressió de membrana (precisió 0.2% TRAFAG, Mannëdorf, Suïssa) i la temperatura amb un termoparell tipus K. L'autoclau pot contenir un filtre intern d'acer inoxidable, F1, situat al fons de l'autoclau per retenir les partícules que es puguin formar per precipitació GAS. Els components d'aquesta equip estan connectats mitjançant tub d'acer inoxidable de diàmetre extern d'1/8 de polzada i vàlvules d'alta pressió.

El detall del sistema de filtració que s'ha acoblat a aquest equip (veure Figura 13) per permetre la separació del precipitat que es forma durant el procés DELOS es mostra en la

imatge de la Figura A2. Aquest sistema consta d'un primer filtre F1b (no inclós en la Figura 13) de metall sinteritzat (HEADLINE FILTERS, Kent, UK) situat just abans de la vàlvula de despressurització V4 i que serveix per retenir possibles partícules formades per un procés GAS que hagin sobrepassat el filtre interior de R, F1. Entre el filtre F1b i la vàlvula V4, hi ha un termoparell tipus K per mesurar la temperatura abans de la despressurització de la dissolució, T_W. A la sortida de la vàlvula de despressurització trobem un altre termoparell del mateix tipus per mesurar la temperatura després de la despressurització, T_F, i un filtre F2 de major capacitat que l'anterior (HEADLINE FILTERS, Kent, UK) per a retenir les partícules produïdes per la cristal·lització DELOS®. F2 està també precedit per un manòmetre manual que serveix com a indicador d'obturacions d'aquest filtre.

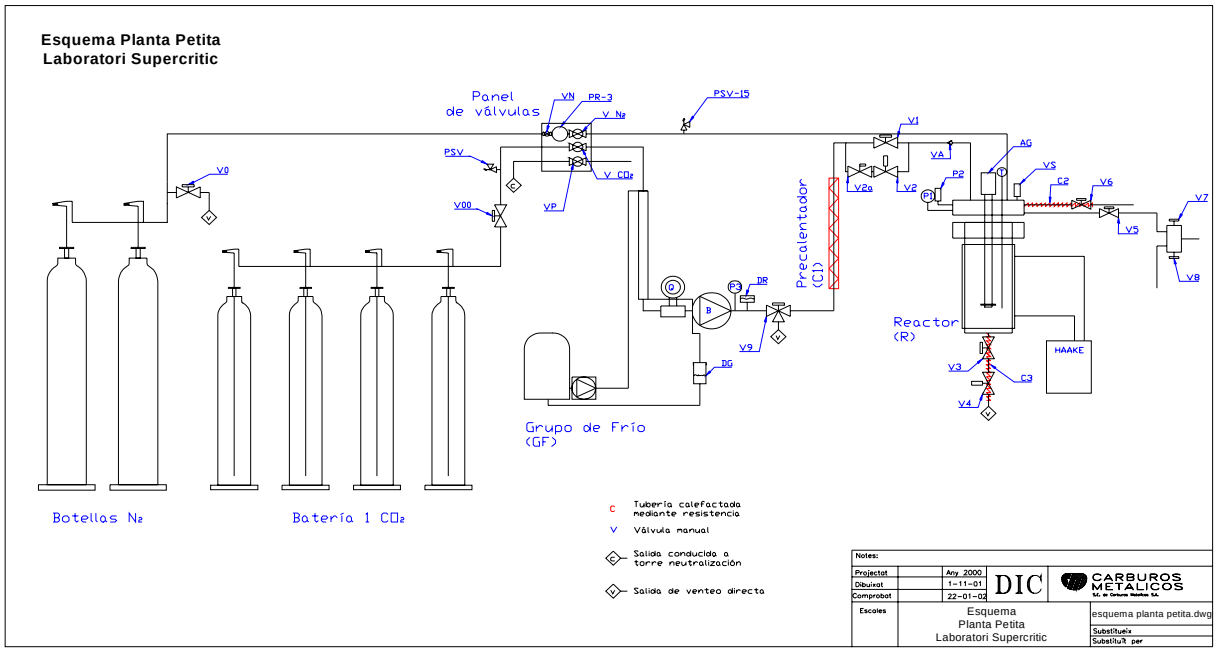

Figura A1. Esquema de l'equip d'alta pressió a escala de laboratori.

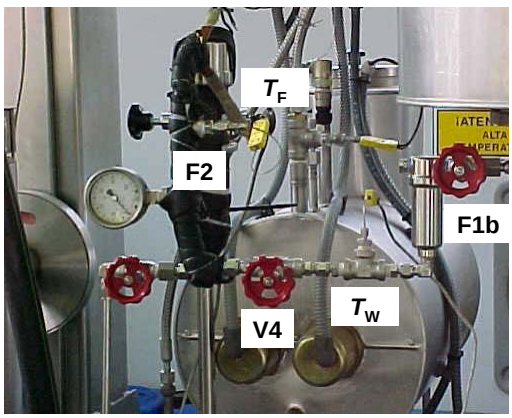

Figura A2. Esquema del sistema de filtració adaptat a l'equip d'alta pressió a l'escala de laboratori.

En qualsevol moment de l'experiment, la pressió i temperatura interna de l'autoclau R, el cabal d'addició mesurat pel caudalímetre màssic i les temperatures dels termoparells anterior i posterior a la vàlvula V4 apareixen en dispositius de visualització connectats als dispositius de mesura corresponents. Cada 5 segons, els valors mitjos d'aquests paràmetres s'enregistren en un ordinador acoblat als dispositius de visualització. Aquest ordinador permet crear un registre de temperatures, pressions i cabals en funció del temps associat a cada experiment. El registre del cabal de CO_2 introduït, s'utilitza per a calcular la massa total introduïda a R, i així poder obtenir el valor de X_{CO2} del sistema. Aquest càlcul es realitza per integració amb mètode de trapezi de la zona de la gràfica temps versus cabal, corresponent a l'etapa d'addició de CO_2. Per altra banda, la diferència entre T_W i T_F permet calcular el valor de ΔT instantani i mitjà de tot el procés de despressurització.

Planta pilot d'altes pressions i altes temperatures

La configuració mostrada en la Figura 13 també ha estat adaptada a una planta pilot equipada amb un reactor de 2 L. En aquesta planta es poden realitzar experiments a una escala un ordre de magnitud superior a la de l'equipament a escala de laboratori anteriorment descrit. L'esquema complet de la planta pilot utilitzada es mostra en la Figura A3. Dels tres reactors de què consta aquesta planta s'ha utilitzat el que en aquest Figura es nombra com a R3. El volum del reactor R3 és de 2 litres (Autoclave Engineers, Erie, USA) i compta amb un agitador impulsat per un sistema pneumàtic. El control de temperatura d'aquest reactor es realitza mitjançant un serpentí intern connectat a una bomba de recirculació d'oli provinent d'un bany termostatitzat. Aquest reactor també compta amb dues mirilles de quars a través de les quals és possible visualitzar el seu interior. El sistema de bombeig del CO_2 consta d'un liquador de 85 litres alimentat per una bateria d'un total de vuit cilindres de CO_2. El CO_2 líquid provinent d'aquest liquador és bombejat per una bomba d'alta pressió (LEWA, Leonberg, Alemanya) capaç de proporcionar un cabal màxim de 40 Kg/h. Un caudalímetre màssic d'efecte coriolis (RHEONIK, Odelzhausen, Alemanya) permet la mesura d'aquest cabal. Una línia independent connectada a dos cilindres de N_2 comprimit permet l'addició d'aquest gas a R3. La pressió a l'interior de R3 es mesura amb un transductor de pressió de membrana (WIKA, Klingenberg, Alemanya) amb un incertesa del 0.5% i la temperatura amb un termoparell tipus K. Els components d'aquest equip estan connectats mitjançant tub d'acer inoxidable de diàmetre extern d'1/4 de polzada i vàlvules d'alta pressió.

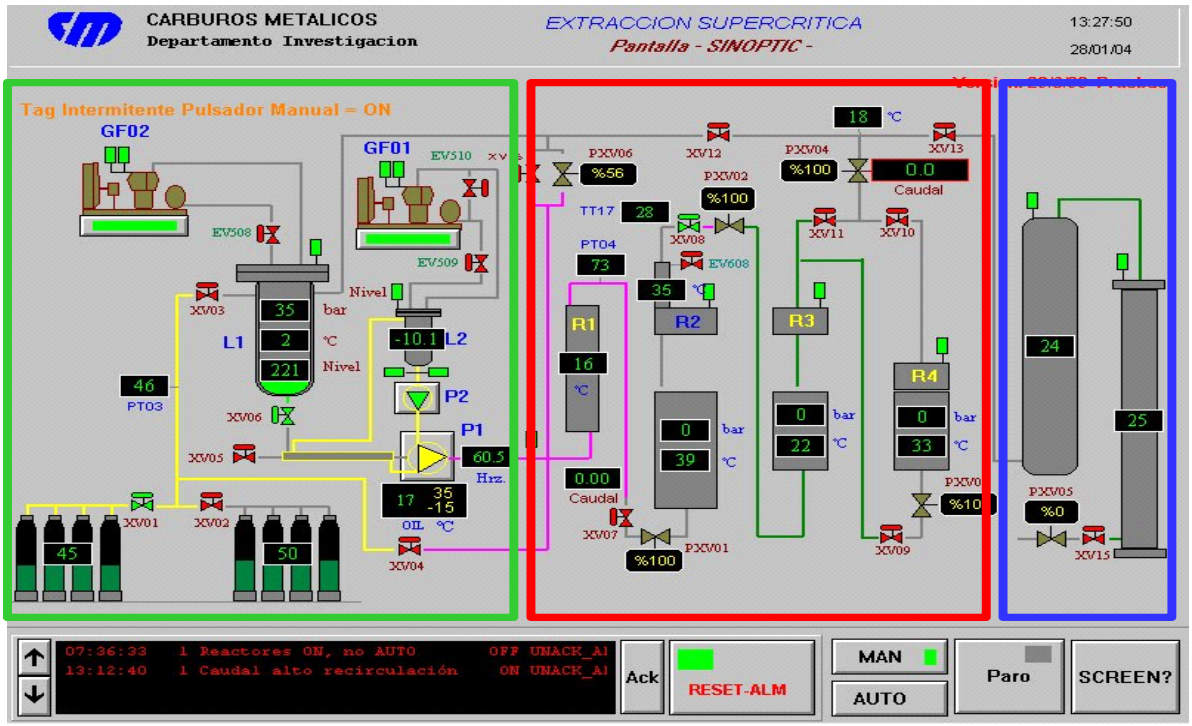

Figura A3. Planta pilot d'alta pressió i alta temperatura amb les seves tres unitats: 1) Requadre verd: Liquador i subministrador de CO_2; 2) Requadre vermell: Reactors; 3) Requadre blau: zona de venteig.

El sistema de filtració de partícules produïdes per GAS presenta algunes diferències en relació a l'utilitzat en l'equipament a escala de laboratori ja que el reactor R3 no compta amb un filtre intern F1. La retenció de la totalitat d'aquestes partícules s'ha realitzat, en aquest cas, amb un filtre exterior de metall sinteritzat F1 (HEADLINE FILTERS, Aylesford, Regne Unit) ubicat a la sortida de R3 i pressuritzat inicialment amb nitrogen a la pressió, P_W. El sistema de filtració de partícules produïdes per DELOS® i la resta de components són equivalents a l'equipament a escala de laboratori. En aquells casos on la quantitat precipitat obtingut per DELOS® és molt gran, s'ha adaptat un sistema de dos filtres en paral·lel (F2a i F2b) per a facilitar-ne la seva separació de les aigües mares, el qual es mostra en la Figura A4.

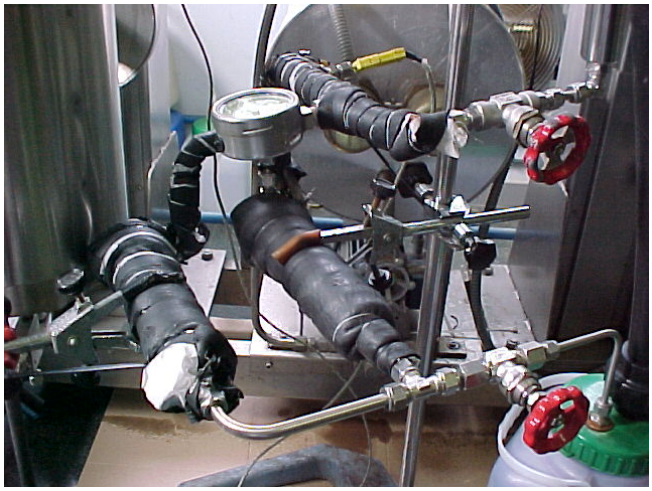

Figura A4. Esquema d'un sistema de filtració amb doble filtre en paral·lel i adaptat a la planta d'altes pressions i altes temperatures.

En qualsevol moment de l'experiment, la pressió i temperatura interna de l'autoclau R3, el cabal d'addició de CO_2, mesurat pel caudalímetre màssic, i les temperatures dels termoparells anterior i posterior a la vàlvula de despressurització s'observen en la pantalla de l'ordinador que actua com a dispositiu de visualització, control i registre de tots els elements de la planta. El registre dels paràmetres anteriorment mencionats també s'actualitza cada 5 segons. El càlcul de la massa total de CO_2 introduïda durant la pressurització i del ΔT associat a la despressurització es realitza de la mateixa manera com s'ha indicat per la planta a escala de laboratori.

B. Equipament i protocol d'operacions emprats en els experiments GAS

La Figura A5 mostra la configuració experimental emprada per a dur a terme processos de cristal·lització GAS. Aquesta configuració ha estat adaptada a l'equipament d'alta pressió a escala de laboratori i a la planta pilot d'altes pressions i altes temperatures.

El procediment operacional seguit durant la realització d'experiments GAS utilitza la configuració experimental mostrada en la Figura A5, i consisteix en la seqüència d'accions que es descriu a continuació:

Un volum conegut de dissolució del solut a cristal·litzar en un dissolvent orgànic convencional, amb una sobresaturació inicial β_I, es carrega en el reactor d'alta pressió R1. Durant tot el procés, el sistema de termostatització es manté connectat al reactor R1, per tal de mantenir la temperatura de treball, T_W, a l'interior del reactor. La dissolució inicial és llavors pressuritzada fins a la pressió de treball P_W, mitjançant l'addició de CO_2 a través de la part inferior del reactor R1. D'aquesta manera s'aconsegueix millorar la cinètica de dissolució del CO_2 en el dissolvent orgànic fins aconseguir arribar al valor desitjat de fracció molar de treball de CO_2, X_W.

Un cop assolits els valors desitjats de P_W i X_W s'inicia el procés de filtrat que permet aïllar el precipitat produit per efecte anti-solvent del CO_2. Els cristalls formats a l'interior de R1 durant l'addició de CO_2, són recollits en el filtre F1. Durant aquest procés de filtrat, la pressió a l'interior de R1 és mantinguda constant a P_W mitjançant la contínua addició de nitrogen pressuritzat a través de la part superior de R1. Un cop finalitzada la filtració, la neteja del precipitat GAS recollit sobre F1, es du a terme mitjançant CO_2 a pressió d'entre 3 i 6 MPa i a temperatura ambient, durant 60 minuts.

Durant el transcurs de l'experiment de cristal·lització, T_W i P_W i el cabal d'addició del CO_2 a R1 queden enregistrats en intervals de 5 s en el sistema de registre de dades que es troba acoblat a la planta.

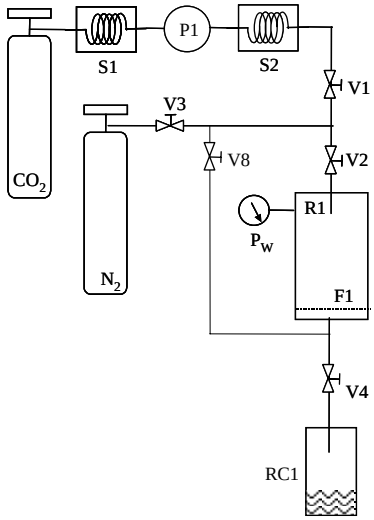

Figura A5. Esquema de l'equipament emprat en els experiments GAS. P: bomba; S: intercanviador de calor; V: vàlvula; F: filtre; R: reactor d'alta pressió; RC: col·lector per reciclatge.

C. Determinació del descens de temperatura obtingut durant la despressurització de mescles "dissolvent convencional/CO_2"

Procediment emprat

Per a la realització d'aquestes mesures s'ha utilitzat l'equipament d'alta pressió a escala de laboratori descrit en l'apartat anterior i s'ha realitzat el procediment que es descriu a continuació. Un volum conegut de dissolvent orgànic convencional es carrega al reactor d'alta pressió R. Durant tot el procés, el bany amb recirculació d'aigua es manté connectat al reactor encamisat R, per tal de mantenir constant la temperatura de treball, T_W, a l'interior del reactor. El dissolvent es pressuritza fins a la pressió de treball, P_W, per mitjà de l'addició de CO_2. Després de deixar el sistema amb agitació a les condicions de treball durant 30-60 minuts per tal d'aconseguir la completa homogeneïtzació del sistema i el seu equilibri tèrmic, la mescla "dissolvent convencional/CO_2" es despressuritza a través de la vàlvula V4 des de P_W fins a pressió atmosfèrica. Durant el procés de despressurització, la pressió a l'interior de R es manté constant a P_W per mitjà de la continua addició de nitrogen pressuritzat a través de la part superior de R. Durant el transcurs de l'experiment, T_W, T_F, P_W i el cabal d'addició del CO_2 a R queden enregistrats en intervals de 5 s en el sistema de registre de dades que es troba

acoblat a la planta. Això permet calcular el valor de X_W i el valor de ΔT ($\Delta T = T_F - T_W$) obtingut durant el transcurs de la despressurització.

Taula A1. Experiments de despressurització de mescles d'"acetona/CO_2"

EXPERIMENT	T_W (K)	P_W(MPa)	X_W[a]	F (Kg/h)	ΔT
TERMO 1	298	10	0.27	52.1	-27
TERMO 2	298	6	0.27	43.0	-28
TERMO 3	298	10	0.3	26.6	-31
TERMO 4	298	8	0.29	33.1	-31
TERMO 5	298	6	0.31	23.3	-35
TERMO 6	298	10	0.4	25.5	-41
TERMO 7	298	8	0.4	33.7	-41
TERMO 8	298	6	0.4	18.9	-45
TERMO 9	298	10	0.44	19.7	-52
TERMO 10	298	8	0.45	21.1	-53
TERMO 11	298	6	0.46	30.0	-55
TERMO 12	298	15	0.5	22.2	-58
TERMO 13	298	10	0.5	15.8	-58
TERMO 14	298	8	0.51	12.1	-60
TERMO 15	298	6	0.5	10.8	-61
TERMO 16	298	10	0.6	5.7	-71
TERMO 17	298	8	0.6	9.9	-72
TERMO 18	298	6	0.61	15.3	-73
TERMO 19	298	10	0.71	23.0	-86
TERMO 20	298	6	0.71	19.0	-87

Taula A2. Experiments de despressurització de mescles "dissolvent convencional/CO_2"

EXPERIMENT	DISSOLVENT	T_W (K)	P_W(MPa)	X_W	ΔT	$\Delta H^s_{V(CO2)}$ (KJ/mol)
TERMO 21	Metanol	298	10	0,2	-32	10,52
TERMO 22	Metanol	298	10	0,3	-44	8,31
TERMO 23	Metanol	298	10	0,4	-58	7,06
TERMO 24	Metanol	298	10	0,6	-88	4,77
TERMO 25	Acetat d'etil	298	10	0,3	-27	10,81
TERMO 26	Acetat d'etil	298	10	0,5	-49	8,42
TERMO 27	Acetat d'etil	298	10	0,6	-64	7,35
TERMO 28	Acetat d'etil	298	10	0,7	-77	5,67
TERMO 29	Acetona	298	10	0,31	-35	10,62
TERMO 30	Acetona	298	10	0,5	-61	7,71
TERMO 31	Acetona	298	10	0,61	-73	5,9
TERMO 32	Acetona	298	10	0,71	-87	4,44
TERMO 33	Etanol	298	10	0,3	-33	8,74
TERMO 34	Etanol	298	10	0,5	-58	6,52
TERMO 35	Etanol	298	10	0,6	-72	5,39
TERMO 36	Etanol	298	10	0,7	-93	4,46

[a] En l'Equació 11 $n_{(CO2)}$ i $n_{(dis)}$ han estat substituits per X_W i 1- X_W, respectivament.

En la Taula A1 es mostren el conjunt d'experiments de despressurització de mescles d'"acetona/CO_2", amb els paràmetres operacionals T_W, P_W, X_W i F emprats i el valor de ΔT obtingut en cada experiment. Aquests experiments han estat utilitzats per a realitzar l'estudi

mostrat en l'Apartat 1.1.4.1, en el qual s'avalua la influència dels paràmetres P_W, X_W i F sobre el valor de ΔT que s'obté al despressuritzar mescles d'acetona com a dissolvent convencional i CO_2 com a fluid comprimit.

En la Taula A2 es mostren el conjunt d'experiments de despressurització de mescles "dissolvent convencional/CO_2" que s'han realitzat per estudiar la influència de la naturalesa del dissolvent convencional sobre el valor de ΔT obtingut en un procés DELOS®. Aquest estudi es troba descrit en l'Apartat 1.1.4.2. En aquesta Taula es mostra el dissolvent utilitzat en cada experiment, els paràmetres operacionals emprats, la composició de la mescla dissolvent, el valor de ΔT obtingut i el valor de l'entalpia de vaporització del CO_2 dissolt, $\Delta H^s_{V(CO2)}$ (kJ/mol), calculat tal i com es descriu en l'Apartat 1.1.4.4.

D. Instrumentació i tècniques utilitzades en la caracterització dels precipitats obtinguts

Mesura de distribució de mida de partícula per dispersió de llum (LS; Light Scattering technique)

Les distribucions volumètriques de mida de partícula dels materials finament dividits obtinguts en les cristal·litzacions GAS i DELOS®, van ser mesurades mitjançant la tècnica de dispersió de llum amb els aparells MALVERN de model Mastersizer/E i Beckman Coulter de model LS13320. La preparativa de les mostres va consistir en la suspensió d'una quantitat determinada de mostra en un medi dispersant líquid. Aquesta suspensió es sotmet a ultrasons durant uns minuts per assegurar la disgregació de les partícules i l'estabilització de la suspensió. El medi dispersant utilitzat per a mesurar la mida de partícula del colorant **1**, l'àcid esteàric i el colesterol va ser una solució amb 0.05% del tensoactiu TWEEN 80 (SIGMA-ALDRICH) en aigua, mentre que pel què fa a l'aspirina i el paracetamol es va utilitzar una fracció de petroli amb punts d'ebullició entre 180 i 220ºC (Petroleum Special, FLUKA-ALDRICH). El model matemàtic utilitzat per l'aparell de mesura per transformar el senyal òptic rebut pel detector en la distribució de mida de partícula va ser l'anomenat Model Independent d'Anàlisi.

Microscopia Electrònica d'Escombrat (SEM)

La morfologia de les partícules va ser observada per mitjà d'un microscopi electrònic d'escombrat HITACHI de model S-570. Igualment com en les mesures de distribució de mida de partícula, la preparativa de mostra va consistir en la preparació d'una suspensió en un medi

dispersant determinat. En el cas del colorant 1 s'utilitzà una solució etanol/aigua (1/1), en el cas de l'àcid estearic s'utilitzà etanol/aigua (1/10), en el cas del colesterol aigua, i en el cas de l'aspirina i l'acetaminofè s'utilitzà el petroli ja emprat en les mesures de dispersió de llum. Es van dipositar unes poques gotes de la suspensió preparada sobre el portamostres del microscopi i es va assecar el dissolvent amb paper absorbent. Finalment es va dipositar una capa de metal·litzat d'or sobre les mostres.

Difracció de Raigs X en Pols (PXRD)

Els difractogrames de raigs X en pols dels materials obtinguts van ser enregistrats per mitjà d'un Difractòmetre RIGAKU DS5000 amb ànode de Coure (λ=1.540598), amb valors de 2θ entre 3 i 60º i increments de 0.02º.

Calorimetria Diferencial d'Escombrat (DSC)

Els perfils de DSC van ser mesurats mitjançant un Calorímetre Diferencial d'Escombrat PERKIN ELMER de model DSC7. L'Indi (T_f=156.6º; ΔH_f=28.45 J g^{-1}) va ser utilitzat com a patró de calibració. La quantitat de mostra analitzada en cada mesura fou de 0.8-1.2 mg, els quals foren pesats amb una precisió de 0.001mg i dipositats en portamostres d'alumini. Les velocitats d'escombrat de temperatura emprades van oscilar entre 1ºC/min i 40ºC/min.

Espectroscòpia d'Infraroig de Transformada de Fourier (FTIR)

Es va utilitzar un Espectròmetre d'Infraroig de Transformada de Fourier PERKIN ELMER model Spectrum One amb resolució de 4 cm^{-1}. Les mesures en fase sòlida es varen realitzar mitjançant la barreja de 1 mg de mostra i 100 mg de KBr, i la formació d'una pastilla.

E. Mètode de determinació de solubilitats en dissolvents orgànics

Mescles saturades (sòlid en equilibri amb dissolució saturada) del solut en el dissolvent orgànic es mantingueren en agitació durant una hora a la temperatura desitjada. Es van utilitzar banys d'aigua termostatitzats per a determinacions per sobre de 273 K, i mescles d'aigua i gel quan la temperatura és 273K. Per a temperatures més baixes, es van utilitzar banys criogènics amb CO_2 sòlid (p. ex. mescla CCl_4/CO_2 per a 249 K i mescla acetonitril/CO_2 per a 228K). Acabat aquest període, l'agitació es va aturar i la mescla es mantingué a la mateixa temperatura durant 30 minuts. Després, un volum conegut de dissolució saturada fou extret, filtrat, pesat amb una balança de precisió (±0.0001 g), obtenint-se $n^0_{SOLUT}+n^0_{ORG}$, i finalment, evaporat fins a sequedat per tal de conèixer la quantitat la sòlid dissolt, n^0_{SOLUT}. Aquest sòlid sec (dues hores en bomba de buit) va ser també pesat en la balança de precisió.

El procediment es realitzà dues vegades. Les solubilitats foren expressades en termes de mols de solut/mols de dissolvent, $n^0_{SOLUT}/\ n^0_{ORG}$. La utilització d'aquest procediment de mesura comporta un error sistemàtic inferior al 0.1%.

F. Mètodes de determinació de solubilitats en fluids comprimits

Mètode estàtic gravimètric de determinació de solubilitats en dissolvents expandits amb CO_2

La configuració experimental emprada per a portar a terme les mesures de solubilitat mitjançant el procediment anomenat mètode estàtic gravimètric, es mostra a la Figura A6. Aquesta configuració ha estat adaptada a la planta d'altes pressions a escala de laboratori anteriorment descrita.

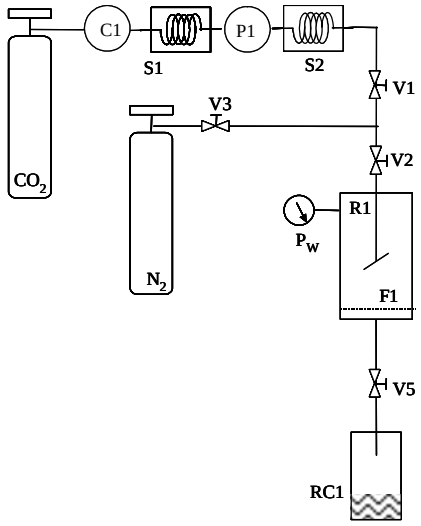

Figura A6. Esquema de l'equipament en el mètode de mesura de solubilitats estàtic gravimètric. P: bomba; C:caudalímetre; S: intercanviador de calor; V: vàlvula; F: filtre; R: reactor d'alta pressió; RC: col·lector per reciclatge.

El procediment de mesura consisteix en la següent seqüència d'accions: una mescla del solut, del qual es desitja mesurar la solubilitat, n^0_{SOLUT} (mols corresponents a una massa pesada amb balança de precisió ±0.001 g), i de dissolvent orgànic, n^0_{ORG} (mols corresponents a volums mesurats amb precisió de ±1 mL), es carrega en el reactor R1. La sobresaturació inicial d'aquesta mescla és superior a 1 i per tant la mescla és una dispersió. A continuació s'activa el circuit de recirculació de la camisa d'aigua del reactor que manté constant la temperatura interna d'aquest a la temperatura desitjada, T_W, i s'inicia el bombeig de CO_2 líquid sobre la mescla. La pressurització es prolonga fins a arribar a la pressió de treball desitjada, P_W. La quantitat total de CO_2 introduïda en el reactor, n^0_{CO2} (mols calculats a partir de mesures de cabal amb precisió relativa de 0.1% a la planta a escala de laboratori i 0.2% a la planta pilot),

és mesurada mitjançant el caudalímetre, la qual cosa permet calcular la fracció molar de CO_2 de la mescla dissolvent, $X_{CO2}=X_W$. En el present treball, X_W ha estat sempre calculat sense tenir en compte la contribució de la concentració de solut, la qual acostuma a ser suficientment baixa com per a ser menyspreable. El sistema s'agita durant una hora a fi d'assolir condicions d'equilibri. Una vegada assolit l'equilibri, l'agitació s'atura i es procedeix a la filtració del sòlid que roman encara en l'interior de R1. Durant aquesta etapa, un flux continu de nitrogen a la mateixa pressió P_W és afegit per la part superior de R1 fins a aconseguir la completa evacuació de la dissolució. Després de la filtració, la neteja del sòlid retingut pel filtre F1 es du a terme mitjançant CO_2 pur amb una pressió 3-6 MPa. Una vegada despressuritzat el sistema es recupera aquest sòlid retingut en F1 i es pesa en una balança de precisió (±0.001 g). La diferència entre la quantitat inicial de solut introduït, n^0_{SOLUT}, i la quantitat de sòlid retingut en F1, n^f_{SOLUT}, correspon a la massa de solut que s'ha dissolt en el dissolvent expandit amb CO_2 a la pressió i temperatura de treball. La solubilitat del solut (S) ha estat calculada mitjançant l'Equació A1:

$$S = \frac{n^o_{SOLUT} - n^f_{SOLUT}}{n_{SOLVENT} + n_{CO_2}} \qquad \text{(A1)}$$

La utilització d'aquest procediment de mesura tant en la planta a escala de laboratori com en la planta pilot comporta un error sistemàtic inferior al 0.5% en la determinació de solubilitats i inferior al 1% en la determinació de valors de fracció molar de CO_2.

Mètode de determinació de solubilitats en dissolvents expandits amb CO_2 segons el mètode de "vanishing-point" mitjançant una cel·la de volum variable

Durant la realització de la present tesi doctoral, mitjançant una estreta col·laboració entre el Laboratori de Materials Orgànics de l'ICMAB i el departament d'investigació de l'empresa CARBUROS METÀLICOS, s'ha dissenyat i construït un analitzador de fases a alta pressió basat en una cel·la de volum variable, el qual ha permès mesurar solubilitats mitjançant el mètode conegut amb el nom de "vanishing-point". El diagrama de flux de l'esmentat analitzador de fases es troba representat en la Figura A7.

Els diferents elements que composen aquesta configuració experimental han estat agrupats en els diferents sistemes que es troben representats en els diferents requadres de la Figura A7, i el contingut dels quals es descriu a continuació:

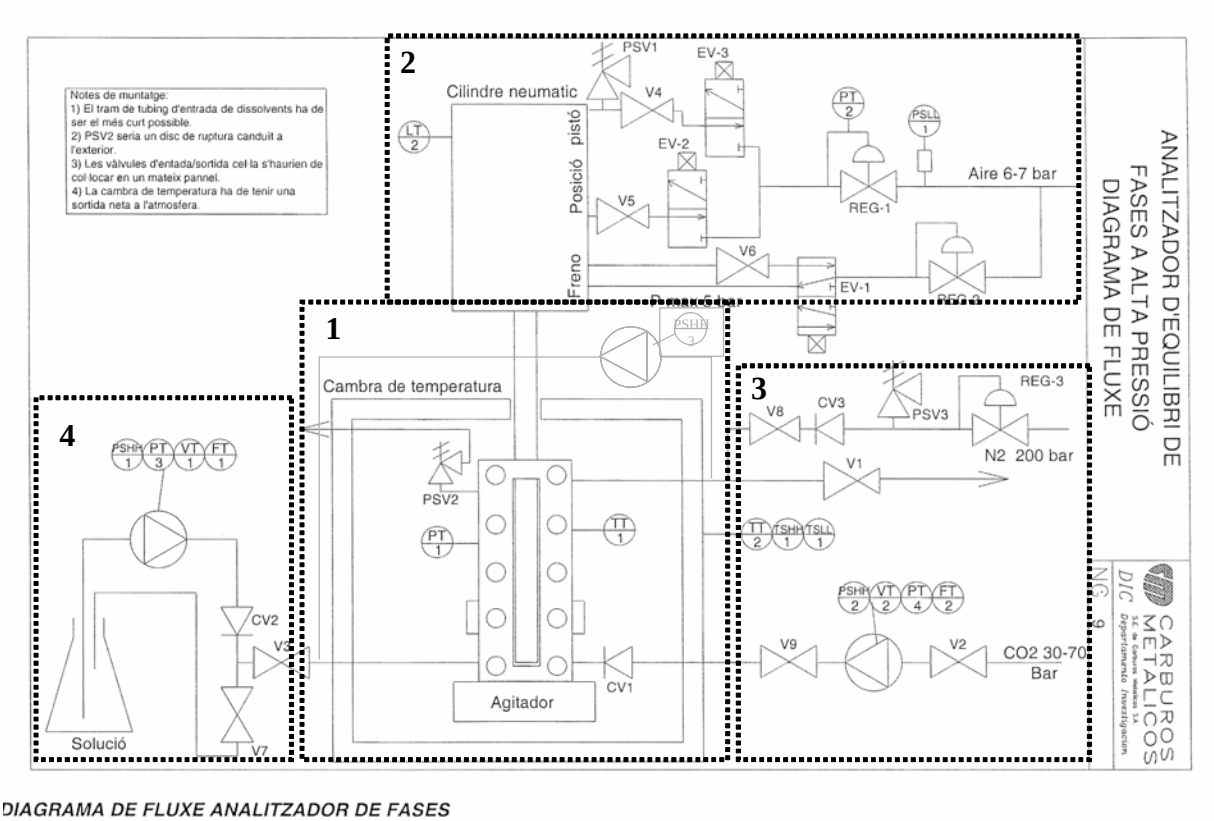

Figura A7. Diagrama de flux de l'analitzador de fases emprat amb el "vanishing-point method".

Requadre 1: La cel·la de volum variable està basada en un reactor de mirilla d'alta pressió de la marca Jerguson model 16-T-40 i està construït en acer inoxidable 316 i vidre trempat en la part corresponent a la mirilla (vidres transparents frontal i posterior). Aquesta cel·la ha estat mecanitzada per la part inferior per a adaptar-hi un tap portasubstàncies per introduir substàncies sòlides en el seu interior. S'hi ha incorporat dues mirilles laterals de safir per a realitzar mesures de terbolesa com a sistema de detecció del "vanishing-point" (encara no disponible). Compta amb una sonda de temperatura (pt-100) i un transductor de pressió (Keller sèrie 8). L'element que permet la variació del volum intern de la cel·la és un pistó d'acer inoxidable 316 que s'introdueix dins del reactor fins a una profunditat màxima, comptada des de la junta de guia i estanquitat, de 20 cm. La cel·la de volum variable està situada a l'interior d'una cambra de temperatura fred/calor Binder model MK 53. La temperatura mínima de treball d'aquesta cambra és -35ºC i la màxima 180ºC. El fluid intern de la cel·la és homogeneïtzat mitjançant una bomba externa de recirculació Micropump sèrie 180. La Figura A8 mostra una imatge frontal de la cel·la.

Requadre 2: Aquest requadre inclou el cilindre pneumàtic de marca SMC i model CE2B63-200J que governa el moviment del pistó amb bloqueig i lectura de carrera. Està preparat per treballar amb una pressió mínima en el pistó de 0.1 MPa i màxima de 1 MPa.

El moviment del cilindre està comandat per tres electrovàlvules de bloqueig, moviment ascendent i descendent i per una línia d'aire comprimit de 0.55 MPa i de pressió regulada a través d'un transductor electropneumàtic de pressió (SMC model ITV2050).

Figura A8: Imatge frontal de la cel·la de volum variable.

Requadre 3: Inclou les línies d'alimentació de fluids comprimits. La línia de N_2 (superior) arriba directament d'una bombona amb control de pressió per mitjà d'un manorreductor. La línia de CO_2 (inferior) disposa d'una bomba de xeringa d'alta pressió marca ISCO i model 260D per a produir fluxos a pressió (màxim 50 MPa) o a cabal constant (màxim 90 mL/min).

Requadre 4: Correspon a la línia d'alimentació de dissolvents orgànics o dissolucions orgàniques. Compta amb una bomba de bombeig per micropistons d'alta pressió marca JASCO i model PU-1580. També permet treballar amb modes de pressió i cabal constant fins a una pressió màxima de 50 MPa i cabal màxim de 10 mL/min.

Figura A9. Imatge completa de l'equip on es visualitza la cambra de fred/calor que conté la cel·la (esquerra), la bomba de líquids (centre sobre estructura) i la bomba de CO_2 (dreta)

La Figura A9 mostra una imatge completa del conjunt instrumental que composa l'analitzador de fases. La Figura A10 mostra el diagrama de visualització del software dissenyat per CARBUROS METÀLICOS per a controlar l'equip.

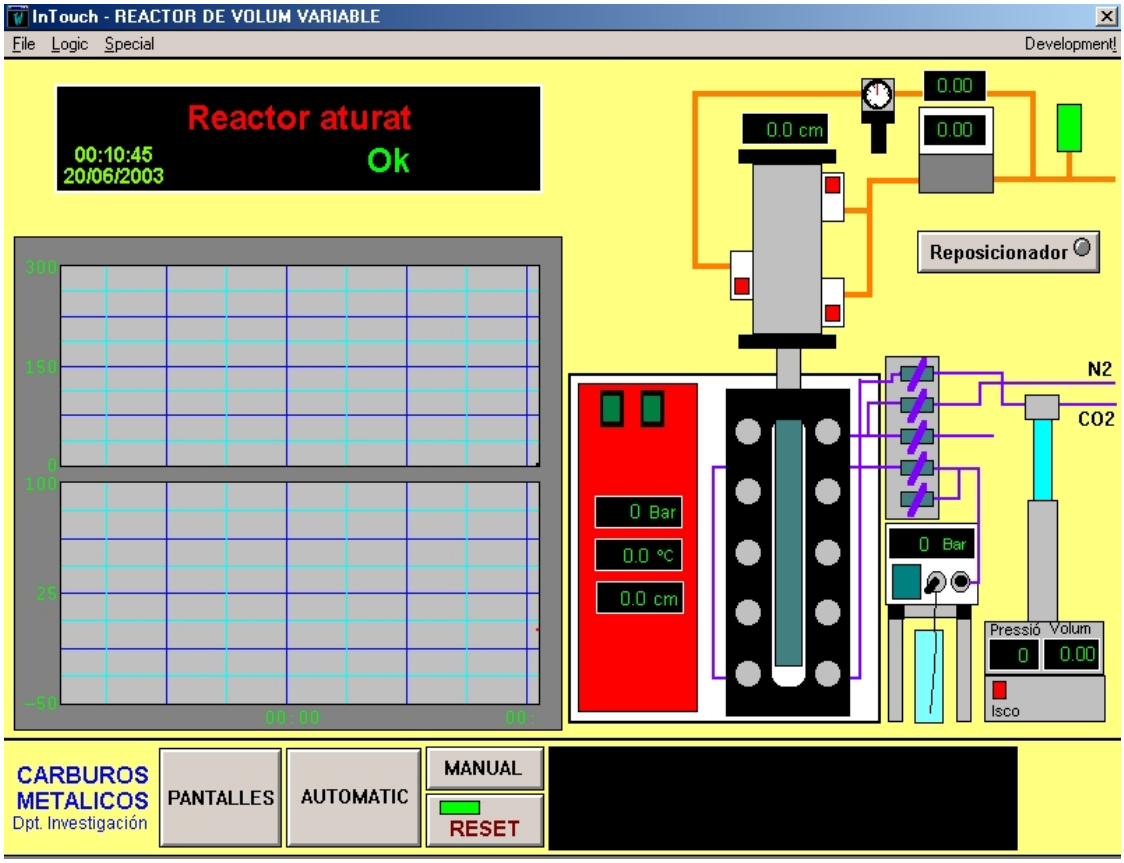

Figura A10. Programa de control i visualització de paràmetres dels components de l'analitzador de fases

El mètode de "vanishing-point" de determinació de solubilitats en fluids comprimits es troba descrit en treballs de F. E. Wubbolts i col.[1] Aquest mètode està inspirat en el procediment de determinació de solubilitats de sals inorgàniques en barreges d'aigua i dissolvents orgànics a pressió atmosfèrica, descrit en un treball de P. H. Karpinski i J. Nývlt i que aquests autors anomenen "Mètode de dissolució de l'últim cristall visible".[2] Les sals inorgàniques presenten una major solubilitat en aigua que en els dissolvents orgànics. Així, en aquest procediment es realitza l'addició d'una quantitat determinada de dissolvent orgànic sobre una dissolució de sal en aigua, prou elevada com per provocar la precipitació del solut. Posteriorment, s'addiciona sobre la mescla, de manera lenta i controlada, aigua fins a obtenir la dissolució de l'última partícula sòlida de solut. La realització del balanç de les quantitats de sal inorgànica, aigua i dissolvent orgànic que han permès arribar en aquest punt on l'últim cristall s'ha dissolt, permet determinar el valor de la solubilitat del solut en el sistema ternari.

El mètode de "vanishing-point" és una adaptació d'aquest procediment i es basa en l'addició d'una dissolució d'un compost C en un dissolvent A, sobre un altre dissolvent B miscible amb el dissolvent A i en el qual el compost C hi té una solubilitat significativament més baixa. Durant aquesta addició, la representació de la variació de la composició del sistema en mols de solut C/mols de dissolvent, a mesura que es va introduint dissolució de C en A, es comporta segons la línia de treball que es mostra en la Figura A11. Aquesta línia de treball depèn de la concentració de la dissolució de C en A, C_A. En el cas hipotètic d'una corba de solubilitat del compost C en la mescla A/B com la que es mostra en la Figura A11, l'addició de dissolució sobre el dissolvent B provoca l'inici de la precipitació de C a partir del punt a de la línia de treball indicat en l'ampliació de la representació gràfica en la zona propera a X_{CO2}=1. Aquest punt a consisteix en el primer punt de tall entre la línia de treball i la corba de solubilitat quan la trajectòria de la primera segueix el sentit des de X_B=1 fins a X_B=0. Quan més baixa és la solubilitat de C en B més proper és el punt a a X_B=1. L'anomenat "vanishing-point" és el segon punt de tall entre la línia de treball i la corba de solubilitat en la mateixa trajectòria (veure Figura A11). Aquest punt correspon al moment en què les partícules sòlides, que han aparegut a partir del punt a i que al llarg del recorregut de la línia de treball s'han anat redissolent, desapareixen definitivament i per tant s'assoleix una mescla homogènia i d'una sola fase.

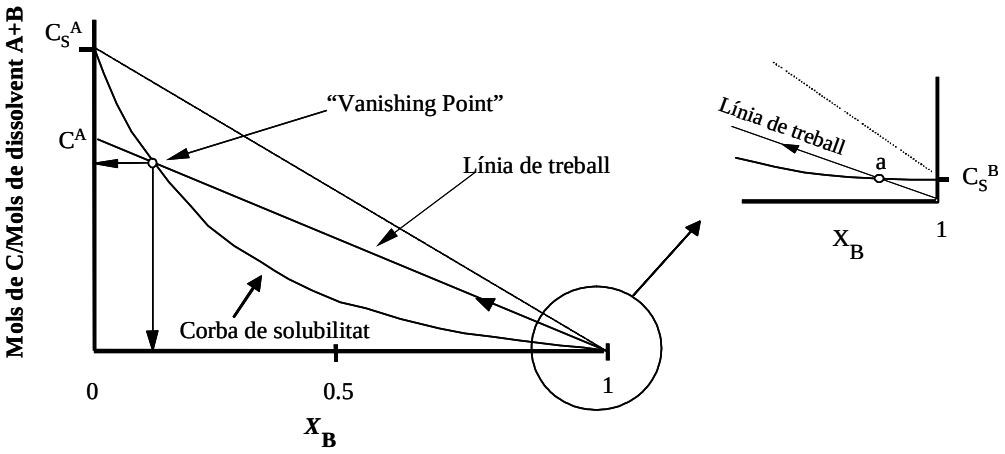

Figura A11. Descripció gràfica del mètode de "vanishing-point"

En definitiva, el principi fonamental que governa les tècniques de "vanishing-point" i "dissolució de l'últim cristall visible" és l'objectiu d'observar la progressiva, i finalment total, redissolució d'un sòlid que es troba en equilibri amb una fase saturada, i que es va redissolent

degut a que es va canviant la composició de la fase dissolvent binària, donant-li a aquesta major capacitat per a dissoldre el sòlid.

En l'analitzador de fases descrit anteriorment no només es poden mesurar corbes de solubilitat com la que es mostra en la Figura A11, o sigui amb una evolució exponencial i amb un clar comportament d'antisolvent del dissolvent B en relació a la dissolució de C en A, sinó també es poden mesurar corbes de solubilitat amb comportaments de co-solvència del dissolvent B i fins i tot amb possibles efectes sinèrgics de la capacitat solvatadora de la mescla binària de dissolvents. En la Figura A12 es mostren alguns exemples dels tipus de comportaments de solubilitat susceptibles de ser mesurats amb aquest equipament.

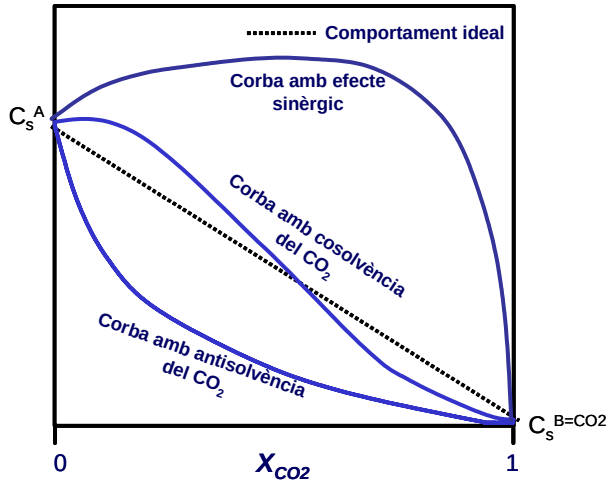

Figura A12. Diferents tipus de corbes de solubilitat en sistemes "solut/dissolvent orgànic/CO_2"

Així, la metodologia de determinació de solubilitats en dissolucions expandides amb CO_2 que s'ha emprat en aquest treball utilitzant l'analitzador de fases a alta pressió anteriorment descrit, es pot resumir en les dues etapes següents:

1) Preparació dins de la cel·la de volum variable d'una mescla "solut/dissolvent convencional/CO_2" sobresaturada a les condicions de pressió i temperatura desitjades.
2) Addició del dissolvent apropiat (dissolvent orgànic o fluid comprimit) seguint una línia de treball determinada, per tal de facilitar la progressiva dissolució del solut en estat sòlid, fins a observar-ne la completa desaparició. Aquest moment correspon al punt de tall entre la línia de treball i la corba de solubilitat, i per tant, determina el valor de solubilitat.

La manera com es prepara la mescla de l'etapa 1, la qual ha de tenir la presència de sòlid en equilibri amb la dissolució saturada, i la direcció, en termes de composició de la fase dissolvent "dissolvent convencional/CO_2", que pren la línia de treball que porta a creuar la corba de solubilitat, permeten definir diferents variants de procediment de mesura:

Cas A: Mesura de corbes amb efecte anti-solvent del CO_2

Correspon al mètode de "vanishing-point" clàssic descrit anteriorment el qual permet mesurar corbes de solubilitat en sistemes amb efecte anti-solvent del CO_2 en relació a la dissolució del solut en el dissolvent orgànic. Es basa en el bombeig d'una dissolució de solut en el dissolvent convencional sobre CO_2 a les condicions de pressió i temperatura de mesura fins a creuar el punt a. A partir d'aquest punt a ja es té l'equilibri solut sòlid/dissolució saturada buscat en l'etapa 1(veure Figura A11). Si es continua l'addició de dissolució de solut en dissolvent orgànic es segueix la línia de treball, que ve definida per la concentració d'aquesta dissolució, C^A, fins a arribar al "vanishing-point". Com s'observa en la Figura A13, en funció de quina sigui la concentració de la dissolució de solut en el dissolvent orgànic ($C^A(1)$, $C^A(2)$,..... $C^A(n)$) es pot aconseguir la mesura de diferents punts de la corba de solubilitat.

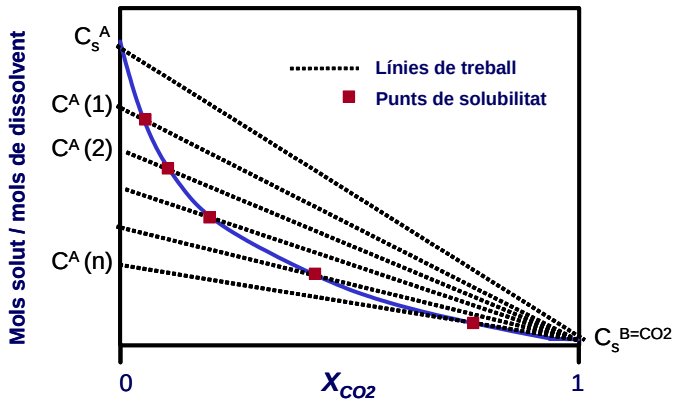

Figura A13. Exemples de punts de solubilitat mesurats en el CAS A

Cas B: Mesura de corbes amb efecte co-solvent del CO_2 o efecte sinèrgic a partir de línies de treball $X_{CO2}=1 \rightarrow X_{CO2}=0$

El procediment associat a aquesta cas permet realitzar mesures complementàries a les que es realitzen en el CAS A. Quan el comportament de solubilitat del sistema es caracteritza per un comportament de cosolvent del CO_2 en un rang determinat de concentracions de la fase dissolvent, el procediment amb addició de dissolució de solut en dissolvent orgànic sobre CO_2 a les condicions de mesura (cas A), només permet determinar un nombre limitat de punts de solubilitat situats en zones properes a $X_{CO2}=1$. La Figura A14 descriu gràficament aquesta limitació.

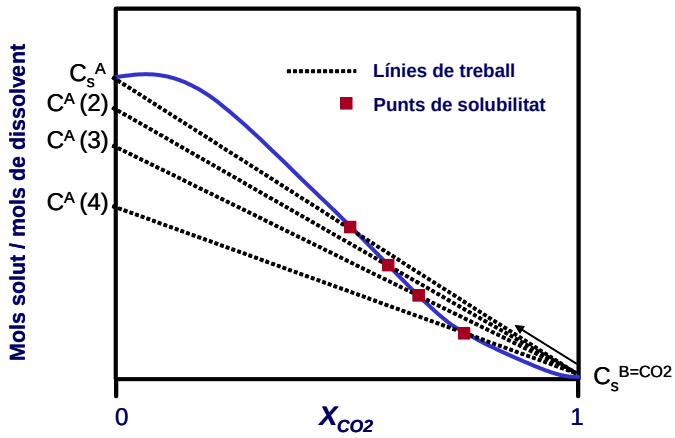

Figura A14. Punts de solubilitat mesurables segons el mètode descrit en el cas A per una corba de forma sigmoidea (co-solvència de CO_2).

Per a poder realitzar la mesura de punts de solubilitat situats a menor X_{CO2} que els mostrats en la Figura A14, es fa necessari realitzar una major càrrega de la cel·la en solut. En el cas de la cel·la de volum variable descrita en el present annex, aquesta càrrega addicional es realitza mitjançant la introducció de sòlid a través del portamostres situat sobre el tap inferior de la cel·la. La Figura A15 mostra una imatge d'aquest portamostres. Un cop introduït el portamostres a la cel·la, es pressuritza la cel·la amb CO_2 a la pressió i temperatura de mesura. Posteriorment es bombeja, sobre la barreja sòlid/CO_2, dissolució de solut en el dissolvent orgànic d'una concentració determinada. Com en el cas A, durant aquest addició es produeix la progressiva dissolució del sòlid degut a l'enriquiment de la mescla en dissolvent orgànic. Les línies de treball seguides depenen de la quantitat de solut introduït en el portamostres i de la concentració de solut en la dissolució que s'addiciona. Tal i com s'observa en la Figura A16, aquestes línies de treball es creuen amb la corba de solubilitat en punts de la corba situats a menor valor de X_{CO2} que els corresponents als punts ja determinats amb el mètode de "vanishing-point" clàssic. La corba de solubilitat queda per tant completament descrita en tot el rang complet de composicions de la mescla dissolvent.

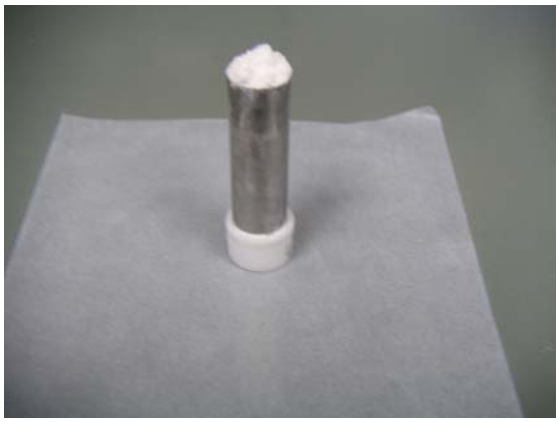

Figura A15. Vista del cilindre portamostres utilitzat per a la introducció de sòlids a la cel·la de mesura.

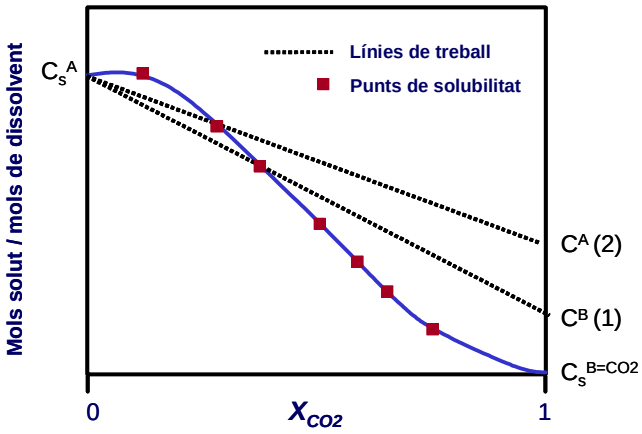

Figura A16. Punts de solubilitat d'una corba amb co-solvència del CO_2, mesurables amb la càrrega addicional de la cel·la mitjançant el portamostres (cas B)

El procediment de càrrega addicional de la cel·la abans de la pressurització és de realització obligada en el cas de determinacions de solubilitat en sistemes que presenten un efecte sinèrgic de la capacitat solvatadora de la mescla binària en relació a les solubilitats en els dissolvents purs. En la Figura A17 es demostra que per arribar a determinar els punts de solubilitat indicats sobre la corba, cal realitzar el bombeig de dissolució de solut en el dissolvent orgànic sobre una quantitat inicial bastant elevada de sòlid pressuritzat amb CO_2. Existeix també la possibilitat de realitzar bombeig de dissolvent A pur sobre la barreja inicial de solut i CO_2, i així determinar altres punts com els indicats en la mateixa Figura.

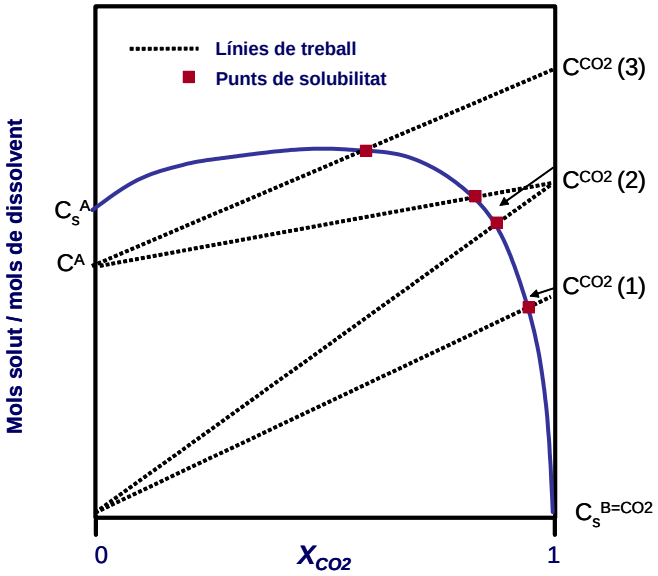

Figura A17. Punts de solubilitat d'una corba amb efecte sinèrgic, mesurables amb la càrrega addicional de la cel·la mitjançant el portamostres

Cas C: Mesura de corbes amb efecte sinèrgic a partir de línies de treball $X_{CO2}=0 \rightarrow X_{CO2}=1$

Fins aquest punt, els procediments d'operació introduïts descriuen línies de treball que evolucionen des de $X_{CO2}=1$ fins a $X_{CO2}=0$ en la determinació del punt de tall amb la corba de solubilitat. A continuació es demostra que en alguns casos, pot ser útil servir-se de línies de treball que evolucionin en sentit contrari, és a dir, des de $X_{CO2}=0$ fins a $X_{CO2}=1$. Aquest és el cas, en la determinació de punts de solubilitat en la zona propera a $X_{CO2}=0$ de la corba ja mostrada en la Figura A17. Si el procediment d'operació es basa en la preparació d'una dissolució inicial sobresaturada del solut en el dissolvent orgànic i es realitza, a continuació, l'addició de CO_2 a la pressió i temperatures de mesura sobre aquesta dissolució inicial, les línies de treball que es seguiran són les mostrades en la Figura A18. S'observa que els punts de tall d'aquestes línies amb la corba de solubilitat permeten trobar valors de solubilitat en la zona no coberta per les mesures realitzades pel procediment descrit en el cas B. En aquest cas també es requereix l'ús del portamostres per a introduir més sòlid del que és capaç de dissoldre el dissolvent orgànic A ($C^A > C_S^A$). Tot i el diferent mode de realització d'aquest nou procediment, aquest es regeix segons el mateix principi que els anteriors casos i per tant, que el del "Mètode de dissolució de l'últim cristall visible" i el "vanishing-point method", és a dir, s'observa l'evolució des d'una mescla en equilibri "sòlid/dissolució saturada" fins a la completa dissolució del sòlid causada pel canvi en la composició de la mescla dissolvent.

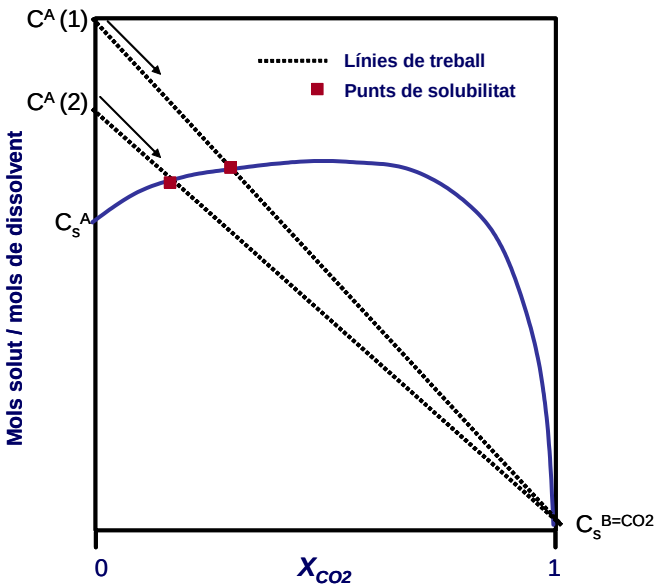

Figura A18. Punts de solubilitat d'una corba amb efecte sinèrgic, mesurables amb les línies de treball amb sentit $X_{CO2}=0 \rightarrow X_{CO2}=1$ (CAS C)

Procediments detallats de mesura

A continuació es procedeix a descriure de manera més detallada la seqüència d'operacions que defineixen els procediments de mesura descrits en els tres casos exposats. L'ordre de realització de les operacions dependrà del sentit de línia de treball que s'esculli (X_{CO2}=0→X_{CO2}=1 o X_{CO2}=1→X_{CO2}=0):

Operació 1) Es fixa la posició del pistó en la seva posició més baixa, és a dir, introduït 20 cm en l'interior de la cel·la de mesura. Si ens trobem en els casos B i C, s'introdueix per l'orifici inferior una massa coneguda de sòlid continguda en el portamostres i pesada anteriorment en un balança de precisió ±0.0001. Es fa el buit a dins la cel·la mitjançant la connexió de la vàlvula 1 (veure Figura A6) a una bomba de buit. Es selecciona la temperatura de mesura, T_W, mitjançant la cambra de fred/calor.

Operació 2) Si es treballa en el sentit X_{CO2}=1→X_{CO2}=0, es bombeja dins la cel·la una quantitat coneguda de CO_2 mitjançant la bomba ISCO. Per a realitzar aquesta operació de bombeig, s'utilitza el mode de pressió constant de la bomba. Això fa possible que per diferència de contingut en volum de la bomba abans i després del bombeig, es pugui calcular, per mitjà dels valors de densitat tabulats, la massa de CO_2 introduïda.[3,4] A continuació, es bombeja dins la cel·la mitjançant la bomba JASCO, la quantitat de dissolvent orgànic o dissolució del solut en el dissolvent orgànic necessària per a arribar a la pressió de mesura, P_W. El recipient que conté el dissolvent o la dissolució de bombeig està suportat a sobre una balança de precisió (±0.01), la qual cosa permet determinar la massa de líquid introduït. En aquest punt s'engega la bomba de recirculació MICROPUMP per tal d'aconseguir, el més ràpidament possible, una mescla "sòlid/dissolució saturada" en equilibri.

Si es treballa en el sentit X_{CO2}=0→X_{CO2}=1, es realitzen les operacions anteriors de forma inversa. És a dir, es bombeja primer una quantitat determinada de dissolució de solut en el dissolvent orgànic. A continuació, es bombeja CO_2 fins a assolir P_W. S'inicia la recirculació de la mescla fins a assolir l'equilibri de la mescla "sòlid/dissolució en saturada".

Operació 3) En aquest punt ens trobem al damunt de la línia de treball que ve definida per les quantitats inicials de sòlid i dissolvents introduïts dins la cel·la, i per la concentració de la dissolució que s'addicionarà. A continuació es realitza

l'evolució al llarg de la línia de treball en direcció a creuar la corba de solubilitat en el punt de solubilitat. En el sentit $X_{CO2}=1 \rightarrow X_{CO2}=0$, aquesta evolució es realitza mitjançant la lenta i controlada addició de dissolució de solut/dissolvent convencional o dissolvent convencional pur sobre la mescla. Durant aquest addició, la pressió d'aire que regula el moviment del pistó es fixa de manera que permeti mantenir la pressió interna de la cel·la, P_W, mitjançant el moviment ascendent del pistó. El cabal de bombeig és reduït en funció de la velocitat amb què s'observa la desaparició de sòlid en suspensió. Quan s'observen els darrers cristalls s'atura el bombeig i es manté el sistema en recirculació durant un mínim de 30 minuts per comprovar si aquests romanen presents. En cas afirmatiu es realitzen petites i discretes addicions fins a observar la definitiva desaparició del sòlid.

Quan es treballa en sentit $X_{CO2}=0 \rightarrow X_{CO2}=1$, l'evolució de la línia de treball es realitza mitjançant el bombeig de CO_2 sobre la mescla "sòlid/dissolució saturada" en equilibri inicial, la qual es manté a P_W mitjançant el moviment ascendent del pistó. El procediment d'addició és similar a l'utilitzat en el sentit $X_{CO2}=1 \rightarrow X_{CO2}=0$, ja que aquesta és progressivament alentida a mesura que s'observa desaparició de sòlid en suspensió. En observar la presència d'unes poques partícules en suspensió s'atura l'addició i es deixa estabilitzar la mescla (30 minuts). En el cas de restar partícules en suspensió, es prossegueix l'addició fins a observar la desaparició d'aquestes.

Operació 4) Un cop assolida una sola fase homogènia es realitza el balanç màssic de tots els elements introduïts a dins de la cel·la. Aquest balanç permet calcular la fracció molar de CO_2 de la mescla, X_{CO2}, i el valor de solubilitat obtingut a partir de l'Equació A1.

La utilització d'aquest procediment de mesura en el nostre equip analitzador de fases comporta un error sistemàtic inferior al 1% en la determinació de solubilitats i inferior al 2% en la determinació de valors de fracció molar de CO_2.

Mètode dinàmic de determinació de solubilitats en CO_2

La configuració experimental utilitzada per aquest mètode es mostra en la Figura A19 i ha estat adaptada a la planta pilot d'alta pressió i alta temperatura anteriorment descrita. Aquesta configuració consta de dos reactors R1 i R2 d'alta pressió amb volums interns de 2 i 1 L, respectivament. El reactor R1 és alimentat amb CO_2 per la seva part inferior mitjançant la bomba P1. El flux de CO_2 surt de R1 després de passar per un cilindre extractor CE de 22 cm de llarg i 0.9 cm de diàmetre connectat al capçal del reactor, i que conté la mostra a extraure. Aquest cilindre compta a un únic orifici d'entrada per la part inferior consistent en una malla reixada. Al final del cilindre CE, i abans de la connexió amb el capçal de R1, hi ha una vàlvula de seguretat que en cas de obturació de CE s'obre i deixa pas lliure al flux de CO_2. S'ha adaptat a la sortida de R1 un cilindre mostrejador CM situat entre dues vàlvules i amb un by-pass amb una tercera vàlvula. Tant R1 com el tub que surt d'aquest i connecta amb CM poden ser calefactats elèctricament fins a la temperatura desitjada. A la sortida del sistema de mostreig es troba el reactor R2 que connecta amb el regulador de pressió VR2 i caudalímetre C1 que permeten controlar la pressió i cabal de CO_2 de tot el sistema. Els components d'aquesta configuració estan connectats mitjançant tub d'acer inoxidable de diàmetre extern d'1/4 de polzada. Manòmetres, controladors de temperatura i vàlvules d'alta pressió completen la planta. La pressió i la temperatura interna de R1 i R2 i el cabal de CO_2 mesurat per C1 són visualitzats i enregistrats cada 5 segons en un ordinador acoblat als dispositius de control i mesura d'aquests paràmetres.

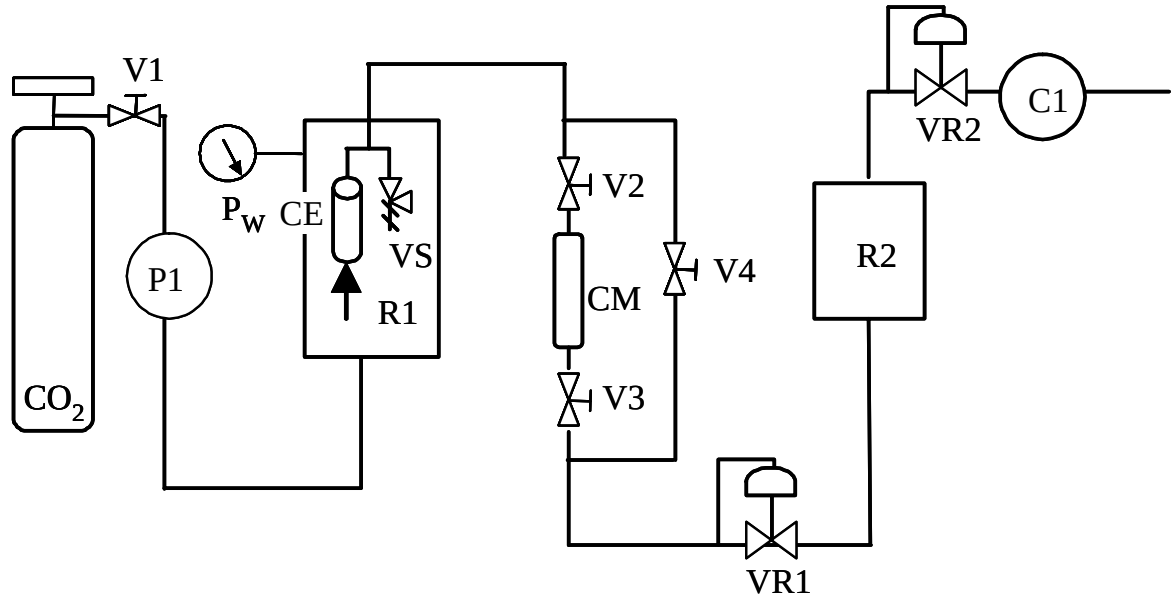

Figura A19. Configuració experimental per a mesurar solubilitats en CO_2. R: reactor, V: vàlvula, P: bomba, CE: cilindre extractor, VS: vàlvula de seguretat, CM: cilindre mostrejador, VR: regulador de pressió, C: caudalímetre.

El procediment d'operació per a portar a terme les mesures de solubilitat implica la preparació prèvia del cilindre extractor CE. Aquest es carrega amb una mescla del compost sòlid, del qual se'n desitja mesurar la solubilitat, i de boles de vidre que pretenen afavorir el contacte entre el flux de CO_2 i la mostra a extraure. També es dipositen a la part inferior i superior de CE més boles de vidre que actuen com a difusors. Un cop instal·lat el cilindre en el capçal de R1 es tanca el sistema i es pressuritza aquest fins a la pressió de mesura, P_W. Quan s'assoleix P_W s'obren les vàlvules V2 i V3 de manera que el corrent de CO_2 saturat amb el compost contingut en CE passi a través del cilindre mostrejador CM. Aquest cilindre ha estat prèviament pressuritzat amb nitrogen a la pressió P_W per evitar la precipitació d'aquest compost per despressurització. El flux de CO_2 es manté durant 15 minuts amb un cabal de 1 Kg/h controlat pel regulador de pressió VR. Passat aquest temps s'aïlla el cilindre i es manté la circulació de CO_2 a través del by-pass. En aquest punt es pot acoblar un nou cilindre mostrejador en substitució de l'anterior per a realitzar novament el mateix procediment i prendre una nova mostra de dissolució de CO_2 saturada en el compost en qüestió.

Per tal determinar el contingut del cilindre CM, aquest ha d'haver estat prèviament tarat i el seu volum intern determinat. La dissolució continguda en CM és despressuritzada lentament sobre una dissolució de dissolvent orgànic en el qual el compost dissolt en CO_2 hi sigui significativament soluble. Un cop despressuritzat, el cilindre es neteja acuradament amb el mateix dissolvent. La dissolució orgànica resultant és rotavaporada fins a sequedat, la qual cosa permet recuperar el sòlid que estava contingut en CM. La massa d'aquest sòlid és determinada amb una balança de precisió (±0.0001). La massa de CO_2 que estava continguda en el mateix cilindre es determina mitjançant el volum intern del cilindre i la densitat del CO_2 a les condicions de mesura.[3] El valor de solubilitat és expressat en mols de solut/mols de dissolvent. Tot el procediment es repeteix fins a tres vegades. L'error relatiu associat a aquest procediment en les mesures realitzades va ser inferior al 1%.

G. Dades de solubilitats descrites en la memòria

En la Taula A3 s'enumeren les dades de solubilitat, C^S, que s'han emprant en el present treball i que han estat utilitzades per a descriure les corbes de solubilitat de soluts en dissolvents expandits amb CO_2. Aquestes corbes de solubilitat han estat obtingudes per ajust de les dades de solubilitat a l'Equació A2.[1b]

$$C^S = A\cdot(1-X_{CO2})^{B+C\cdot X_{CO2}} + D\cdot X_{CO2} \qquad (A2)$$

Taula A3. Mesures de solubilitat descrites en el present treball

Mètode utilitzat	X_{CO2}	C^S **(mol/mol)**
Sistema "colorant **1**/acetona/CO_2" T_W=293 K, P_W=10 MPa		
"Vanishing point"[a]	0	1.63E-03
Estàtic gravimètric[b]	0.30	1.31E-03
Estàtic gravimètric[b]	0.40	1.01E-03
"Vanishing point"[a]	0.604	5.70E-04
"Vanishing point"[a]	0.65	4.56E-04
Estàtic gravimètric[b]	0.73	2.31E-04
"Vanishing point"[a]	0.733	2.63E-04
Estàtic gravimètric[b]	0.81	1.79E-04
Sistema "aspirina/acetona/CO_2" T_W=296 K, P_W=7 MPa		
"Vanishing point"[c]	0	8.70E-02
"Vanishing point"[c]	0.4311	4.58E-02
"Vanishing point"[c]	0.6028	1.75E-02
"Vanishing point"[c]	0.7472	7.08E-03
"Vanishing point"[c]	0.87	1.74E-03
Sistema "paracetamol/etanol/CO_2" T_W=315 K, P_W=10 MPa		
"Vanishing point"[c]	0	8.30E-02
Estàtic gravimètric[b]	0.22	5.90E-02
Estàtic gravimètric[b]	0.23	5.70E-02
Estàtic gravimètric[b]	0.3	4.90E-02
Estàtic gravimètric[b]	0.38	3.79E-02
"Vanishing point"[c]	0.47	2.42E-02
"Vanishing point"[c]	0.53	1.60E-02
"Vanishing point"[c]	0.64	7.68E-03
"Vanishing point"[c]	0.75	2.96E-03
"Vanishing point"[c]	0.76	2.90E-03
"Vanishing point"[c]	0.79	1.35E-03
Sistema "paracetamol/acetona/CO_2" T_W=315 K, P_W=10 MPa		
"Vanishing point"[c]	0	5.85E-02
"Vanishing point"[c]	0.18	3.12E-02
"Vanishing point"[c]	0.26	2.13E-02
"Vanishing point"[c]	0.34	1.49E-02
"Vanishing point"[c]	0.44	6.40E-03
"Vanishing point"[c]	0.58	2.63E-03
"Vanishing point"[c]	0.69	1.09E-03
Sistema "colesterol/acetona/CO_2" T_W=308 K, P_W=10 MPa		
Mètode en dissolvents orgànics[b]	0	6,42E-03
"Vanishing point"[b]	0.353	4.71E-03
"Vanishing point"[b]	0.401	4.46E-03
"Vanishing point"[b]	0.423	3.92E-03
Estàtic gravimètric[b]	0.52	2.66E-03
Estàtic gravimètric[b]	0.64	1.74E-03
Estàtic gravimètric[b]	0.65	1.75E-03
Estàtic gravimètric[b]	0.70	1.18E-03
Estàtic gravimètric[b]	0.72	1.16E-03
Estàtic gravimètric[b]	0.79	6.05E-04
Mètode dinàmic en CO_2[b]	1	5,00E-05

Continuació de la Taula A3

Mètode utilitzat	X_{CO2}	C^S (mol/mol)
Sistema "metenamina/etanol/CO_2" T_W=313 K, P_W=10 MPa		
Mètode en dissolvents orgànics[b]	0	1.54E-02
"Vanishing point"[b]	0.2	1.87E-02
"Vanishing point"[b]	0.44	2.20E-02
"Vanishing point"[b]	0.45	2.23E-02
"Vanishing point"[b]	0.65	2.06E-02
"Vanishing point"[b]	0.731	2.04E-02
"Vanishing point"[b]	0.737	2.06E-02
"Vanishing point"[b]	0.79	1.80E-02
"Vanishing point"[b]	0.87	1.67E-02
"Vanishing point"[b]	0.92	1.30E-02
"Vanishing point"[b]	0.946	1.26E-02
Mètode dinàmic en CO_2[b]	1	5.30E-04

[a] Mesures de la referència 5. [b] Mesures realitzades en el present treball
[c] Mesures de la referència 1a

H. Mesures d'espectroscopia d'IR en dissolució

L'espectròmetre de FTIR utilitzat en les mesures dels espectres dels compostos paracetamol i fenacetin en dissolució de diferents dissolvents orgànics (veure taula 10, Apartat 3.2.3.2) va ser un PERKIN ELMER model Spectrum One. La resolució va ser fixada a 2 cm^{-1}. Per a fer aquestes mesures es va utilitzar una cel·la per a líquids PERKIN ELMER equipada amb finestres de ZnSe i espaiadors de tefló amb gruixos des de 25 fins a 250 μm.

L'espectròmetre de FTIR utilitzat en les mesures de dissolucions expandides amb CO_2 i acoblat a la configuració experimental mostrada en la Figura 51 (Apartat 3.2.2.1), fou un espectròmetre Bio-Rad (tipus FTS-60A). En les mesures realitzades amb aquest aparell la resolució espectral fou de 2 cm^{-1} i el nombre d'espectres acumulats per a cada mesura fou de 50. En la Taula A4 es mostren els valors dels màxims de banda utilitzats per a calcular els desplaçaments de banda $\Delta\nu_{CO}$ i $\Delta\nu_{NH}$ representats en la Figura 57 (Apartat 3.2.2.2).

Taula A4. Valors de nombre d'ona (en cm^{-1}) dels màxims de banda dels modes ν_{CO} i ν_{NH} del paracetamol en acetona i etanol expandits amb CO_2, en relació a X_{CO2}

X_{CO2}	0	0.15	0.20	0.25	0.3	0.35	0.4	0.45	0.5	0.55	0.6	0.75
Sistema "Paracetamol/acetona/CO_2" T_W=315 K, P_W=10 MPa												
$\tilde{\nu}_{CO}$	1687.8	1688.7	1688.7	1689	1689.7	1690.6	1690.6	1691.7	1691.9	1692.6	1694.1	-
$\tilde{\nu}_{NH}$	3361	3362	3363	3364	3366	3368	3370	3372	3373	3375	-	-
Sistema "Paracetamol/etanol/CO_2" T_W=315 K, P_W=10 MPa												
$\tilde{\nu}_{CO}$	1656.7	1656.8	-	-	1657.0	-	-	1657.8	-	-	1658.6	1659.8
$\tilde{\nu}_{NH}$	3335	3338	-	-	3342	-	-	3348	-	-	3353	3357

REFERÈNCIES

1. a) F. E. Wubbolts, Ph. D. Thesis, University of Delft (Netherlands), **2000**; b) F. E. Wubbolts, O. S. L. Bruinsma, G. M. van Rosmalen, *J. Supercrit. Fluids* **2004**, *32*, 79.
2. P. H. Karpinski, J. Nývlt, *Crystal Res. and Technol.* **1983**, *18*, 959.
3. Carbon Dioxide. International Thermodynamic Tables of the Fluid State – 3. Compiled by S. Angus, B. Armstrong, K. M. Reuck. IUPAC Project Centre, Imperial College, London.
4. L'error associat a la mesura de la massa de CO_2 és conseqüència de la precisió del caudalímetre màssic(0.5%) i de l'error correspondent a l'equació d'estat utilitzada per a construir les taules de densitats de CO_2 (0.2%).
5. N. Ventosa i col·laboradors. Pendent de publicació.

Annex 2 – Articles relacionats amb el Capítol 1

ARTICLE A:

Títol: Depressurization of an Expanded Liquid Organic Solution (DELOS): A New Procedure for Obtaining Submicron- or Micron-Sized Crystalline Particles

Autors: Nora Ventosa, Santiago Sala, Jaume Veciana, Joaquim Torres, Joan Llibre

Publicació: Crystal Growth and Design **2001**, *1*, 299-303

(Presentat a la comissió de doctorat)

CRYSTAL GROWTH & DESIGN
2001
VOL. 1, NO. 4
299−303

Depressurization of an Expanded Liquid Organic Solution (DELOS): A New Procedure for Obtaining Submicron- or Micron-Sized Crystalline Particles

Nora Ventosa, Santiago Sala, and Jaume Veciana*

Institut de Ciència de Materials de Barcelona (CSIC), Campus Universitari de Bellaterra, 08193-Cerdanyola, Spain

Joaquim Torres and Joan Llibre

Carburos Metálicos S.A., Psg. Zona Franca 14-20, 08038-Barcelona, Spain

Received March 8, 2001; Revised Manuscript Received May 25, 2001

ABSTRACT: The depressurization of an expanded liquid organic solution (DELOS) crystallization technique is a new eco-efficient, one-step process for the straightforward production of submicron- or micron-sized crystalline particles. This novel method is based upon the large, fast, and very homogeneous temperature decreases experienced by an organic solution, previously expanded with a gaslike compressed fluid (e.g., CO_2), when it is depressurized. Through a DELOS process, it is possible to achieve the size reduction of different kinds of organic compounds that are difficult to comminute by conventional techniques.

Industry rather often faces the need for the manufacturing of micron-sized solid particles in the production of different compounds, such as dyes, polymers, waxes, explosives, salts, and pharmaceuticals, including proteins. The conventional techniques for particle-size reduction currently practiced involve mechanical comminution (crushing, grinding, and milling) and suffer from many disadvantages. The limitations of mechanical comminution are the shock sensitivity associated with the solid, the thermal degradation due to heat generation during mechanical comminution, and/or the lack of brittleness, as occurs with most polymers and waxes.

Within the last two decades, new alternative eco-efficient processes for the production of micron-sized crystalline particles have emerged using compressed fluids (CF) either under supercritical (SC) conditions or in the liquid state. Most of these technologies use CO_2 as a CF because it is nontoxic, nonflammable, cheap, and easily recyclable. These methods can be classified into three groups according to the solvating behavior of the compressed fluid.[1]

(i) Compressed Fluid as a Solvent. The crystallization technique called rapid expansion of a supercritical solution (RESS) involves the dissolution of the solute of interest in a pure CF, generally under SC conditions, followed by a rapid expansion of the resulting solution to atmospheric pressure through a nozzle, which produces a rapid decrease of the solvation power, resulting in the precipitation of monodisperse particles.[2]

(ii) Compressed Fluid as an Anti-Solvent. The solute of interest is dissolved in a conventional organic solvent to form a solution. The solute is then precipitated from this solution in two alternative ways: (a) In the first method, called gas anti-solvent (GAS) crystallization, a batch of the liquid solution is expanded severalfold by mixing it with the CF. This expansion produces a solvating power decrease of the mixture that becomes supersaturated, and then the solute precipitates as microparticles.[3] (b) The second method, named precipitation with compressed anti-solvents (PCA), involves the spraying of the organic solution through a nozzle into the CF as fine droplets. In this process, the CF diffuses into the sprayed droplets causing a rapid expansion of the solvent, decreasing its solvating capacity and forcing the solute to precipitate or crystallize as microparticles.[4] In the case of a continuous flow of the solution and the anti-solvent, the process is also termed an aerosol solvent extraction system (ASES)[5] if it uses a countercurrent flow, while the term solution-enhanced dispersion by supercritical fluids (SEDS)[6] is used in the case of co-current flow.

(iii) Compressed Fluid as a Solute. The technique called particles from gas saturated solutions (PGSS)[7] involves the solubilization, at a given pressure and temperature, of a CF in the pure liquid substance (melted) to be crystallized to form a gas saturated solution. By expansion of such solution, the CF is evaporated and the solution is cooled. When the melting temperature is reached, the substance is subcooled and solid particles are formed.

In this paper, we present a new method, called depressurization of an expanded liquid organic solution (DELOS),[8] where a CF is used for the straightforward production of micron-sized and submicron-sized crystalline particles from an organic solution. This process differs from the above-mentioned techniques in that the CF acts as *cosolvent* being completely miscible, at a given pressure and temperature, with the organic solution of the solute to be crystallized. The role of the CF is to produce a homogeneous subcooling of the solution with solid particle precipitation. The DELOS process comprises the following three steps:

(i) Dissolution of the solute to be crystallized in a conventional solvent (e.g., organic solvent), at atmospheric pressure and at a working temperature, T_W, to

* To whom correspondence should be addressed. E-mail: vecianaj@icmab.es.; tel: 34-93-580 18 53; fax: 34-93-580 57 29.

10.1021/cg0155090 CCC: $20.00
Published on Web 06/14/2001

Chart 1. Colorant Solvent Blue 35

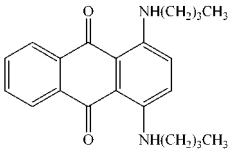

1

form a solution with a solute concentration, C, which is below the saturation limit, C^S; that is, with an initial supersaturation ratio, β_I, less than one, where $\beta_I = C/C^S$.

(ii) Addition of a CF (e.g., CO_2) over the organic solution to obtain a volumetric expanded liquid solution, at the working temperature (T_W) and at a high working pressure (P_W) containing a given molar fraction of the CF (X_W), which we call the working composition of CF. The solute concentration in this step must remain below the saturation limit in the expanded mixture of the conventional solvent and the CF.

(iii) Rapid reduction of the pressure of the expanded solution, from the working (P_W) to the atmospheric pressure, through a nonreturn valve. During this depressurization process, the evaporation of the CF from the volumetric expanded solution takes place producing a large, fast, and extremely homogeneous decrease of the solution temperature down to the final temperature, T_F. As a consequence, a pronounced and homogeneous increase of the supersaturation ratio over all the solution takes place and the phenomenon of catastrophic nucleation occurs causing the precipitation of submicron- or micron-sized crystalline particles with a narrow particle size distribution.[3]

Experimental Section

The parameters influencing the yield and the characteristics of solid particles obtained through a DELOS process were studied in detail for the crystallization of the colorant solvent blue 35 (**1**),[9] using acetone as the conventional organic solvent and CO_2 as the CF (Chart 1). The experimental equipment employed in this study is schematized in Figure 1. The operational procedure and experimental conditions used in this study are the following: A known volume of a solution of colorant **1** in acetone, with an initial supersaturation ratio of $\beta_I = 0.8$, was loaded in the high-pressure vessel R1. A circulating water jacket was used to maintain, during the process, the working temperature at 293 K inside this vessel. The initial solution was then pressurized up to the working pressure P_W by the addition of a given amount of CO_2 through the top of the vessel. Any precipitate produced through an undesired GAS process inside R1, during the CO_2 addition, was collected in the filter plate, F1, placed inside the vessel R1. After leaving the system at the same conditions for 30−60 min, to achieve a complete homogenization and its thermal equilibration, the solution was depressurized over the nonreturn valve V4 from P_W to atmospheric pressure. This abrupt pressure reduction produces a large solution temperature decrease whose magnitude depends on the CO_2 content of the solution before depressurization, i.e., on the working composition X_W. During the depressurization step, solid particles precipitated and were collected on filter F2 located inside the vessel R2. During this step, the pressure of the solution inside R1 was maintained constant at P_W by a continuous addition of pressurized nitrogen gas from the top of the high-pressure vessel. After the filtration, the cleaning of the precipitate was carried out with pure liquid CO_2 at 6 MPa and 293 K. The CO_2 evolved in the last step of the process was easily separated from the mother liquor after the valve V5, recovered, and, if required, recirculated after compression. Similarly, the mother liquor was disposed in the recycling container RC2 and recycled, if desired.

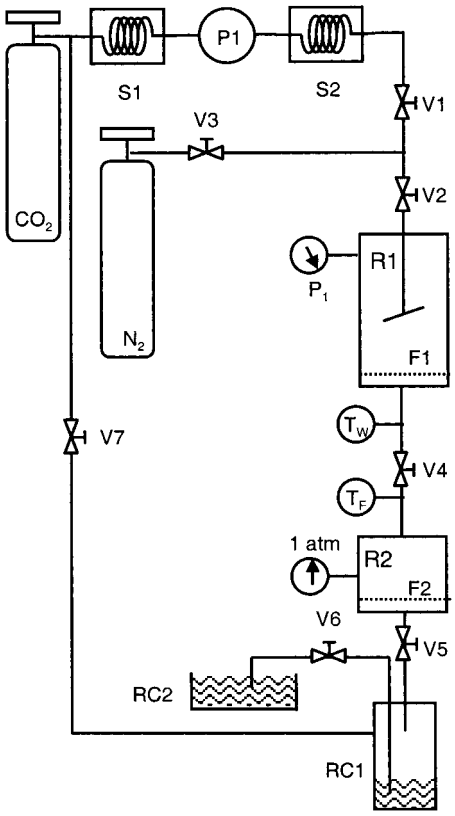

Figure 1. Scheme of the equipment used for DELOS experiments. P: pump; S: heat exchanger; V: valve; F: filter; R: high-pressure vessel; RC: recycling collector.

Results and Discussion

In Table 1 are summarized the results obtained in eight DELOS crystallization experiments of colorant **1**. In all cases, the resulting particles have a median particle diameter smaller than 5 μm, which is 2 orders of magnitude smaller than the median particle diameter of the particles produced through the conventional cooling crystallization technique from methanol solutions. Therefore, through a DELOS process, micron-sized particles are produced straightforward, and the production steps of comminution and homogenization, required after a classical cooling crystallization method, can be suppressed. As ascertained by powder X-ray diffraction, the particles produced in all the experiments have a high degree of crystallinity. Indeed, diffractograms of particles were identical to those of crystals obtained by classical crystallization techniques in acetone.[10]

Experiments DELOS 1−5 were performed over initial solutions of colorant **1** in acetone with the same initial supersaturation ratios and the same working pressures and temperatures. The unique different operational parameter was the working CO_2 molar fraction of the solvent mixture before the depressurization step. As shown in Table 1, the yields of these experiments increase slightly with the increasing X_W. This result can be explained by the larger temperature reduction achieved during the depressurization step. Thus, the higher the CO_2 content in the solution of colorant **1**, the

Table 1. DELOS Experiments Performed with Colorant 1 at T_W = 293 K Using Acetone and CO_2 with an Initial Organic Solution Concentration of β_I = 0.8

					diameter of particles (μm)[b]				
exp	P_W (MPa)	ρ (g cm^{-3})	X_W	ΔT (°C)[a]	X10%	X50%[c]	X90%	GAS yield (%)	DELOS yield[d] (%)
DELOS-1	10	0.90	0.40	−32	0.5	3.9	13.0	0	70
DELOS-2	10	0.96	0.54	−46	0.7	3.1	12.3	0	75
DELOS-3	10	0.95	0.62	−57	0.3	1.0	11.5	0	80
DELOS-4	10	0.96	0.70	−65	0.2	0.5	6.6	5	80
DELOS-5	10	0.97	0.80	−75	0.2	0.5	1.8	15	80
DELOS-6	5	0.94	0.55	−45	0.6	3.9	14.9	0	80
DELOS-7	10	0.96	0.55	−46	0.7	3.2	12.4	0	80
DELOS-8	15	0.97	0.55	−45	0.7	3.5	14.1	0	80

[a] Temperature decrease, $\Delta T = T_F - T_W$, where T_W is the solution temperature before the nonreturn valve V4 and T_F is the solution temperature after this valve. [b] Volumetric particle size distributions, measured with the light scattering technique (Mastersizer/E, Malvern, UK), are given as 10, 50, and 90% quantiles. [c] These values correspond to the medians of the particle distributions. The average diameters of particles were confirmed by SEM images (vide infra). [d] The DELOS yields reported correspond to the ratio between the amount of colorant **1** collected in filter F2 and the quantity of colorant **1** in solution after filter F1.

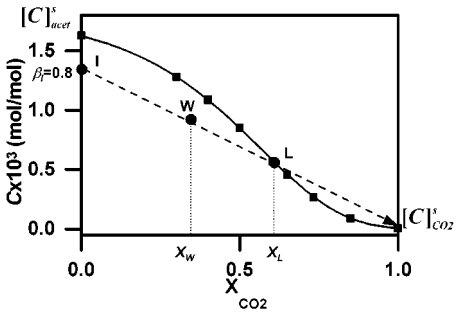

Figure 2. Solubility curve (continuous line) fitted through the experimental solubility data[12] of colorant **1** in the solvent mixture acetone/CO_2, at P_W = 10 MPa and T_W = 293 K. Working line (discontinuous line) depicts the evolution of the concentration of colorant **1** under the same experimental conditions during a DELOS process performed with an initial solution concentration of β_I = 0.8.[13]

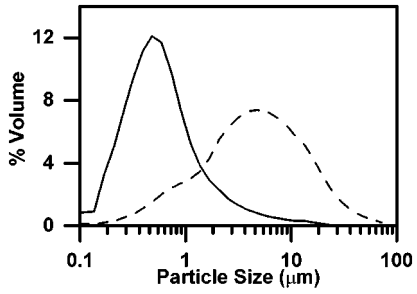

Figure 3. Volume size distributions of the particles obtained in the experiments DELOS-1 (dashed line) and DELOS-5 (continuous line).

higher the heat required for its vaporization when the depressurization step is done, and thereby a larger solution temperature decrease is observed. Consequently, augmenting this temperature reduction increases the supersaturation ratio attained in the organic mixture and improves the precipitation yield. On the other hand, the higher the X_W values are, the higher is the supersaturation ratio attained at the working point (β_W), which also contributes to increase the yield of a DELOS process.[11] There is an upper limit for the molar fraction to be used in a DELOS process since molar fractions larger than this limit produce undesirable GAS precipitation at the vessel R1 (Table 1) during the pressurization step. The limit value, X_L, which can be used for performing a DELOS experiment avoiding a premature GAS precipitation during the addition of CO_2 in step 2, is determined by the characteristics of the so-called working line (Figure 2) and of the solubility curve of colorant **1** in the solvent mixture of acetone/CO_2 at the working pressure P_W and temperature T_W (Figure 2). During the pressurization step, the concentration of the solute in the acetone/CO_2 mixture is reduced, according to the working line depicted in Figure 2, from the initial solution concentration (point I) to the working solution concentration (point W) by the addition of the CO_2. At the same time, the solubility of colorant **1** in the mixture of acetone and CO_2 during this step changes according to the solubility curve, as shown in Figure 2. Therefore, the supersaturation ratio at the working point, β_W, is not the same as that at the initial point, β_I. When performing the pressurization step, it is important that the molar fraction of CO_2 at point W, X_W, is not higher than X_L, which is the limiting CO_2 molar fraction corresponding to the crossing between the solubility curve and the working line (point L in Figure 2). Beyond this point, the mixture becomes supersaturated, $\beta_W > 1$, and undesired GAS precipitation can take place. As shown in Table 1, the X_W of experiments DELOS-4 and DELOS-5 were higher than 0.65, which corresponds to X_L for a initial solution of **1** in acetone with a β_I = 0.8 at P_W = 10 MPa and T_W = 293 K and, as expected, in both experiments part of the solute crystallizes before the depressurization step through a GAS-like process.

The particle size and size distribution resulting from experiments DELOS 1−5 show a clear dependence on the CO_2 content of the mixture before the depressurization step. Thus, when X_W is higher the particles produced are smaller and the particle size distribution is narrower. Therefore, in a DELOS process, it is possible to control the particle size characteristics through the CO_2 content of the pressurized system. Another important result is the wide range of sizes of the particles obtained with this technique. Figure 3 shows the volume size distributions of particles achieved in the experiments performed with the lowest (DELOS-1) and the highest molar fractions (DELOS-5) of CO_2 showing that it is possible to obtain crystalline particles ranging from nanoscopic to microscopic dimensions. Such results were confirmed later by the SEM images of particles (Figure 4) and the corresponding powder X-ray diffractions (not shown).

To study the effect of the extent of the pressure reduction in the depressurization step (step 3) in the

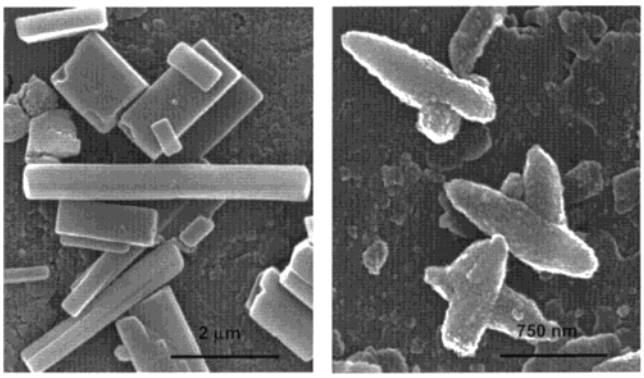

Figure 4. Scanning electron microscopy images of the crystalline particles of **1** produced in the experiments DELOS-1 (left) and DELOS-5 (right).

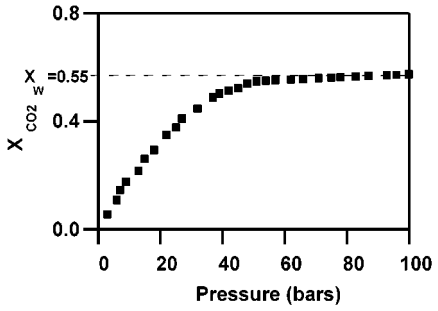

Figure 5. Profile of the composition of CO_2 in function of pressure in the vessel R1 measured during the experiment DELOS-7 (T_W = 293 K).

DELOS process, experiments DELOS 6−8 were performed. The characteristics of the resulting particles (Table 1) show that a variation of the extent of the pressure reduction, at a given X_W, does not affect the temperature decrease of the solution occurring during the depressurization step. In addition, as shown in Table 1, a change on the working pressure P_W when all other process parameters are kept constant, neither affects the DELOS process yield nor the dimensions and size distribution of the particles formed.[14] This result is very important from the practical point of view since it permits the reduction of the working pressure of a DELOS process to a level well below those used in other high-pressure crystallization techniques without changing the yield and the characteristics of crystalline particles. Indeed, in the vapor−liquid equilibria of an acetone−CO_2 mixture below the critical temperature of the CO_2,[15] the pressure fixes the composition of the liquid phase until the saturation pressure, $P^{sat}_{CO_2}$, is reached.[16] In addition, the volume of the acetone−CO_2 liquid mixture is determined by the volumetric expansion of acetone by the CO_2.[17] Therefore, in a DELOS experiment performed over an initial acetone solution, the molar fraction of CO_2, X_{CO_2}, of the final liquid expanded solution, which fills the total volume of the high-pressure vessel, depends on the vapor−liquid equilibria and the volumetric expansion behavior of the binary system acetone/CO_2. As is shown in Figure 5, as the pressure augments an increase of X_{CO_2} occurs until reaching a certain point, where the expanded solution occupies the total volume of the high-pressure vessel. From this point, a further pressure increase is completely useless because, as shown in Table 1, it does not practically affect the solution density and does not cause any further increase of the X_{CO_2}, which becomes the working molar fraction (X_W) of the CF, the real operational parameter for the control of the temperature decrease in the DELOS process.

Finally, it was observed that a decrease of the initial supersaturation ratio β_I from 0.8 to 0.6, when all other operational parameters were kept constant, produces a decrease from 80 to 55% on the yield of the DELOS process, as initially expected from consideration of the relative concentration of the solute at the working point.

In conclusion, the results summarized in Table 1 reveal that the yields and the characteristics of crystalline particles resulting from the DELOS process depend only on the initial supersaturation ratio (β_I) and on the composition of the solution mixture before the depressurization step (X_W), and they do not show any significant dependence on the working pressure P_W.

In comparison with other high-pressure crystallization techniques, like RESS and PCA, the DELOS process requires moderate working pressures, which is a very important parameter in the economical evaluation of the process for industrial applications. In addition, the equipment needed is relatively simple and is easily scalable following the good manufacturing practices (GMP) specifications. In the DELOS process, the supersaturation profile is ideally homogeneous over all solutions during all the experiments because the compressed fluid is dissolved in the solution when the precipitation, caused by the CF evaporation in the depressurization step, takes place. Therefore, in this process, in contrast with a GAS precipitation, the size and size distribution of the particles do not depend on the efficiency of the mixing between the solution and the CF, and low stirring requirements are needed.

Summarizing, the DELOS process is an efficient high-pressure crystallization method for the straightforward production of submicron- or micron-sized particles of organic compounds with narrow size distribution, provided that a "solute/organic solvent/CF" system that exists in liquid solution phase is found. The DELOS crystallization technique has also been used successfully for obtaining submicron- and micron-sized crystalline particles of other anthraquinonic dyes as well as of some drugs of interest (acetylsalicylic acid, acetaminophen, etc.). Application of this process for the precipitation of polymers is under way in this laboratory.

Acknowledgment. This work was supported by grants from DGI, Spain (project MAT2000-1388-C03-01), and DGR, Catalunya (project 2000 SGR 00114). We thank J. Fraile for and R. Solanes (ICMAB) for particle size measurements and the operation of high-pressure facilities at the ICMAB as well as Dr. D. Amabilino (ICMAB) for correcting the manuscript.

References

(1) Kikic, I.; Lora, M.; Bertucco, A. *Ind. Eng. Chem. Res.* **1997**, *36*, 5507.

(2) (a) Matson, D. W.; Fulton, J. L.; Petersen, R. C.; Smith, R. D. *Ind. Eng. Chem. Res.* **1987**, *26*, 2298. (b) Tom, J. W.; Debenedetti, P. G. *J. Aerosol Sci.* **1991**, *22*, 555. (c) Chang, C. J.; Randolph, A. D. *AIChE J.* **1989**, *35*, 1876. (d) Mohamed, R. S.; Debenedetti, P. G.; Prud'homme, R. K. *AIChE J.* **1992**, *38*, 742.

(3) (a) Gallagher, P. M.; Coffey, M. P.; Krukonis, V. J.; Klasutis, N. *ACS Symp. Ser.* **1989**, *406*, 334. (b) Yeo, S.-D.; Lim, G.-B.; Debenedetti, P. G.; Bernstein, H. *Biotechnol. Bioeng.* **1992**, *41*, 341. (c) Randolph, T. W.; Randolph, A. D.; Mebes, M.; Yeung, S.; *Biotechnol. Prog.* **1993**, *9*, 429. (d) Berends, E. M.; Bruinsma, O. S. L.; de Graauw, J.; Van Rosmalen, G. M. *AIChE J.* **1996**, *42*, 431. (e) Reverchon, E.; Porta, G. D.; Trolio, A. D. *Proc. 4th Conf. On Supercritical Fluids and Their Applications, Capri, Italy*, 1997, pp 335, 385.

(4) (a) Dixon, D. J.; Johnston, K. P. *J. Appl. Polym. Sci.* **1993**, *50*, 1929. (b) Mawson, S.; Yates, M. Z.; O'Neil, M. L.; Johnston, K. P. *Langmuir* **1997**, *13*, 1519. (c) Mawson, S.; Johnston, K. P.; Betts, D. E.; McClain, J. B.; DeSimone, J. M. *Macromolecules* **1997**, *30*, 71.

(5) (a) Bleich, J.; Muller, B. W.; Wabmus, W. *Int. J. Pharm.* **1993**, *97*, 111. (b) Bleich, J.; Müller, B. W. *Microencapsulation* **1996**, *13*, 131.

(6) Palakodaty, S.; York, P.; Hanna, M.; Pritchard, J. *Proc. 5th Meeting on Supercritical Fluids, Nice, France*; 1998, *T1*, 275.

(7) Weidner, E.; Knez, Z.; Novak, Z. *Proceedings of the 3rd International Symposium on Supercritical Fluids*; ISASF: Strasbourg, 1994; p 229.

(8) Ventosa, N.; Veciana, J.; Rovira, C.; Sala, S. *Spanish Patent Appl.* 200002129, 2000.

(9) CAS number: [17354-14-2].

(10) Chippendale, A.; Mathias, A.; Aujla, R. S.; Harris, R. K.; Packer, K. J.; Say, B. J. *J. Chem. Soc., Perkin Trans 2* **1983**, 1357−1363.

(11) It is possible to calculate the supersaturation at the working point, that is, the working supersaturation ratio of the solute (β_W) as the ratio between the actual concentration of the solute at the working point (C_W) and the concentration at the saturation limit (C_W^S) for a mixture with a composition of the CF of X_W; i.e., $\beta_W = C_W/C_W^S$. The calculated values of β_W for experiments DELOS 1−8 were 0.7, 0.8, 0.9, 1.2, 1.7, 0.8, 0.8, and 0.8, respectively.

(12) Solubitily data of colorant **1** at such conditions were measured with a variable volume high-pressure cell and will be published elsewhere.

(13) The supersaturation ratio in pressurized pure solvent β_I was assumed to be close to that at atmospheric pressure. For related considerations see: Wubbolts, F. E. In *Supercritical Crystallization. Volatile Components as (Anti-)Solvents*; Universal Press Science Publishers: The Netherlands, 2000; Chapter 2, pp 45−52.

(14) It has also been confirmed that different flow rates (from 5 to 50 kg/h) through the nonreturn valve V4 have no significant influence on the temperature decrease and therefore on the yield and particle characteristics.

(15) The critical temperature and pressure of CO_2 is 304.3 K and 7.38 MPa.

(16) Kato, M.; Aizawa, K.; Kanahira, T.; Ozawa, T. *J. Chem. Eng. Jpn.* **1991**, *24*, 767−771.

(17) Gallagher, P. M.; Coffey, M. P. Krukonis, V. J. *J. Supercritical Fluids* **1992**, *5*, 130−142.

CG0155090

ARTICLE B:

Títol: DELOS process: A crystallization technique using compressed fluids. 1. Comparison to the GAS crystallization method.

Autors: Nora Ventosa, Santiago Sala, Jaume Veciana

Publicació: The Journal of Supercritical Fluids **2003**, *26*, 33-45

(Presentat a la comissió de doctorat)

Available online at www.sciencedirect.com
SCIENCE DIRECT®
J. of Supercritical Fluids 26 (2003) 33–45
THE JOURNAL OF Supercritical Fluids
www.elsevier.com/locate/supflu

DELOS process: a crystallization technique using compressed fluids
1. Comparison to the GAS crystallization method

N. Ventosa, S. Sala, J. Veciana *

Institut de Ciència de Materials de Barcelona (CSIC), Campus Universitari de Bellaterra, 08193-Cerdanyola, Spain

Received 12 November 2001; received in revised form 27 June 2002; accepted 2 July 2002

Abstract

The depressurization of an expanded liquid organic solution (DELOS) crystallization technique is a new one-step process, which uses a compressed fluid (CF) (e.g. CO_2), for the straightforward production of sub-micron- or micron-sized crystalline particles. The driving force of a DELOS crystallization process is the fast, large and extremely homogeneous temperature decrease experienced by a solution, which contains a CF, when it is depressurized from a given working pressure to atmospheric pressure. In contrast to other already reported high-pressure crystallization techniques (RESS, GAS, PCA, PGSS), in a DELOS process the CF behaves as co-solvent over the initial organic solution of the solute to be crystallized. Through a DELOS process it is possible to produce fine powders of a compound provided that a system 'compound/organic solvent/CF' in a liquid one-phase state is found. In order to compare DELOS and gas anti-solvent (GAS) procedures, 1,4-bis-(*n*-butylamino)-9,10-anthraquinone has been crystallized from 'acetone/CO_2' mixtures by both methods. The crystallization results obtained have been analyzed upon the solubility behavior of 1,4-bis-(*n*-butylamino)-9,10-anthraquinone in 'acetone/CO_2' mixtures with different composition. It will be seen how important is the knowledge of the solute solubility behavior in the CO_2-expanded solvent in order to choose the most convenient crystallization technique (GAS like or DELOS) and the best operational parameters. Finally, it has been experimentally determined which are the operational parameters that control the temperature decrease experienced in a DELOS crystallization. The results obtained have been corroborated through thermodynamic considerations.

Keywords: Carbon dioxide; High pressure crystallization; Micron-particles; GAS; DELOS

1. Introduction

The particle size and size distribution of solid materials produced in industrial processes are frequently not those desired for its subsequent use, and therefore further down stream operations, like comminution and homogenization operations,

* Corresponding author. Tel.: +34-93-5801853; fax: +34-93-5805729
E-mail address: vecianaj@icmab.es (J. Veciana).

0896-8446/02/$ - see front matter © 2002 Elsevier Science B.V. All rights reserved.
PII: S0896-8446(02)00189-4

are carried out on a large scale in different industrial sectors (chemical, pharmaceutical, dyes, polymers, explosives, etc.) in order to achieve the desired particle characteristics. The processes used to accomplish particle-size reduction are as diverse as the materials used (crushing, grinding, ball milling, air micronization, jet milling, etc.). However many materials such as certain dyes, chemical intermediates, pharmaceutical and biological compounds, speciality polymers and explosives, which are chemical sensitive, thermo-labile, waxy or soft, are difficult to comminute by the above conventional techniques. Within the last two decades, new eco-efficient processes for the production of micron-sized crystalline particles have emerged using compressed fluids (CF) either under supercritical conditions or in the liquid state [1]. Most of these technologies have in common the use of CO_2 as CF (it is non-toxic, non-flammable, cheap and easy recyclable) and also their final purpose: i.e; to produce micro- and even submicro- or nanoparticles with a narrow particle size distribution. Moreover, such crystallization methods permit to avoid problematic comminution and homogeneization down stream process steps, which are often required after conventional crystallization processes. These crystallization techniques can be classified in three groups according to the solvating behavior of the CF [2]. (1) *CF as a solvent:* The crystallization technique called rapid expansion of a supercritical solution (RESS) involves the dissolution of the solute of interest in a pure CF, generally under supercritical conditions, followed by a rapid expansion of the resulting solution to atmospheric pressure through a nozzle, which produces a rapid decrease of the solvation power, resulting in the precipitation of monodisperse particles [3–6]. (2) *CF as an anti-solvent:* The solute of interest is dissolved in an organic solvent to form a solution. The solute is then precipitated from this solution in two alternative ways. In the first method, called gas anti-solvent (GAS) crystallization, a batch of the liquid solution is expanded several-fold by mixing it with the CF. This expansion produces a solvating power decrease of the mixture, which becomes supersaturated and then the solute precipitates as micron-particles [7–11]. The second method, named precipitation with compressed anti-solvents (PCA), involves the spraying of the organic solution through a nozzle, into the CF, as fine droplets. In this process the CF diffuses into the sprayed droplets causing a rapid expansion of the solvent, decreasing its solvating capacity and forcing the solute to precipitate or crystallize as micron-particles [12–14]. In the case of a continuous flow of the solution and the anti-solvent, the process is also termed aerosol solvent extraction system (ASES) [15,16], if it uses a countercurrent flow, while the term solution-enhanced dispersion by supercritical fluids (SEDS) [17] is used in the case of co-current flow. (3) *CF as a solute:* The technique called particles from gas saturated solutions (PGSS) [18] involves the solubilization, at a given pressure and temperature, of a CF in the pure liquid substance (melted) to be crystallized in order to form a gas saturated solution. By expansion of such solution the CF is evaporated and the solution is cooled. When the melting temperature is reached, the substance is sub-cooled and solid particles are formed.

In this paper we present a new method, called depressurization of an expanded liquid organic solution (DELOS) [19,20], where a CF is used for the straightforward production of micron-sized and sub-micron-sized crystalline particles from an organic solution. This process differs from the other high-pressure techniques in that the CF acts as co-solvent being completely miscible, at a given pressure and temperature, with the organic solution of the solute to be crystallized [21]. The role of the CF is to produce, through its vaporization, a homogeneous sub-cooling of the solution with solid particle precipitation.

In any crystallization process, a compound (solute) changes from the solvated state to the solid state. The supersaturation ratio, β, defined as the ratio between the actual concentration, C, and the saturation concentration, or solubility, C_s, of the solute to be crystallized, is the driving force for the nucleation and crystal growth.

Therefore, the crystallization yield and the physical characteristics (size, size distribution, morphology, polymorphic nature, etc.) of the particles produced depend strongly on the evolution of the solution β profile during the crystal-

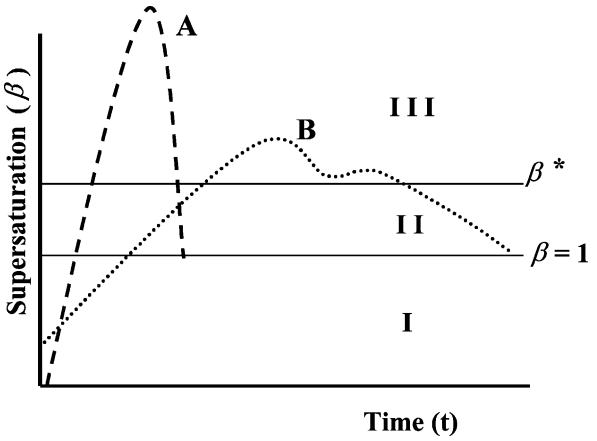

Fig. 1. Trace A: qualitative supersaturation profile corresponding to a crystallization process where nucleation phenomena is enhanced over crystal growth. Trace B: qualitative supersaturation profile corresponding to a crystallization process where crystal growth is enhanced over nucleation.

lization process. In those crystallization processes where large levels of supersaturation are steeply attained (trace A in Fig. 1) and there exists a high homogeneity of this supersaturation profile over all the bulk solution, nucleation phenomena will be enhanced over crystal growth and very small and essentially monodisperse particles will be produced. On the contrary, in the crystallization processes with a β profile more comparable to trace B of Fig. 1, the solute in solution is depleted by both nucleation and crystal growth mechanisms and, thereby, large crystals with broad particle size distribution are formed. Therefore, the efficiency of a given crystallization is highly related to the compound solubility and the actual solute concentration evolution, which determine the progress of the solution supersaturation during the crystallization process.

In this work we present a comparative study of the crystallization results achieved when colorant 1,4-bis-(*n*-butylamino)-9,10-anthraquinone (**1**) is crystallized from 'acetone/CO_2' solvent mixtures through a GAS-like method and by the new DELOS process. It will be shown that using the same experimental setup both crystallization processes, GAS and DELOS, may occur simultaneously although their extension can be controlled by the CO_2 content of the 'solute/organic solvent/CO_2' mixture, being possible to favor exclusively one of such processes. The yields of GAS and DELOS crystallization processes obtained in the different experiments, as well as the characteristics of the particles produced using both methods, have been analyzed and discussed upon the solubility data of colorant **1** in pressurized solvent mixtures of 'acetone/CO_2'.

2. Description of the DELOS crystallization method

The DELOS process comprises the following three steps, which are schematized in Fig. 2. (1) Dissolution of the solute to be crystallized in a conventional organic solvent, at atmospheric pressure and at a working temperature, T_W, to form a solution with an initial supersaturation ratio, β_I, where $\beta_I = C_I/C^S$, C_I is the concentration of this initial solution and C^S is its saturation limit at T_W. (2) Addition of a CF (e.g. CO_2) over the organic solution in order to obtain a volumetric expanded liquid solution, at the working temperature (T_W) and at a high working pressure (P_W) containing a given molar fraction of the CF (X_W), named as the working composition of CF. The solute concentration in this step (C_W) must remain below the saturation limit in the expanded mixture of the organic solvent and the CF (C^S_W); that is, the supersaturation ratio, β_W, of the expanded solution must be less than one, where $\beta_W = C_W/C^S_W$. (3) Rapid reduction of the pressure of the liquid expanded solution, from the working pressure to the atmospheric one through a non-return valve, which produces a large, fast and extremely homogeneous decrease of the solution temperature down to the final temperature, T_F. As a consequence a pronounced and homogeneous increase of the supersaturation ratio, over all the solution, takes place and the phenomenon of catastrophic nucleation occurs causing the precipitation of submicron- or micron-sized crystalline particles with a narrow particle size distribution.

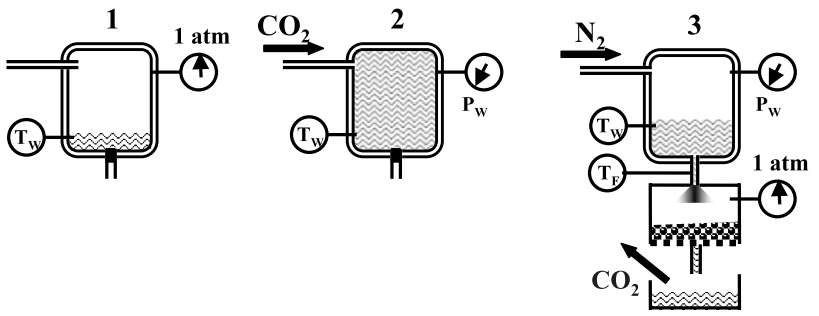

Fig. 2. Different steps of a DELOS process: (1) A liquid solution of the compound to be crystallised is added to the autoclave. (2) Addition of CO_2 produces a new expanded liquid solution which fills all the autoclave volume at a given pressure, P_W, temperature, T_W, giving rise to a solution with a molar fraction of CO_2 of X_W. (3) Depressurization of the expanded liquid solution through a valve leading to precipitation of monodispersed nano- or micron-sized particles.

3. Apparatus, materials and methods

3.1. Materials and characterizations

Colorant 1,4-bis-(*n*-butylamino)-9,10-anthraquinone (**1**) (purity 98%) was purchased from SIGMA-ALDRICH (Steinheim, Germany), acetone (purity 99.5%) was bought from QUIMIVITA (Barcelona, Spain) and CO_2 (purity 99.9%) was supplied by Carburos Metálicos S.A. (Barcelona, Spain). Volumetric particle size distributions of the particles of colorant **1** were measured by light scattering technique with a Malvern (model Mastersizer/E) apparatus. The particle morphology was observed using a HITACHI model S-570 scanning electron microscope. Powder X-ray diffraction analysis was performed using a RIGAKU DS5000 diffractometer to ascertain if changes occurred in the crystallinity of the precipitated colorant **1** as a consequence of the GAS and the DELOS process.

3.2. Apparatus and procedure for DELOS precipitations

Fig. 3 shows the experimental apparatus used to perform all the experiments described in this work. Liquid CO_2 was pumped with a high-pressure pump (Dosapro Milton Roy, Pont-Saint-Pierre, France), P1, after being cooled with a heat exchanger, S1, to prevent cavitation. The CO_2 was heated to the desired temperature in a spiral heat exchanger, S2, before being introduced into the high-pressure vessel, R1. The autoclave R1 (Autoclave Engineers, Erie, USA), of 300 cm^3

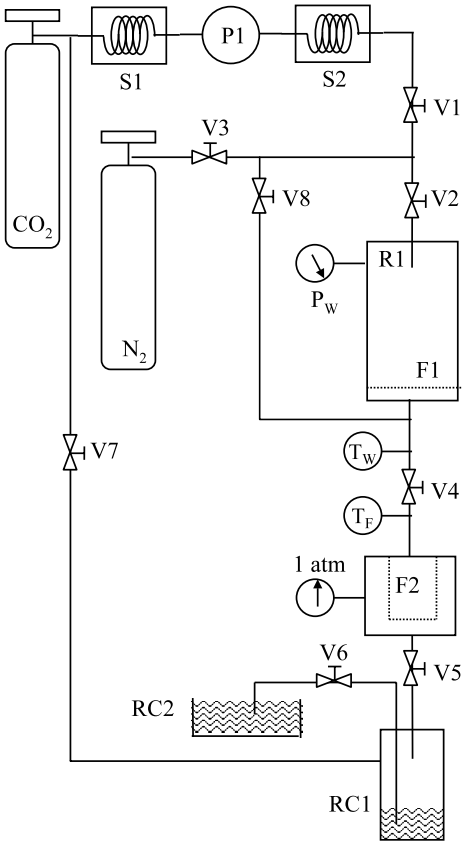

Fig. 3. Scheme of the equipment used for DELOS experiments. P: pump; S: heat exchanger; V: valve; F: filter; R: high-pressure vessel; RC: recycling collector.

internal volume, is provided with a stainless steel frit, F1, at the bottom of the vessel. In addition, this autoclave is connected through valve V4 to one stainless steel filter housing (Headline Filters, Aylesford, England), F2, where the solid particles, produced by DELOS crystallization, are collected. In order to determine T_W and T_F, two thermocouples type K were used for the continuous register of the temperatures inside the tube, before and after the depressurization valve V4. Manometers, temperature controllers, and high-pressure valves complete the plant.

The crystallization experiments of colorant **1** either by a GAS or a DELOS method have been performed using the equipment schematized in Fig. 3, and the operational procedure and experimental conditions used were as follows. A known volume of a solution of colorant **1** in acetone, with a known initial supersaturation ratio, β_I, was loaded in the high-pressure vessel R1. A circulating water jacket was used to maintain, during all the process, the working temperature, T_W, at 293 K inside this vessel. The initial solution was then pressurized up to the working pressure, P_W, by the addition of CO_2 through the bottom of the vessel in order to ensure a faster CO_2 dissolution rate, until a molar fraction of CO_2 of X_W was reached. After leaving the system under the same conditions for 30–60 min, in order to achieve a complete homogenization and its thermal equilibration, the solution was depressurized over the non-return valve V4 from P_W to atmospheric pressure. As it is shown in Fig. 4, when the solution depressurization starts, the temperature registered after V4 decreases suddenly till reaching a constant value. This temperature value is taken as T_F.

The crystals produced through a GAS process inside the vessel R1, during the CO_2 addition, were collected at P_W on the filter plate, F1, placed inside the vessel R1, whereas the precipitate produced through a DELOS process, during the depressurization, was collected at atmospheric pressure on filter F2. During the filtration process step, the pressure of the solution inside R1 was maintained constant at P_W by a continuous addition of pressurized nitrogen gas from the top of the high-pressure vessel. After the filtration, the cleaning of the precipitates was carried out with CO_2 at

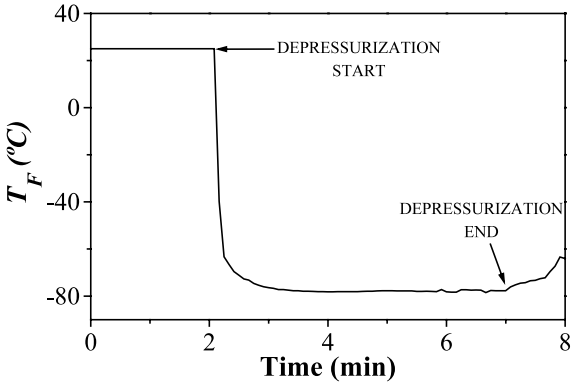

Fig. 4. Variation of the temperature registered inside the tube after valve V4 during the solution depressurization step in a DELOS crystallization.

3 MPa and 293 K during 60 min. The CO_2 evolved in the last step of the process was easily separated from the mother liquor after the valve V5, recovered and, if required, recirculated after compression. Similarly, the mother liquor was disposed in the recycling container RC2 and recycled, if required.

4. Results and discussion

*4.1. Comparison of the crystallization of colorant **1** from acetone/CO_2 mixtures through a DELOS procedure and a GAS method*

Several crystallization experiments of colorant **1** from acetone/CO_2 solvent mixtures at $P_W = 10$ MPa and $T_W = 293$ K were carried out, using the equipment schematically represented in Fig. 3. The GAS and the DELOS crystallization yields, as well as the characteristics of the particles produced by both processes in each crystallization experiment, are summarized in Table 1. As ascertained by powder X-ray diffraction, the particles produced in all the experiments, either through a GAS or by a DELOS process, have a high degree of crystallinity (Fig. 5). However, the diffraction pattern differences shown by the three samples may correspond to different solid polymorphic phases, which are at present under study.

Table 1
DELOS and GAS crystallizations of colorant **1** from acetone/CO_2 solvent mixtures at $T_W = 293$ K and $P_W = 10$ MPa

Exp. No.	β_1	X_W	ΔT(°C)	GAS yield (%)	Diameter of GAS particles (μm)[a]			DELOS yield (%)[c]	Diameter of DELOS particles (μm)[a]		
					X10%	X50%[b]	X90%		X10%	X50% [b]	X90%
E1	0.8	0.40	−32	0	–	–	–	70	0.5	3.9	13.0
E2	0.8	0.54	−46	0	–	–	–	75	0.7	3.1	12.3
E3	0.8	0.62	−57	0	–	–	–	80	0.3	1.0	11.5
E4	0.8	0.70	−65	5	21.3	94.3	163.4	75 (80)	0.2	0.5	6.6
E5	0.8	0.80	−75	15	40.2	86.5	127.8	65 (80)	0.2	0.5	1.8
E6	0.9	0.90	−86	60	30.9	87.0	159.4	25 (60)	3.0	14.2	50.8
E7	0.9	0.94	−91	75	32.9	70.8	137.9	0	–	–	–
E8	0.9	0.97	−93	80	21.5	73.7	156.2	0	–	–	–

The flow rate of CO_2, during the pressurization step, used in all the experiments was 8 kg/h.

[a] Volumetric particle size distributions, measured with the light scattering technique (Mastersizer/E, Malvern, UK), are given as 10, 50, and 90% quantiles.

[b] These values correspond to the medians of the particle distributions. The average diameters of particles were confirmed by SEM images (vide infra).

[c] The DELOS yields reported in parentheses correspond to the ratio between the amount of colorant **1** collected in filter F2 and the quantity of this compound in solution after filter F1.

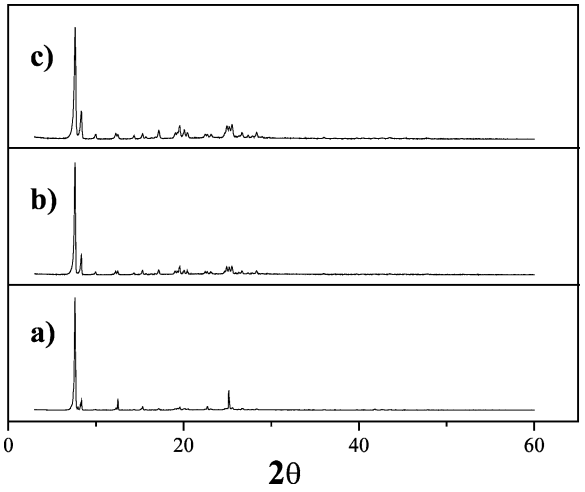

Fig. 5. Powder XRD diffractograms of unprocessed 4-bis-(*n*-butylamino)-9,10-anthraquinone (trace **a**), GAS processed (trace **b**) and DELOS processed (trace **c**).

The experimental data gathered in Table 1 shows that, for solutions of colorant **1** with initial supersaturation ratios between 0.8 and 0.9, the efficiency of the GAS and the DELOS process is tightly related to the CO_2 content, X_W, of the ternary system 'colorant **1**/acetone/CO_2' at the working conditions. It is interesting to compare the results obtained in series of experiments performed under the same experimental conditions and where only the operational parameter X_W is changed.

Thus, experiments E1–E5, performed with an initial supersaturation ratios of $\beta_I = 0.8$, and at the same working pressures and temperatures, show that at CO_2 contents lower than 0.65 it is not possible to crystallize colorant **1** through a GAS process, while the precipitation through a DELOS process gives high crystallization yields. At X_W values higher than 0.65, part of the colorant **1** of the pressurized solution precipitates through a GAS process. From this threshold value, it has been observed that the yield of the GAS crystallization increases with the increase of the CO_2 content. Experiments E6–E8, performed with a $\beta_I = 0.9$ and at higher molar fraction of CO_2 than those employed in experiments E1–E5, show a similar trend. In this series, however, higher molar fractions of CO_2 are required to produce crystals by a GAS process, and the DELOS crystallization of colorant **1** is not achievable from pressurized solutions with a greater X_W than 0.9. The two series of experiments, E1–E5 and E6–E8, show that the X_W threshold value, from which GAS crystallization starts to be possible and, from where a decrease in the DELOS yield is notable, depends on the initial supersaturation ratio. All the above-described results can be rationalized as follows.

In all these experiments, during the addition of CO_2 the concentration of the solute in the acetone/CO_2 mixture is reduced, according to the working line depicted in Fig. 6, from the initial solution concentration (point I) to the working solution concentration (point W). At the same time the solubility of the colorant **1** in the mixture acetone/CO_2 changes according to the solubility curve shown in Fig. 6 [22]. Therefore, the supersaturation ratio at the working point, β_W, is not the same as that at the initial point, β_I. In order to crystallize colorant **1** through a GAS process, it is necessary that X_W becomes higher than X_L, which is the CO_2 molar fraction corresponding to the crossing between the solubility curve and the working line (point L in Fig. 6). Beyond this point—the so-called threshold value—the solution of colorant **1** in the acetone/CO_2 solvent

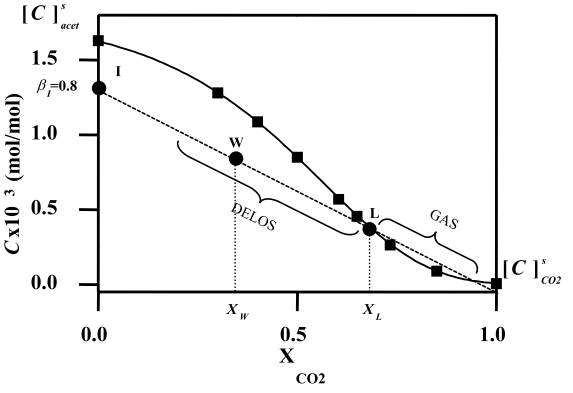

Fig. 6. Solubility curve (continuous line) fitted through the experimental solubility data [22] of colorant **1** in the solvent mixture acetone/CO2, at $P_W = 10$ MPa and $T_W = 293$ K. Working line (discontinuous line) depicts the evolution of the concentration of colorant **1** under the same experimental conditions during the addition of CO_2 over a initial solution of **1** in acetone with a $\beta_I = 0.8$.

mixture becomes supersaturated, $\beta_W > 1$, and GAS precipitation may take place. As shown by the results of experiments E1–E5 of Table 1, starting from a initial solution of **1** in acetone with a $\beta_I = 0.8$, an X_W larger than 0.65 is necessary, which corresponds to X_L for an initial solution of **1** in acetone with a $\beta_I = 0.8$, in order to produce some crystals through a GAS process. Above X_L, the higher the X_W the higher is the GAS crystallization yield achieved (see experiments E4 and E5). Experiments E1–E3 were performed at X_W below X_L, and therefore, GAS precipitation was not detected. In these experiments, it was observed that the higher the X_W the greater is the solution temperature decrease down to the final temperature T_F, during the depressurization step. The lower the T_F the lower is the solubility of colorant **1** in acetone (C^S (261 K) = 3.46E−4 mol/mol; C^S (247 K) = 1.76E−4 mol/mol; C^S (236 K) = 1.24E−4 mol/mol), and higher DELOS yields are attained. The above rationalization allows us to explain the observed trends of the GAS and DELOS crystallizations yields, as well as the fact that the threshold X_W value depends on the initial supersaturation ratio.

Experimental data summarized in Table 1 also reveal that, when using the equipment facilities represented in Fig. 3, the crystalline particles of colorant **1** produced through a DELOS process have median particle diameters that are one or even two orders of magnitude smaller than those produced by a GAS process. Moreover, the results obtained in experiments E1–E5 show a clear dependence of the particle size on the CO_2 composition for the particles produced through a DELOS process, whereas this relationship is nonexistent for the GAS precipitated particles, as can be inferred from the results of experiments E6–E8. Such results were confirmed by SEM images of the particles (Figs. 7 and 8).

The size and size distribution differences can be attributed to the different evolution of the supersaturation profile during a GAS and a DELOS crystallization process. The supersaturation profile occurring during a DELOS process is ideally homogeneous over all solution due to the fact that the magnitude and rate of the solution temperature decrease is identically experienced in any solution point (Fig. 4). In a GAS process, however, the homogeneity of the supersaturation profile over all the solution, when the crystallization takes place, depends on the efficiency of the mixing system during the CO_2 addition over the solution of **1** in acetone. Implementation of active stirring in the mixing vessel would be required in order to produce smaller particles with a narrower particle size distribution of colorant **1**.

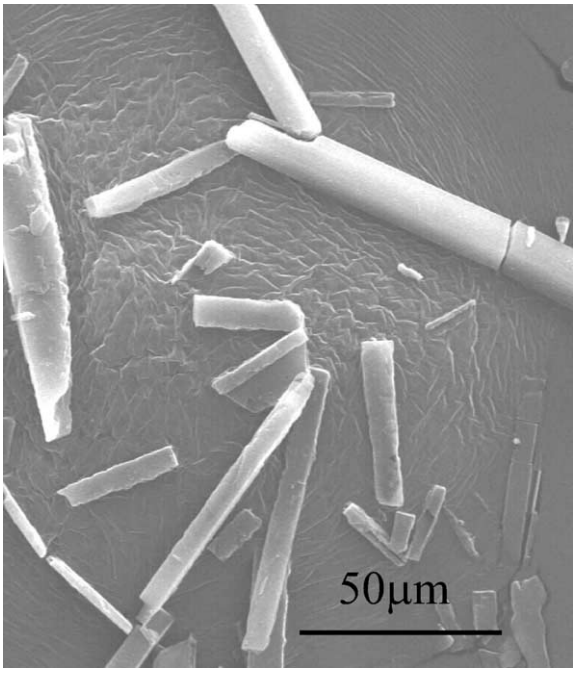

Fig. 7. Scanning Electron Microscopy image of crystalline colorant **1** particles precipitated from acetone/CO2 mixtures at $P_W = 10$ MPa, $T_W = 293$ K, $X_W = 0.94$ and $\beta_I = 0.9$ through a GAS process.

From the results summarized above, it can be concluded that the DELOS method is more efficient than the GAS procedure for the production of micro- and sub-micro crystalline particles of colorant **1** from acetone/CO_2 mixtures. Through a DELOS crystallization smaller particles with a narrower particle size distribution are obtained, and the X_W required to achieve good crystallization yields is far smaller than the one required in the GAS crystallization procedure.

Finally it is interesting to analyze the CO_2 solvating behavior over the system 'colorant

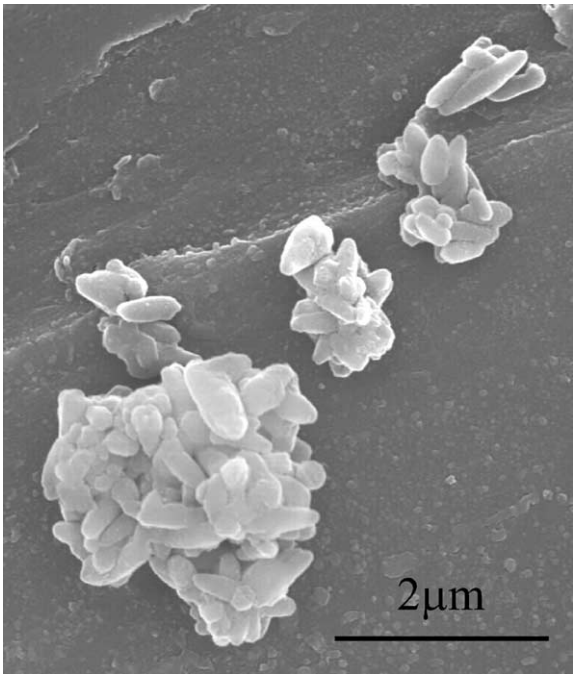

Fig. 8. Scanning Electron Microscopy image of crystalline colorant **1** particles precipitated from acetone/CO2 mixtures at $P_W = 10$ MPa, $T_W = 293$ K, $X_W = 0.62$ and $\beta_I = 0.8$ through a DELOS process.

1/acetone/CO_2'. The solubility data represented in Fig. 6 shows that the CO_2 behaves as co-solvent over this ternary system at lower CO_2 contents; i.e. from $X_{CO_2} = 0$ to the threshold value which corresponds to $X_{CO_2} = 0.57$. Beyond this point the CO_2 starts to act as anti-solvent over the system. Therefore, from this solubility data it can be inferred that the DELOS process is a suitable technique for the crystallization of colorant **1** from pressurized acetone/CO_2 mixtures, since the 'colorant **1**/acetone/CO_2' system exists in one phase liquid solution for a wide range of X_{CO_2}. On the contrary, the crystallization of **1** by a GAS process from this ternary system is not efficient because higher values of X_{CO_2} are required in order to obtain a supersaturated solution and the phenomena of precipitation.

We can conclude that in those 'solute/organic solvent/CO_2' ternary systems where the CO_2 behaves as co-solvent, the DELOS process can be an alternative to the GAS crystallization method, where the CO_2 behaves as anti-solvent.

4.2. Influence of different operational parameters in a DELOS process

The driving force of a DELOS precipitation is the high, steep and greatly homogeneous temperature decrease, from T_W to the final temperature T_F, experienced by the expanded solution when it is depressurized from P_W to atmospheric pressure. As shown in the previous section, in a DELOS crystallization over a given 'solute/organic solvent/CF' system, the magnitude of the temperature decrease, defined as $\Delta T = T_F - T_W$, determines the yield and the characteristics of the crystalline particles produced. In order to identify which are the operational parameters that govern this temperature decrease, a set of depressurization experiments were performed over different 'organic solvent/CO_2' liquid mixtures with different CO_2 content, X_W, at different working pressures, P_W, and using different flow rates through the depressurization valve V4 (Fig. 3), F.

In Fig. 9 are depicted the temperature decrease observed during the depressurization of various acetone/CO_2 high-pressure liquid mixtures under different conditions. The distinct ΔT values mea-

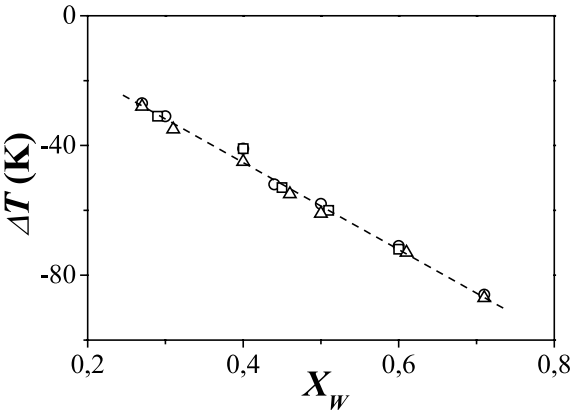

Fig. 9. Dependence of the temperature decrease magnitude, ΔT, on: the mixture CO_2 content, X_W, during the depressurization of acetone/CO_2 mixtures from P_W to atmospheric pressure: (○) acetone/CO_2 mixtures at $P_W = 10$ MPa; (□) acetone/CO_2 mixtures at $P_W = 8$ MPa; (△) acetone/CO_2 mixtures at $P_W = 6$ MPa.

sured during the depressurization of these mixtures were fitted to the corresponding values of the operational parameters X_W, P_W and F by means of a multivariable linear regression method [23]. Models M1 and M2, described in Table 2, were generated by fitting, respectively, the experimental data to Eq. (1) and Eq. (2). Both statistical models have F-test values greater than the corresponding F_{99}, which indicates that both models are valid at the 99% significance level. However, the statistical model M1, obtained by fitting the experimental data to Eq. (1), has the pressure coefficient, b, and the flow coefficient, c, with a much lower statistical significance than the CO_2 content coefficient, a, as revealed by the corresponding t-test values. On the other hand, the value of the adjusted coefficient of multiple determination, R_a^2, of the statistical model M2, which only includes the independent term, k, and the CO_2 molar fraction term, is practically equal to the R_a^2 value of model M1. This indicates, that the addition of the pressure and the flow term do not represent any improvement to the fitting.

$$\Delta T = k + aX_W + bP_W + cF \quad (1)$$

$$\Delta T = k + aX_W \quad (2)$$

The statistical results given in Table 2 together with the plot represented in Fig. 9, clearly demonstrate that the operational parameter that controls the temperature decrease experimented by the solution mixture, when it is depressurized, is its CO_2 content. From this result it can be inferred that in a DELOS crystallization over a given 'solute/organic solvent/CO_2' ternary system, the magnitude of the temperature decrease is mainly governed by the CO_2 concentration, X_W, of the ternary mixture before its depressurization. The higher is the CO_2 content the higher is the heat required for its vaporization when the depressurization takes place, and a higher temperature decrease is produced. Moreover, the results of this study show that ΔT experienced in a DELOS process is linearly related to X_W. On the other hand, it has been demonstrated that changes on the flow rate, F, through the depressurization valve V4, and on the working pressure, P_W, when X_W is kept constant, do not affect ΔT. This result is very important from the practical point of view since it permits to reduce the working pressure of a DELOS process to a level well below those used in other high-pressure crystallization techniques without changing the yield and the characteristics of the particles produced. Indeed, in the vapor–liquid equilibrium of a 'organic solvent/CO_2' mixture, below the critical temperature of the CO_2 [24], the pressure fixes the composition of the liquid phase until the saturation pressure, $P_{CO_2}^{sat}$, is reached. In addition,

Table 2
Dependence of the temperature decrease, ΔT on the working pressure, P_W, the flow rate through the depressurization valve, F, and the CO_2 molar fraction, X_W, when acetone/CO_2 mixtures are depressurized from P_W to P_{atm}

Mod	n[a]	N[b]	Coefficient (t test)[c]				Statistics				
			k	a	b	c	R[d]	s[e]	R_a^2[f]	F[g]	F_{99}[h]
M1[i]	20	16	4.2	−131.2 (36.2)	0.03 (1.63)	0.04 (0.89)	0.997	1.6	0.993	843	5.29
M2[j]	20	18	8.2	−133.3 (48.1)	–	–	0.996	1.6	0.992	2315	8.29

[a] Number of data points.
[b] Degrees of freedom.
[c] Number in parentheses is the student's test values in the same range as the other parameters.
[d] Coefficient of multiple correlation.
[e] Standard error of the estimate.
[f] Adjusted coefficient of multiple determination.
[g] F-test value for derived equation.
[h] F-test value from statistical tables appropriate for the 99% confidence level.
[i] Fit to model $\Delta T = k + aX_W + bP_W + cF$.
[j] Fit to model $\Delta T = k + aX_W$.

the volume of the 'organic solvent/CO_2' liquid mixture is determined just by the volumetric expansion of 'organic solvent' by the liquid CO_2. Therefore, in a DELOS experiment performed over an initial solution with acetone as organic solvent, the molar fraction of CO_2 of the final liquid expanded solution, which fills the total volume of the high-pressure vessel, depends on the vapor–liquid equilibrium and on the volumetric expansion behavior of the binary system acetone/CO_2 [25,26].

As is shown in Fig. 10, as the pressure raises an increase of X_{CO_2} occurs until reaching a certain point, where the expanded solution occupies the total volume of the high-pressure vessel. From this point, a further pressure increase is completely useless because it does not cause any further increase of the X_{CO_2}. This limit CO_2 content becomes the working molar fraction (X_W) of the CF, which is the real operational parameter for the control of the temperature decrease in the DELOS process.

In Fig. 11 is depicted the dependence of ΔT on the CO_2 content, X_W, for different 'organic solvent/CO_2' mixtures. For each of the different organic solvents studied, it was corroborated that ΔT is linearly related to X_W. But, as it can be observed, the slopes of the represented straight lines corresponding to the different organic solvents studied are different from solvent to solvent.

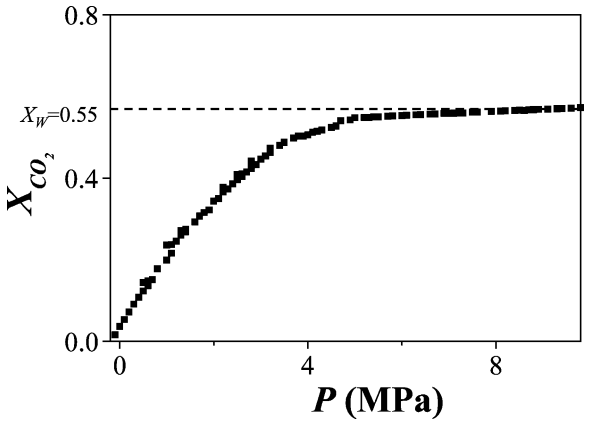

Fig. 10. Dependence of the solution CO_2 content on the pressure when CO_2 is added over an initial volume of acetone, which fills 2/3 of the total autoclave volume.

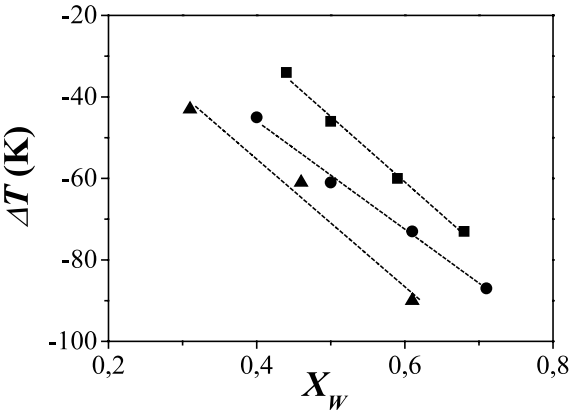

Fig. 11. Dependence of the temperature decrease magnitude, ΔT, on the mixture CO_2 content, X_W, during the depressurization of various 'conventional solvent/CO_2' mixtures from P_W to atmospheric pressure: (●) acetone, (■) ethyl acetate and (▲) methanol.

Summarizing, the magnitude of the temperature decrease, which is the driving force of a DELOS crystallization, is determined by the nature of the solvent employed and by the CO_2 content of the expanded solution before its depressurization.

The experimental results exposed above are in good agreement with the following thermodynamic considerations. Thus, during the DELOS depressurization step, the compressed CO_2 present in the one liquid phase system 'solute/organic solvent/CO_2' at P_W, goes from the liquid state at P_W to the vapor state at atmospheric pressure. The vaporization heat required for performing this change of phase (q_A) is related, through Eq. (3), to the enthalpy of vaporization of the dissolved CO_2, $\Delta H^s_{V(CO_2)}$, and to the quantity of CO_2 present in the ternary system. The value of $\Delta H^s_{V(CO_2)}$ depends on the organic solvent nature and on the composition of the 'solute/organic solvent/CO_2' ternary system [27].

$$q_A = n_{(CO_2)} \cdot \Delta H^S_{V(CO_2)} \quad (3)$$

Since the heat transfer to the surroundings occurring in a DELOS crystallization can be considered as non existent, the heat required for the CO_2 vaporization (q_A) must be extracted from the liquid solution (q_E), and as a consequence a solution temperature decrease is observed. Consequently for this adiabatic process the temperature

decrease, ΔT, depends, following Eq. (4), on the mass, $n_{(sol)}$,?and the heat capacity, $C_{p(sol)}$, of the liquid solution.

$$q_E = n_{(sol)} \cdot C_{p(sol)} \Delta T \quad (4)$$

$$\Delta T = -n_{(CO_2)} \cdot \Delta H^S_{V(CO_2)} / n_{(sol)} \cdot C_{p(sol)} \quad (5)$$

Therefore as it is inferred from Eq. (5), which is obtained by making equal q_A to $-q_E$, the temperature decrease observed during a DELOS crystallization performed over a given 'solute/organic solvent/CO_2' system can be modulated through its CO_2 content at P_W, as it was experimentally observed.

5. Conclusion and perspectives

It has been shown that the DELOS process is an efficient high-pressure crystallization method for the straightforward production of crystalline micron-sized particles provided that a system 'compound/organic solvent/CO_2' in a liquid one-phase state is found. In those ternary systems where the CO_2 behaves as co-solvent over a wide range of X_{CO_2}, like the case of 'colorant **1**/acetone/CO_2' system, this new process can be an alternative to the already reported GAS and PCA crystallization methods, where the CO_2 is used as anti-solvent. In a DELOS process the extent of CO_2 vaporization at any point of the liquid solution is exactly the same, as a consequence the solution temperature decrease and the evolution of the supersaturation profile are extremely uniform over all the system. Therefore, the design of the stirring system, which is usually a problem in many industrial processes performed in solution, is not a key point because the characteristics of the particles produced do not depend on the mixing efficiency.

Summarizing, the DELOS process is a promising new high-pressure crystallization technique, which can be a useful processing tool in the particle engineering of different compounds and materials of industrial interest.

Acknowledgements

The authors acknowledge financial support from CARBUROS METALICOS S.A., and Joan Llibre and Joaquim Torres for their valuable comments. We also thank R. Solanes (ICMAB) for the operation of high-pressure facilities at the ICMAB, as well as Dr Felicià Plana and Rafael Bartolí for their assistance during the performance of particle size measurements. This work was supported by grants from DGI, Spain (project MAT2000-1388-C03-01), and DGR, Catalunya (project 2001 SGR 00362).

References

[1] J. Jung, M. Perrut, Particle design using supercritical fluids: literature and patent survey, J. Supercrit. Fluids 20 (2001) 179.
[2] I. Kikic, M. Lora, A. Bertucco, A thermodynamic analysis of three-phase equilibria in binary and ternary Systems for applications in Rapid Expansion of a Supercritical Solution (RESS), Particles from Gas-Saturated Solutions (PGSS), and Supercritical Antisolvent (SAS), Ind. Eng. Chem. Res. 36 (1997) 5507.
[3] D.W. Matson, J.L. Fulton, R.C. Petersen, R.D. Smith, Rapid expansion of supercritical fluid solutions: Solute formation of powders, thin films and fibers, Ind. Eng. Chem. Res. 26 (1987) 2298.
[4] J.W. Tom, P.G. Debenedetti, Formation of bioerodible polymeric microspheres and microparticles by rapid expansion of supercritical solutions, Biotechnol. Prog. 7 (1991) 403.
[5] C.J. Chang, A.D. Randolph, Precipitation of microsize organic particles from supercritical solutions, AIChE J. 35 (1989) 1876.
[6] R.S. Mohamed, P.G. Debenedetti, R.K. Prud'homme, Effects of process conditions on crystals obtained from supercritical mixtures, AIChE J. 38 (1992) 742.
[7] P.M. Gallagher, M.P. Coffey, V.J. Krukonis, N. Klasutis, Gas Antisolvent Recrystallization: new process to recrystallize compounds insoluble in SCF, in: K.P. Johnston, J.M. Penninger (Eds.), ACS Symposium Series 406, American Chemical Society, Washington, DC, 1989, p. 334.
[8] S.-D. Yeo, G.-B. Lim, P.G. Debenedetti, H. Bernstein, Formation of microparticulate protein powders using a supercritical fluid anti-solvent, Biotechnol. Bioeng. 41 (1993) 341.
[9] T.Z. Randolph, A.D. Randolph, M. Mebes, S. Yeung, Sub-micrometer-sized biodegradable particles of poly(L-lactic acid) via the gas antisolvent spray precipitation process, Biotechnol. Prog. 9 (1993) 429.

[10] E.M. Berends, O.S.L. Bruinsma, J. de Graauw, G.M. Van Rosmalen, Crystallization of phenanthrene from toluene with carbon dioxide by the GAS Process, AIChE J. 42 (1996) 431.
[11] E. Reverchon, G.D. Porta, A.D. Trolio, Morphological analysis of nanoparticles generated by SAS, in: E. Reverchon (Ed.), Proceedings of the Fourth Conference On Supercritical Fluids and Their Applications, Capri, Italy, 1997, p. 335.
[12] D.J. Dixon, K.P. Johnston, Formation of microporous polymer fibers and oriented fibrils by precipitation with a compressed fluid anti-solvent, J. Appl. Polym. Sci. 50 (1993) 1929.
[13] S. Mawson, M.Z. Yates, M.L. O'Neil, K.P. Johnston, Stabilized polymer microparticles by precipitation with a compressed fluid anti-solvent. 2 Poly (propyleneoxide)- and poly(butyleneoxide) -based co-polymers, Langmuir 13 (1997) 1519.
[14] S. Mawson, K.P. Johnston, D.E. Betts, J.B. McClain, J.M. DeSimone, Stabilized polymer microparticles by precipitation with a compressed fluid antisolvent, 1. Poly (fluoro acrilates), Macromolecules 30 (1997) 71.
[15] J. Bleich, B.W. Muller, W. Wabmus, Aerosol solvent extraction system—a new microparticle production technique, Int. J. Pharm. 97 (1993) 111.
[16] J. Bleich, B.W. Müller, Production of drug loaded microparticles by the use of supercritical gases with the Aerosol Solvent Extraction System (ASES) process, J. Microencapsulation 13 (1996) 131.
[17] S. Palakodaty, P. York, M. Hanna, J. Pritchard, Crystallization of lactose using solution enhanced dispersion by supercritical fluids (SEDS) Technique, in: M. Perrut, P. Subra (Eds.), Proceedings of the Fifth Meeting on Supercritical Fluids, Nice, France 1998, vol. 1, ISBN 2-905-267-28-3, p. 275.
[18] E. Weidner, Z. Knez, Z. Novak, PGSS (Particles from Gas saturated Solutions) a new process for powder generation, in: G. Brunner, M. Perrut (Eds.), Proceedings of the Third International Symposium on Supercritical Fluids, Strasbourg, France 1994, vol. 3, IBSN 2-905-267-23-8, p 229.
[19] N. Ventosa, S. Sala, J. Torres, J. Llibre, J. Veciana, Depressurization of an Expanded Liquid Organic Solution (DELOS): a new procedure for obtaining submicron- or micron-sized crystalline particles, Crystal Growth and Design 1 (2001) 299.
[20] N. Ventosa, J. Veciana, C. Rovira, S. Sala, S (Carburos Metàlicos S.E.), Method for Precipitating Finely Divided Solid Particles PCT/ES01/00327, August 2000.
[21] A. Shariati, C.J. Peters, Phase behavior of the system CO_2+1-propanol+salicylic acid, in: E. Reverchon (Ed.), Proceedings of the Sixth Conference on Supercritical Fluids and Their Applications, Maiori, Italy 2001, ISBN 88-87030-35-9, p. 329.
[22] Solubility data of colorant 1 at such conditions were measured with a variable volume high-pressure cell and will be published elsewhere.
[23] SYSTAT for windows, version 5, SYSTAT inc., Evaston, Illinois, 1992.
[24] The critical temperature and pressure of CO_2 is 304.3 K and 7.38 MPa.
[25] M. Kato, K. Aizawa, T. Kanahira, T.J. Ozawa, A new experimental method of vapor–liquid equilibria at high pressures, Chem. Eng. Jap. 24 (1991) 767.
[26] P.M. Gallagher, M.P. Coffey, V.J. Krukonis, Gas antisolvent recrystallization of RDX: formation of ultrafine particles of a difficult-to-comminute explosive, J. Supercritical Fluids 5 (1992) 130.
[27] F.W. Giacobbe, Thermodynamic solubility behaviour of carbon dioxide in acetone, Fluid Phase Equilibria 72 (1992) 277.

ARTICLE C:

Títol: Micronization of pharmaceuticals by a compressed fluids-based technique: the DELOS process

Autors: Santiago Sala, Nora Ventosa, Maria Muntó, Jaume Veciana

Publicació: En preparació

(No presentat a la comissió de doctorat)

Micronization of pharmaceuticals by a compressed CO_2-based technique: the DELOS process

Santiago Sala, Nora Ventosa, Maria Muntó, and Jaume Veciana*

Institut de Ciència de Materials de Barcelona (CSIC), Campus de la UAB; E-08193 Cerdanyola (Spain)

Corresponding author. Tel.: +34-93-5801853; fax: +34-93-5805729

E-mail address: vecianaj@icmab.es

ABSTRACT

Purpose. The aim of this work is to evaluate the feasibility of preparing finely divided crystalline particles of pharmaceutical compounds by the DELOS process, a technique based in the use of compressed fluids in the form of CO_2-expanded solutions. The influence of various process parameters on particles characteristics is also going to be studied.

Methods. Taking into account the solubility behaviour of different drugs in their respective "drug/organic solvent/CO_2" systems, Aspirin, Ibuprofen and Cholesterol were crystallized from CO_2-expanded acetone and Acetaminophen was crystallized from CO_2-expanded ethanol by the DELOS process. Particle size distributions from the powders obtained were measured by Light Scattering Technique, particles morphology was evaluated by Scanning Electron Microscopy and crystallinity was determined by X-Ray Powder Diffraction.

Results. Particles with micronic and sub-micronic sizes have been crystallized for all the pharmaceutical compounds by the DELOS technique. It is possible to control the particle size by modifying some process parameters such us CO_2 molar ratio and initial supersaturation ratio. In all cases, pure polymorps were obtained.

Conclusions. The DELOS process is a promising high-pressure crystallization technique, which can be a useful single-stage processing tool in the particle engineering of different compounds and materials of industrial interest such as pharmaceuticals.

Keywords:

High-pressure crystallization, Micron-particles, DELOS, Carbon dioxide-expanded solvents, polymorph.

INTRODUCTION

There is increasing investment in new and more effective drug delivery systems because the acceptance of new drug formulations is expensive and slow, taking up to 15 years to obtain full accreditation for some drugs, with no guarantee of success. Pharmaceutical companies are keen to investigate new techniques that can more effectively deliver or target existing drugs, as this offers a new and less costly route to increasing their product portfolio. Research into micro- and nano-particles of pure drugs has not been very extensive, although it is clear that unique properties of such particles warrant closer investigation. Not only their production is considered as a challenge, but also the improvement of their stability after the precipitation process is observed as a problem to resolve. This research will contribute to the development of new drug formulations as nano-suspensions for intravenous injection or as dry powders for pulmonary delivery, which in many cases are far more efficient than the conventional oral routes.

It is well known that conventional crystallization/precipitation processes may suffer from lack of control over the drug material characteristics and often subsequent processing, such as drying and milling, is needed if a certain particle size is required.(1) Within the last two decades, new alternative eco-efficient processes for the straightforward production of micron-sized crystalline particles have emerged using compressed fluids (CF) either under supercritical conditions or in the liquid state.(2, 3, 4) Most of these technologies have in common the use of CO_2 as CF (it is non-toxic, non-flammable, cheap and easy recyclable) and also their purpose: to produce micro- and even submicro- or nanoparticles with a narrow particle size distribution. These methods can be classified in four groups according to the solvating behavior of the compressed fluid.(5, 6) 1) Compressed fluid as a solvent: The crystallization technique called Rapid Expansion of a Supercritical Solution (RESS) involves the dissolution of the solute of interest in a pure CF, generally under supercritical (SC) conditions, followed by a rapid expansion of the resulting

solution to atmospheric pressure through a nozzle, which produces a rapid decrease of the solvation power, resulting in the precipitation of monodisperse particles.(7, 8, 9, 10) 2) Compressed fluid as an anti-solvent: The solute of interest is dissolved in a conventional organic solvent to form a solution. The solute is then precipitated from this solution in two alternative ways. In the first method, called Gas Anti-Solvent (GAS) crystallization, a batch of the liquid solution is expanded several-fold by mixing it with the CF. This expansion produces a solvating power decrease of the mixture that becomes supersaturated and then the solute precipitates as micron-particles.(11, 12, 13, 14, 15) The second method, named Precipitation with Compressed Anti-solvents (PCA), involves the spraying of the organic solution through a nozzle or a capillary tube, into the CF, as fine droplets. In this process the CF diffuses into the sprayed droplets causing a rapid expansion of the solvent, decreasing its solvating capacity and forcing the solute to precipitate or crystallize as micron-particles.(16,17, 18, 19) In the case of continuous flows of solution and anti-solvent introduced in different points of the precipitation vessel, the process is also termed Aerosol Solvent Extraction System (ASES),(20, 21, 22), while the term Solution-Enhanced Dispersion by Supercritical Fluids (SEDS) (23) is used in the case of employing a coaxial nozzle to achieve intense mixing of solution and anti-solvent flows. 3) Compressed fluid as a solute. The technique called Particles from Gas Saturated Solutions (PGSS) (24) involves the solubilization, at a given pressure and temperature, of a CF in the pure liquid substance (melted) to be crystallized in order to form a gas saturated solution. By expansion of such solution through a nozzle the CF is evaporated and the solution is cooled. When the melting temperature is reached, the substance is sub-cooled and solid particles are formed. 4) Compressed fluids as a co-solvent. Recently we have reported the technique called Depressurization of an Expanded Liquid Organic Solution (DELOS), (25-26) which involves the use of a CF for the straightforward production of micron-sized and sub-micron-sized crystalline

particles from an organic solution. This process differs from the other high-pressure techniques in that the CF acts as co-solvent being completely miscible, at a given pressure and temperature, with the organic solution of the solute to be crystallized.(27) The role of the CF is to produce a homogeneous sub-cooling of the solution with solid particle precipitation.

Solvent media used in GAS and DELOS crystallization techniques are known as carbon dioxide-expanded solvents. This name arises from the fact that, when CO_2 is added and condensed into the solution of compound to crystallize/conventional organic solvent, there is a process of volumetric expansion in the liquid phase. It should be remarked that CO_2-expanded solvents have a much higher capacity to dissolve polar compounds than pure CO_2, and thus chemical processes can be performed under milder and hence more cost-efficient conditions.(7, 28-29) In a previous work, the DELOS process has been described as a better tool to produce micron and sub-micron particles of the colorant Solvent Blue 35 than the GAS process, when employing CO_2 as CF and acetone as conventional organic solvent.(30) The expansion of Solvent Blue 35/acetone solutions with CO_2 does not provokes the precipitation of colorant particles up to a pretty high value of CO_2 concentrations, otherwise it maintains the colorant dissolved in the new expanded solvent for a wide range of CO_2 compositions. In this range the system "Solvent Blue 35/acetone/CO_2" is found in a liquid one-phase, which implies that CO_2 presents a remarkable co-solvency effect. The measurement of solubility curve from this system has allowed to find the feasibility limits of both DELOS and GAS crystallization techniques.

In the present work the feasibility to straightforward produce fine particles from pharmaceuticals through the DELOS process is tested. Aspirin and acetaminophen, as analgesic and antipyretic compounds, ibuprofen, as anti-inflammatory agent and cholesterol, as steroid model compound not soluble in water, were the chemicals chosen to carry out this study. The

particle size distributions of powders obtained have been characterized. The crystallinity of these powders have also been subject of study.

MATERIALS AND METHODS

Materials

Aspirin (99.5%), acetaminophen (99%) and cholesterol (99%) and ibuprofen (99%) were purchased from SIGMA-ALDRICH (Steinheim, Germany). Concerning solvents, acetone (99.5%) was bought from QUIMIVITA (Barcelona, Spain), and ethanol (99.5%) from PANREAC (Barcelona, Spain). CO_2 (purity 99.995%) was supplied by Carburos Metálicos S.A. (Barcelona, Spain). All chemicals were employed without further purification.

Technological description of DELOS process

The DELOS process comprises the following three steps, which are schematized in Figure 1. 1) Dissolution of the solute to crystallize in a conventional organic solvent, at atmospheric pressure and at a working temperature, T_W, to form a solution with an initial supersaturation ratio, β_I, where $\beta_I = C_I/C^S$, C_I is the concentration of this initial solution and C^S is its saturation limit. 2) Addition of a CF (e.g. CO_2) over the organic solution in order to obtain a volumetric expanded liquid solution, at the working temperature (T_W) and at a certain working pressure (P_W), containing a given molar fraction of the CF (X_W), named as the working composition of CF. The solute concentration in this step (C_W) must remain below the saturation limit in the expanded mixture of the conventional solvent and the CF (C_W^S); that is, the supersaturation ratio, β_W, of the expanded solution must be lower than one, where $\beta_W = C_W / C_W^S$. 3) Rapid reduction of the pressure of the liquid expanded solution, from the working pressure to the atmospheric one, through a non-return valve. During this depressurization process, the evaporation of the liquid CF from the volumetric expanded solution takes place producing a large, fast and extremely

homogeneous decrease of the solution temperature down to the final temperature, T_F. As a consequence a pronounced and homogeneous increase of the supersaturation ratio, over all the solution, takes place and the phenomenon of catastrophic nucleation occurs causing the precipitation of sub-micron- or micron-sized crystalline particles with a narrow particle size distribution.

Insert Figure 1 around here

Apparatus and procedure for DELOS precipitations

Figure 2 shows the experimental apparatus used to perform all the experiments described in this work. Liquid CO_2 was pumped with a high-pressure pump (Dosapro Milton Roy, Pont-Saint-Pierre, France), P1, after being cooled with a heat exchanger, S1, to prevent cavitation. The CO_2 was heated to the desired temperature in a spiral heat exchanger, S2, before being introduced into the high-pressure vessel, R1. The autoclave R1 (Autoclave Engineers, Erie, USA), of 300 cm^3 internal volume, is provided with circulating water jacket to control the temperature. A stainless steel frit, F1, is contained at the bottom of the vessel. In addition, this autoclave is connected through valve V4 to one stainless steel filter housing (Headline Filters, Aylesford, England), F2, where the solid particles, produced by DELOS crystallization, are collected. Manometers, temperature controllers, thermocouples and high-pressure valves complete the plant.

Insert Figure 2 around here

The crystallization of aspirin, ibuprofen, acetaminophen and cholesterol through a DELOS process was performed using the equipment schematized in Figure 2. In aspirin, ibuprofen and cholesterol cases, acetone was employed as conventional solvent along with CO_2 as CF. In acetaminophen crystallizations, ethanol was the conventional solvent. A known volume of a

solution of the drug in the conventional solvent with an initial super-saturation ratio, β_I, was loaded in the high pressure vessel R1. In all experiments temperature T_W was kept constant. By addition of a given amount of CO_2, X_W, this initial solution was expanded several folds until reaching the total volume of the high pressure vessel R1, at a given pressure P_W. After leaving the system at the same conditions for 30-60 minutes, in order to achieve a complete homogenization and its thermal equilibration at T_W, the solution was depressurized over the non-return valve V4 from P_W to atmospheric pressure. During this step the pressure of the solution inside R1 was maintained constant at P_W by a continuous addition of pressurized nitrogen gas from the top of the high-pressure vessel. Any precipitate produced through an undesired GAS process inside R1, during the CO_2 addition, was collected in filter plate F1 placed inside R1. The DELOS precipitate obtained after valve V4, where the depressurization of the solution took place, was collected in filter F2. After the filtration, the cleaning of the precipitate was carried out with CO_2 at 3 MPa and 295 K during 60min.

Drug particles characterization

Volumetric particle size distributions of drug particles were measured with a laser diffraction particle size analyzer (Beckman Coulter model LS13320). Water was employed as dispersing medium in cholesterol and ibuprofen measurements whereas a high-boiling point petroleum fraction was the dispersing media in aspirin and acetaminophen determinations. The particles morphology was observed using a HITACHI model S-570 scanning electron microscope. Powder X-ray diffraction analysis was performed using a RIGAKU DS5000 diffractometer to ascertain if changes occurred in the crystallinity of the precipitated drugs as a consequence of the DELOS process. For each sample, data were collected between 2θ angles of 3 and 40.

Solubility determinations

The solubility measurements of drugs in CO_2-expanded solvents performed in this work were carried out through a static gravimetric method. The experimental set-up employed was the one shown in Figure 2. A mixture of drug, n^0_{drug} (moles), and organic solvent, $n_{SOLVENT}$ (moles), was charged into the high-pressure vessel. The initial super-saturation ratio of this mixture was higher than 1. The circulating water jacket was used to maintain, during all the process, the working temperature, T_W, inside this vessel. Liquid CO_2 was pumped with a high-pressure pump until having the desired working pressure, P_W. The total amount of CO_2 introduced inside the vessel, n_{CO2} (moles), was measured by a Coriolis flow meter and the solvent mixture CO_2 molar fraction was calculated, X_{CO2}. The system was stirred during 1 hour in order to reach equilibrium conditions. After such an equilibration, stirring was stopped and then, the filtration of the solid remaining inside the vessel was carried out. During this step a continuous flow of nitrogen at the same P_W was added from the top of the vessel until the complete evacuation of the solution. After the filtration, the cleaning of this solid was carried out with pure CO_2 at 3 MPa and 315 K. The difference between the initial amount of solid introduced, n^0_{drug}, and the amount of the solid retained by the filter, n^f_{drug}, corresponded to the drug dissolved in the "CO_2-expanded solvent" at T_W, P_W, and X_{CO2}. The drug solubility (S) was calculated using Equation S1:

$$S = \frac{n^o_{drug} - n^f_{drug}}{n_{SOLVENT} + n_{CO_2}} \qquad \text{Equation 1}$$

Solubilities of drugs in pure solvents were also determined through a static gravimetric method. Saturated mixtures of the drug and the corresponding solvent were stirred in a constant temperature bath during 1 hour. Water baths with a thermostat were employed for determinations

above 273K and a water/ice bath for 273K. At lower temperatures, CO_2 cryogenics baths were used (CCl_4/CO_2 at 249K and acetonitrile/CO_2 at 228K). Then, the stirring was stopped and the mixture was kept at the same temperature during half an hour. Afterwards, a known volume of the saturated solution was withdrawn, filtered, weighed with a precision balance and evaporated to dryness in order to isolate the dissolved drug. The dry solid was also weighed in a precision balance. This procedure was performed twice. The solubilities were calculated in terms of drug moles/solvent moles ratio.

RESULTS AND DISCUSSION

Aspirin and cholesterol DELOS crystallizations

Several crystallization experiments of aspirin and cholesterol from CO_2-expanded acetone were carried out through a DELOS process at different values of β_I, X_W. All aspirin experiments were performed at P_W=7MPa and T_W=295K whereas cholesterol experiments at P_W=10MPa and T_W=308K. The particle size distribution of the particles produced in all the experiments were determined and are summarized in Table 2. In aspirin experiments, the resulting particles have a median particle diameter smaller than 50μm, which is less than one order of magnitude smaller than the median particle diameter of the unprocessed aspirin. In cholesterol case, median particle sizes smaller than 5μm were achieved. The volumetric particle size distributions show that an important fraction of the cholesterol particles are included in the sub-micronic range. Therefore, through a DELOS process, it is possible to straightforward produce micron- and submicron-sized particles of aspirin and cholesterol, without the need of further comminution and homogenization process steps, after the crystallization.

Insert Table 1 around here

When performing a DELOS crystallization, there is an upper limit for the CO_2 molar fraction to be used. Molar fractions larger than this limit value produce undesirable GAS precipitation at vessel R1 during the pressurization step. The limit value, X_L, under which DELOS experiments can be performed avoiding premature GAS precipitation during CO_2 addition (step 2), is given by the crossing point between the solubility curve of the solute to crystallize in the CO_2-expanded solvent at the working pressure P_W and temperature T_W, and by the so-called working line. This lines depicts the solute/solvent moles ratio evolution during the process of CO_2 expansion of a solution with a determined initial supersaturation ratio, β_I. The solubility curves of aspirin, (31) and cholesterol in CO_2-expanded acetone are represented in Figure 3, together with two working lines defined by initial solution concentration values of β_I=0.8 and 0.6. As it is shown in this Figure, each working line has a different X_L. At any point from a working line having a certain X_W, the ratio between the solute concentration and the solubility give what is called the supersaturation ratio at the working composition, β_W ($\beta_W = C_S/C^S_W$). When performing the pressurization step, it is important that the molar fraction of CO_2 at point W, X_W, is not higher than X_L, since beyond this point, the mixture becomes supersaturated, β_W>1, and undesired GAS precipitation can take place.

Insert Figure 3 around here

Experiments ASP1 – ASP2 and COL1-COL2 were performed over initial solutions of aspirin and cholesterol with the same initial supersaturation ratio (β_I=0.8) and the same working pressure and temperature. The unique different operational parameter was the CO_2 content, X_W, of the solvent mixture before the depressurization step. As shown in Table 2, as higher is the CO_2 molar fraction of the expanded solution, larger is the temperature reduction achieved during its depressurization, ΔT, and lower is the median particle diameter of the particles obtained. It

has been already reported that the driving force of a DELOS precipitation is the high, steep and greatly homogeneous temperature decrease, from T_W to the final temperature T_F, experimented by the expanded solution when it is depressurized from P_W to atmospheric pressure.(24) This temperature decrease provokes a pronounced and homogeneous increase of the supersaturation over all the solution. Therefore, the particle size reduction observed on aspirin an cholesterol precipitations when X_W increases is consequence of the higher ΔT reached values, which have contributed to reach higher supersaturations during the solution depressurization.

Experiments ASP3-ASP4 and COL3-COL4 were performed over initial aspirin and cholesterol solutions with different initial supersaturation ratios (β_I=0.6, 0.4) and the same CO_2 content, X_W=0.55 in aspirin solutions and X_W=0.71 in cholesterol solutions. From the comparison of the results obtained in these experiments, which are also summarized in Table 2, it can be inferred that when using lower initial supersaturation ratios, the lower resultant β_W values causes an increase in the median diameter of the particles produced. For a same value of X_W, as lower is β_W minor will be the supersaturations attained during the depressurization step. As a consequence particles with a high median diameter will be produced.

Therefore, it has been demonstrated that the higher are X_W and β_I, the smaller is the median particle size of the particles crystallized in a DELOS experiment. When comparing experiments carried out at different working lines and limit working compositions X_W= X_L, it should be noted that if a higher X_W is required, a working line with lower β_I must be followed (see Figure 3). Therefore, experiments performed along the solubility curve (β_W=1) such as ASP2-ASP3 and COL2-COL3 can be used to compare the weight of β_I and X_W parameters on particle characteristics. In aspirin crystallizations, ASP3, which has lower β_I and higher X_W than ASP2, presents a more important particle size reduction than the latter. Contrarily, in those cholesterol

experiments also performed at β_W=1 values, COL2, which has higher β_I and lower X_W than COL3, permits to obtain smaller particles. The reason for the different weights of β_I and X_W on particle characteristics of aspirin and cholesterol DELOS experiments is discussed below by using the solubility evolution of both compounds at decreasing temperature observed in Figure 4. These representations show that the solubility of aspirin and cholesterol in acetone increases linearly and exponentially, respectively, in the range of temperatures including T_W and T_F values of ASP2-ASP3 and COL2-COL3.

Insert Figure 4 around here

The following analysis can accurately define the relationship between the DELOS aspirin and cholesterol results concerning particle size and the solubility versus temperature evolution. To make this, the supersaturation evolution during the three steps listed in the technological description of the DELOS process should be regarded. In ASP2-ASP3 and COL2-COL3 experiments, the mixture solute/conventional solvent in DELOS step 1 is a true solution with a certain solute concentration C_I, which is lower than the solute solubility C^S in the conventional solvent at T_W. In DELOS step 2, the addition of CO_2 lead to obtain a new expanded solution with solute concentration equal to C_W. In step 3 CO_2 is suddenly evaporated from the expanded solution due to the pressure drop and the initial solute concentration C_I is reestablished. The temperature decrease also caused by this pressure drop provokes now that C_I becomes higher than the solute solubility in the conventional solvent at the new reached temperature, C_F^S, and then the solution becomes supersaturated. The difference between C_I and C_F^S, which consist of another common expression of supersaturation ΔC ($\Delta C=C_I-C^S_F$), permits to quantify the nucleation rates involved in a DELOS process. The following empirical relationship has been

introduced by some authors as a more successful expression of primary nucleation in industrial crystallization than those base on classical nucleation theories:

$$J = k_n \Delta C_{max}^n \qquad \text{Equation 2}$$

J is the primary nucleation rate, k_n, the nucleation rate constant and ΔC_{max} is the maximum attainable supersaturation during crystallization process. The exponent n, stands for an order of nucleation and is usually higher than 2. ΔC_{max} is considerably influenced by factors such as the rate at which supersaturation is generated in solution and the intensity of agitation. In the case of DELOS process, and at difference with other conventional sub-cooling techniques, the very sudden CO_2 evaporation phenomenon occurring during depressurization followed by the abrupt temperature decrease taking place along all the solution points, lead to a very fast generation of supersaturation which is homogeneously transmitted over all the bulk solution. At this conditions, ΔC_{max} approximates to ΔC and the maximum possible nucleation rates are reached leading to a crystallization process with remarkable enhancement of nucleation phenomenon over crystal growth. Therefore, the higher is ΔC, the higher can be the maximum supersaturation attained, ΔC_{max}, the more notorious is the dominance of nucleation phenomenon, and the smaller particle sizes are achieved. ΔC values have been represented in Figure 4 for experiments ASP2-ASP3 and COL2-COL3. It can be observed that ΔC^{ASP3} is slightly higher than that of ΔC^{ASP2}, since the difference between solubilites at T_F of ASP3 and ASP2 is higher than the difference between the initial concentrations of both experiments. This justifies the higher particle size reduction obtained in ASP3. In contrast, Figure 4 shows that the ΔC^{COL2} is remarkably higher than that of ΔC^{COL3}. In this case, the difference between solubilities at T_F of COL 2 and COL 3 is an order of magnitude lower than the difference between initial concentrations of both experiments. Therefore, in ASP3 and COL2 it has been possible to reach higher ΔC_{max} values,

and consequently higher nucleation rates, than in ASP2 and COL3, respectively, fact which has allowed to obtain smaller particle sizes in the former experiments. Summarizing, in the aspirin experiments performed over the solubility curve, an increase on X_W is more influent in order to produce high supersaturations than an increase on β_I. Contrarily, in cholesterol experiments higher values of β_I are revealed as more important than higher values of X_W. SEM images from particles of ASP3 and COL2 experiments are shown in Figures 5 and 6, respectively.

Insert Figure 5 around here

Insert Figure 6 around here

These SEM images and the particle size measurements show that the micronization of cholesterol in DELOS experiments has been more effective in terms of particle size reduction than aspirin DELOS experiments. It should be also pointed out that the yield obtained in cholesterol crystallizations is remarkably higher than that obtained in aspirin crystallizations. COL2 presented a yield of 85% in mass of particles produced whereas ASP 3 had a yield of 40%. The reason for this different effectiveness of DELOS process is again a consequence of the different solubility evolution with temperature seen in Figure 4. In cholesterol experiments, the solubility at T_F is an order of magnitude lower than the solubility at T_W. This fact enables to produce a very powerful supersaturation increase during the depressurization step as well as it provokes the precipitation of most of the compound which was dissolved before this step. On the other hand, in aspirin experiments, when temperature passes from T_W to T_F owing to CO_2 evaporation from the depressurized solution, the solubility of the compound is only lowered to a half. Then, the supersaturation generated is less important than in cholesterol case and in addition, an important mass of aspirin remains in solution despite the temperature decrease.

Ibuprofen and acetaminophen DELOS crystallizations

The micronization of ibuprofen and acetaminophen by the DELOS process was also carried out in experiments IBU1 and ACPH1, respectively (see Table 1). In case of ibuprofen, CO_2-expanded acetone at 10MPa and 295K was employed as solvent media. For acetaminophen, this solvent mixture was not able to be used because CO_2 has a strong anti-solvent effect over solutions of acetaminophen in acetone. However, it has been reported in a previous work that the solvating power of CO_2-expanded ethanol over acetaminophen is remarkably different to that of CO_2-expanded acetone.(32) CO_2 has a certain co-solvent behavior along a range of X_W, when it is added to a solution of acetaminophen in ethanol. This co-solvency range has allowed to perform DELOS crystallizations at 315K and 10MPa. The particle size measurements of samples IBU1 and ACPH1 can be seen in Table 1. Figures 7 and 8 contain images of the micron-sized particles obtained in both experiments.

Insert Figure 7 around here

Insert Figure 8 around here

Crystallinity of powders produced

In the pharmaceutical industry it is desirable to produce crystalline particles, exhibiting a good dosing accuracy and storage stability. The usefulness of amorphous and/or meta-stable crystalline particles is limited due to their thermodynamic instability. Such kinds of particles tend to fuse in the presence of moisture, thereby forming hard agglomerates, which are difficult to break up. Furthermore, amorphous or meta-stable crystalline particles exhibit larger batch-to-batch variations as regards bulk density than do well-defined crystalline particles. Crystallinity and Polymorph control is then a key point when evaluating the feasibility to apply a crystallization process to a certain compound.

In all DELOS crystallizations of aspirin, cholesterol, acetaminophen and ibuprofen, the particles obtained were highly crystalline and consisted of pure polymorphic phases. As it can be seen in Figure 9, DELOS cholesterol particles have an identical PXRD pattern than the starting material and the simulated diffractogram of the anhydrous and most stable crystalline structure at ambient temperature.(33) The same Figure shows that DELOS aspirin particles diffractogram is also identical to the simulated diffractogram corresponding to the only crystalline structure of aspirin described in literature.(34) The pattern from aspirin starting material, even though it contains the same peak reflections, presents some differences in some peak relative intensities. This may be explained by preferred orientation caused by the high particle size of the starting material in relation to DELOS processed aspirin.

Insert Figure 9 around here

Insert Figure 10 around here

The same thing happens when comparing DELOS processed acetaminophen and ibuprofen and their corresponding starting materials, as it is shown in Figure 10. The high-sized and polydisperse solid starting materials lead to PXRD patterns with some variations on peak relative intensities in relation to DELOS particles patterns. The latter are identical to simulated diffractograms from the most stable polymorph, in case of acetaminophen,(35) and the only reported crystalline structure, in case of ibuprofen.(36) This result encourage the use of the DELOS crystallization for the straightforward production of micron-sized crystalline particles, which are difficult to be produced by conventional methods like spray drying, freeze drying rapid solvent quenching that usually lead to the formation of particles in an amorphous state or in a meta-stable crystalline form.

CONCLUSION

In conclusion, it has been shown that the DELOS process is an efficient high-pressure crystallization method for the straightforward production of crystalline micron- and submicron-sized particles of pharmaceuticals. This new process can be used as an alternative to the already reported GAS and PCA crystallization methods, where the CO_2 acts as anti-solvent. The driving force of the DELOS process is the large and extremely homogeneous temperature decrease experimented by a CO_2 expanded solution when it is depressurized. Therefore, in a DELOS process the design of the stirring system, which is usually problematic in many industrial processes performed in solution, is not a key point because the characteristics of the particles produced do not depend on the mixing efficiency.

Summarizing, the DELOS process is a promising new high-pressure crystallization technique, which can be a useful processing tool in the particle engineering of different compounds and materials of industrial interest.

ACKNOWLEDGMENTS

The authors acknowledge financial support from CARBUROS METALICOS S.A. We also thank R. Solanes (ICMAB) for the operation of high-pressure facilities at the ICMAB, Dr. Ricard Alvarez and Dr. Jaume Comas for their assistance during the performance of particle size measurements, as well as the UAB Microscopy service for their help in recording SEM images. This work was supported by grants from DGI, Spain (project MAT2000-1388-C03-01), and DGR, Catalunya (project 2000 SGR 00114). Dra. Nora Ventosa is contracted by the Ramon y Cajal Program of Ministerio de Educación y Ciencia in Spain.

REFERENCES

1. B. Yu. Shekunov and P. York. Crystallization processes in pharmaceutical technology and drug delivery design. *J. Crystal Growth.* **211**:122-136 (2000).

2. J. Jung and M. Perrut. Particle design using supercritical fluids: Literature and patent survey. *J. Supercrit. Fluids*. **20**:179-219 (2001).

3. S. Palakodaty and P. York. Phase behavioral effects on particle formation processes using supercritical fluids. *Pharmaceutical Res.* **16**:976-985 (1999).

4. N. Foster, R. Mammucari, F. Dehghani, A. Barret, K. Bezanehtak, E. Coen, G. Combes, L. Meure, A. Ng, H. L. Regtop, and A. Tandya. Processing pharmaceutical compounds using dense gas technology. *Ind. Eng. Chem. Res.* **42**:6479-6493 (2003).

5. I. Kikic, M. Lora and A. Bertucco. A thermodynamic analysis of three-Phase equilibria in binary and ternary Systems for applications in Rapid Expansion of a Supercritical Solution (RESS), Particles from Gas-Saturated Solutions (PGSS), and Supercritical Antisolvent (SAS). *Ind. Eng. Chem. Res.* **36**:5507- (1997).

6. Y. Hakuta, H. Hayashi and K. Arai. Fine particle formation using supercritical fluids. *Curr. Opin. Solid State Mat. Sci.* **7**:341-351 (2003).

7. D. W. Matson, J. L. Fulton, R. C. Petersen and R. D. Smith. Rapid expansion of supercritical fluid solutions: Solute formation of powders, thin films and fibers. *Ind. Eng. Chem. Res.* **26**: 2298- (1987).

8. J. W. Tom and P. G. Debenedetti. Formation of bioerodible polymeric microspheres and microparticles by rapid expansion of supercritical solutions. *Biotechnol. Prog.* **7**: 403- (1991).

9. C. J. Chang and A. D. Randolph. Precipitation of microsize organic particles from supercritical solutions. *AIChE J.* **35**:1876- (1989).

10. R. S. Mohamed, P. G. Debenedetti and R.K. Prud'homme. Effects of process conditions on crystals obtained from supercritical mixtures. *AIChE J.* **38**:742- (1992).

11. P. M. Gallagher, M. P. Coffey, V. J. Kukronis and N. Klasutis. Gas Anti-Solvent recrystallization: A new process to recrystallize compounds insoluble in supercritical fluids. *ACS Symp. Ser.* **406**:334- (1989).

12. S. -D. Yeo, G. -B. Lim, P. G. Debenedetti and H. Bernstein. Formation of microparticulate protein powders using a supercritical fluid anti-solvent. *Biotechnol. Bioeng.* **41**:341- (1992).

13. T. W. Randolph, A. D. Randolph, M. Mebes and S. Yeung. Sub-micrometer-sized biodegradable particles of poly(L-lactic acid) via the gas antisolvent spray precipitation process. *Biotechnol. Prog.* **9**:429- (1993).

14. E. M. Berends, O. S. L. Bruinsma, J. de Graauw, G. M. Van Rosmalen. Crystallization of phenanthrene from toluene with carbon dioxide by the GAS Process. *AIChE J.* **42**:431- (1996).

15. E. Reverchon, G. D. Porta, A. D. Trolio. Morphological analysis of nanoparticles generated by SAS, in: E. Reverchon (Ed.), Proc. 4th Conf. On Supercritical Fluids and Their Applications, Capri, Italy, 1997, p.335.

16. D. J. Dixon and K. P. Johnston. Formation of microporous polymer fibers and oriented fibrils by precipitation with a compressed fluid anti-solvent. *J. Appl. Polym. Sci*. **50**:1929- (1993).

17. R. Bodmeier, H. Wang, D. J. Dixon, S. Mawson and K. P. Johnston. Polymeric microspheres prepared by spraying into compressed carbon dioxide. *Pharmaceutical Res.* **12**:1211-1217 (1995)

18. S. Mawson, M. Z. Yates, M. L. O'Neil and K. P. Johnston. Stabilized polymer microparticles by precipitation with a compressed fluid anti-solvent. 2 Poly (propyleneoxide)- and poly(butyleneoxide) – based co-polymers. *Langmuir*. **13**:1519- (1997).

19. S. Mawson, K. P. Johnston, D. E. Betts, J. B. McClain and J. M. DeSimone. Stabilized polymer microparticles by precipitation with a compressed fluid antisolvent. 1. Poly (fluoro acrilates). *Macromolecules*. **30**:71- (1997).

20. J. Bleich, B. W. Muller and W. Wabmus. Aerosol solvent extraction system – a new microparticle production technique. *Int. J. Pharm.* **97**:111-117 (1993).

21. J. Bleich and B. W. Müller. Production of drug loaded microparticles by the use of supercritical gases with the Aerosol Solvent Extraction System (ASES) process, *J. Microencapsulation*. **13**:131- (1996).

22. R. T. Bustami, H. –K. Chan, F. Dehghani and N. R. Foster. Generation of micro-particles of proteins for aerosol delivery using high pressure modified carbon dioxide. *Pharmaceutical Res.* **17**:1360-1366 (2000).

23. S. Palakodaty, P. York, M. Hanna and J. Pritchard. Crystallization of lactose using solution enhanced dispersion by supercritical fluids (SEDS) Technique. In: M. Perrut and P. Subra (eds.), *Proc. 5th Meeting on Supercritical Fluids, Nice, France 1998*, vol. 1, pp. 275-.

24. E. Weidner, Z. Knez and Z. Novak. PGSS (Particles from Gas saturated Solutions) a new process for powder generation. In: G. Brunner and M. Perrut (eds.), *Proceedings of the 3rd International Symposium on Supercritical Fluids, Strasbourg, France 1994,* vol. 3, pp 229-.

25. N. Ventosa, S. Sala, J. Torres, J. Llibre and J. Veciana. Depressurization of an Expanded Liquid Organic Solution (DELOS): A new procedure for obtaining submicron- or micron-sized crystalline particles. *Cryst. Growth Des*. **1**: 299-303 (2001).

26. N. Ventosa, J. Veciana, C. Rovira, S. Sala, (Carburos Metàlicos S.E.), Method for Precipitating Finely Divided Solid Particles PCT/ES01/00327, August 2000.

27. A. Shariati and C. J. Peters. Measurements and modeling of the phase behavior of ternary systems of interest for the GAS process: 1. The system carbon dioxide + 1-propanol + salicylic acid. *J. Supercrit. Fluids*. **23**:195-208 (2002).

28. M. Wei, G. T. Musie, D. H. Busch and B. Subramaniam. CO_2-expanded solvents: unique and versatile media for performing homogeneous catalytic oxidations. *J. Am. Chem. Soc.* **124**:2513-2517 (2002).

29. P. G. Jessop, M. M. Olmstead, C. D. Ablan, M. Grabenauer, D. Sheppard, C. A. Eckert and C. L. Liotta. Carbon dioxide as a solubility "switch" for the reversible dissolution of highly fluorinated complexes and reagents in organic solvents: application to crystallization. *Inorg. Chem.* **41**:3463-3468 (2002)

30. N. Ventosa, S. Sala and J. Veciana. DELOS process: a crystallization technique using compressed fluids. 1. Comparison to the GAS crystallization method. *J. Supercrit. Fluids*. **26**:33-45 (2003).

31. F.E. Wubbolts. *Ph.D. Thesis: Supercritical crystallization. Volatile components as (anti-)solvents*, Universal Press Science Publishers, The Netherlands, 2000, p. 50.

32. S. Sala, T. Tassaing, N. Ventosa, Y. Danten, M. Besnard and J. Veciana. Molecular insight, through IR spectroscopy, on solvating phenomena occurring in CO_2-expanded solutions. *ChemPhysChem*. **5**:243-245 (2004).

33. H. –S. Shieh, L. G. Hoard and C. E. Nordman. The structure of cholesterol. *Acta Cryst.* **B37**:1538-1543 (1981).

34. P. J. Wheatley. The crystal and molecular structure of aspirin. *J. Chem Soc.* 6036-6048 (1964).

35. M. Haisa, S. Kashino, R. Kawai and H. Maeda. The monoclinic form of p-hydroxyacetanilide. *Acta Cryst.* **B32**:1283-1285 (1976).

36. J. F. McConnell. *Cryst. Struct. Commun.* **3**:73 (1974).

Table1: DELOS crystallizations of drugs from CO_2-expanded solvents

							Diameter of particles (μm)[b]		
exp	P_W **(MPa)**	T_W	β_I	X_W	β_W	ΔT **(K)**[a]	**X10%**	**X50%**[c]	**X90%**
ASP1	7	295	0.8	0.4	0.9	-27	10.5	31.1	73.7
ASP2	7	295	0.8	0.47	1.1	-33	8.1	23.4	59.2
ASP3	7	295	0.6	0.55	1.0	-48	5.9	16.5	42.6
ASP4	7	295	0.4	0.55	0.6	-48	4.3	30.5	58
COL1	10	308	0.8	0.50	0.82	-50	0.3	1.2	9.3
COL2	10	308	0.8	0.64	1.0	-60	0.2	0.5	4.5
COL3	10	308	0.6	0.71	1.0	-70	0.3	1.2	6.0
COL4	10	308	0.4	0.71	0.63	-75	0.5	2.1	10.0
IBU1	10	295	0.7	0.82	1.0	-75	1.4	9.4	21.2
ACPH1	10	315	0.8	0.4	1.0	-40	3.5	18.6	34.5

[a] Temperature decrease, $\Delta T = T_F - T_W$, where T_W is the solution temperature before the non-return valve V4 and T_F is the solution temperature after this valve. [b] Volumetric particle size distributions, measured with the light scattering technique (Beckman Coulter, model LS13320), are given as 10, 50, and 90% quantiles. [c] These values correspond to the medians of the particle size distributions. The average diameters of particles were confirmed by SEM images (*vide infra*).

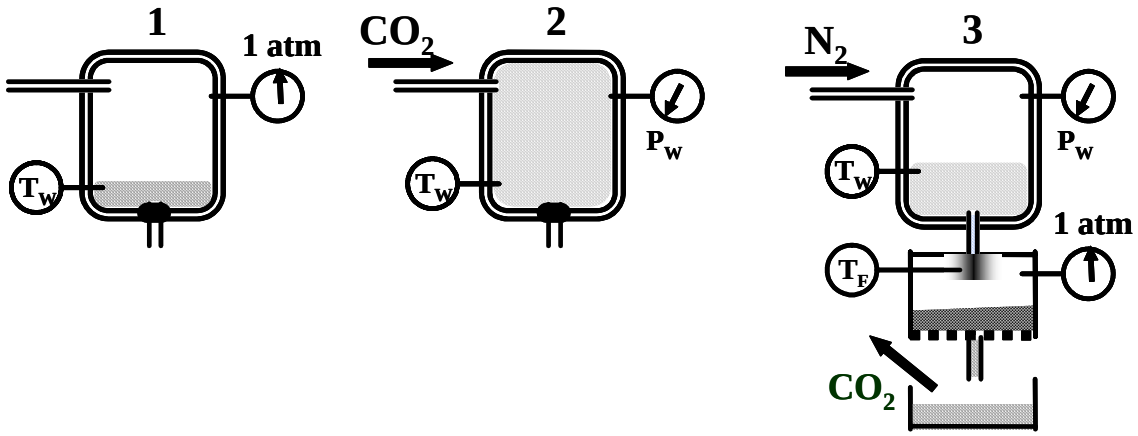

Figure 1

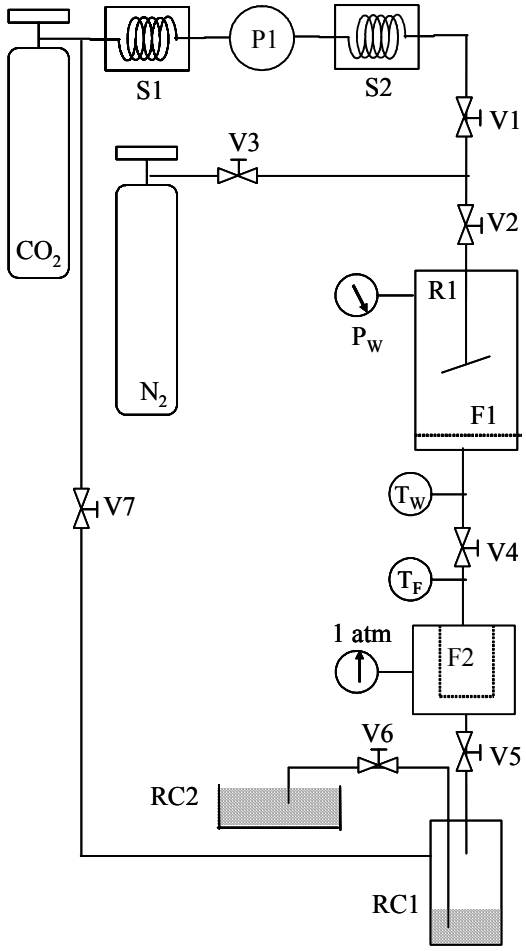

Figure 2

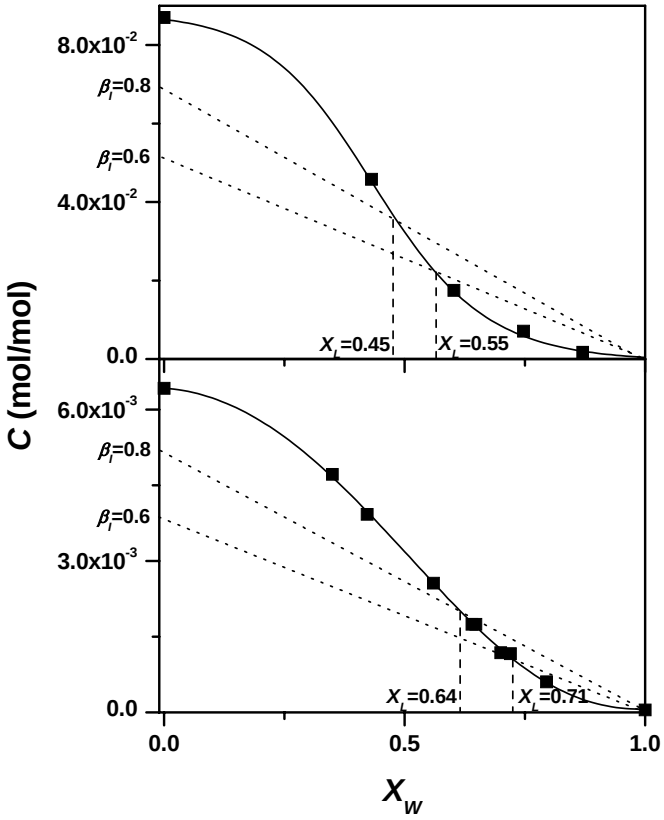
8.0x10-2
βl=0.8
βl=0.6
4.0x10-2
0.0
Xl=0.45
Xl=0.55
6.0x10-3
βl=0.8
βl=0.6
3.0x10-3
0.0
Xl=0.64
Xl=0.71
0.0
0.5
1.0
C (mol/mol)
Xw

Figure 3

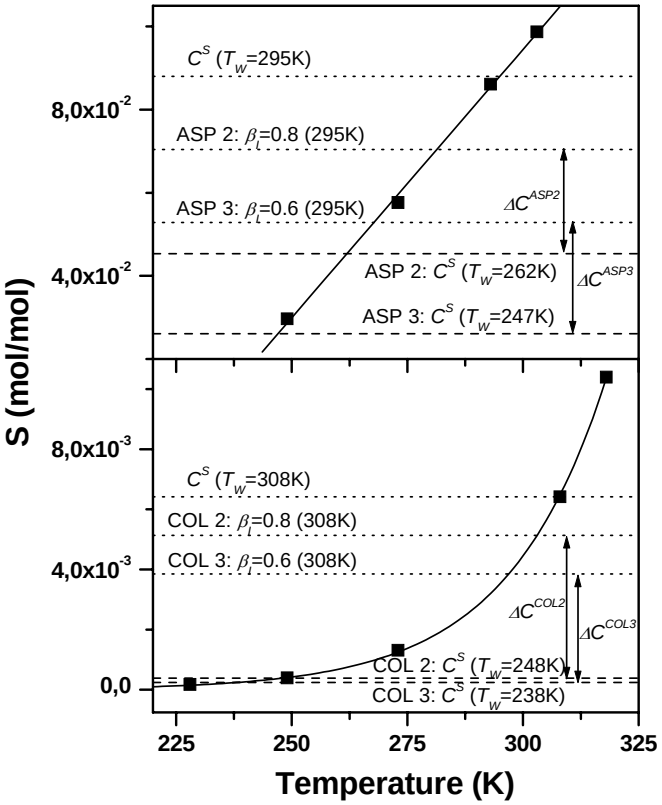
S (mol/mol)
8,0x10-2
4,0x10-2
8,0x10-3
4,0x10-3
0,0
225
250
275
300
325
Temperature (K)
C^S (T_W=295K)
ASP 2: β_l=0.8 (295K)
ASP 3: β_l=0.6 (295K)
ASP 2: C^S (T_W=262K)
ASP 3: C^S (T_W=247K)
ΔC^ASP2
ΔC^ASP3
C^S (T_W=308K)
COL 2: β_l=0.8 (308K)
COL 3: β_l=0.6 (308K)
COL 2: C^S (T_W=248K)
COL 3: C^S (T_W=238K)
ΔC^COL2
ΔC^COL3

Figure 4

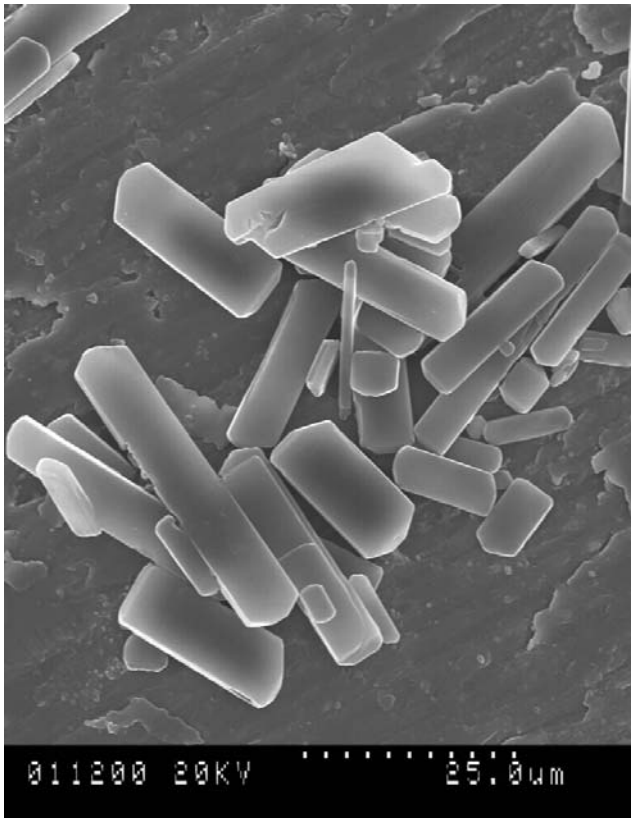

Figure 5

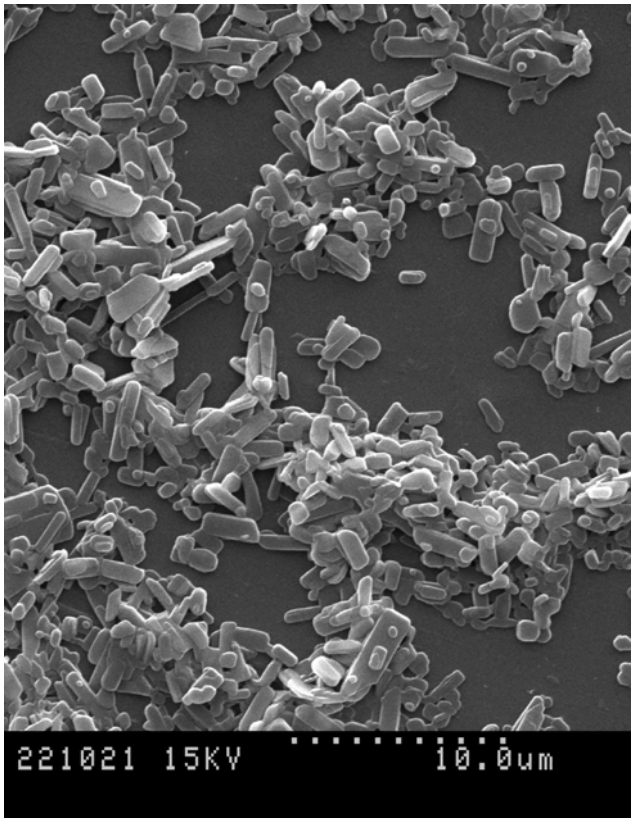

Figure 6

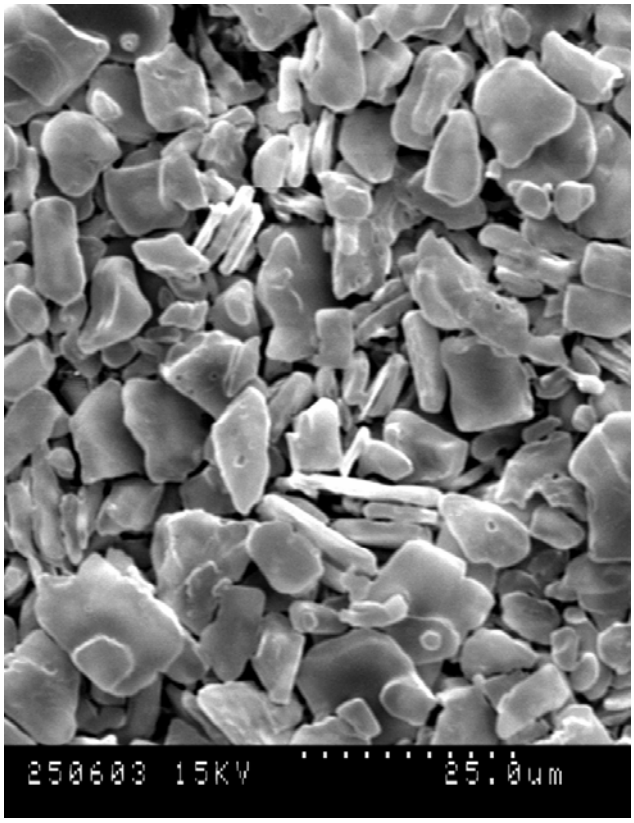

Figure 7

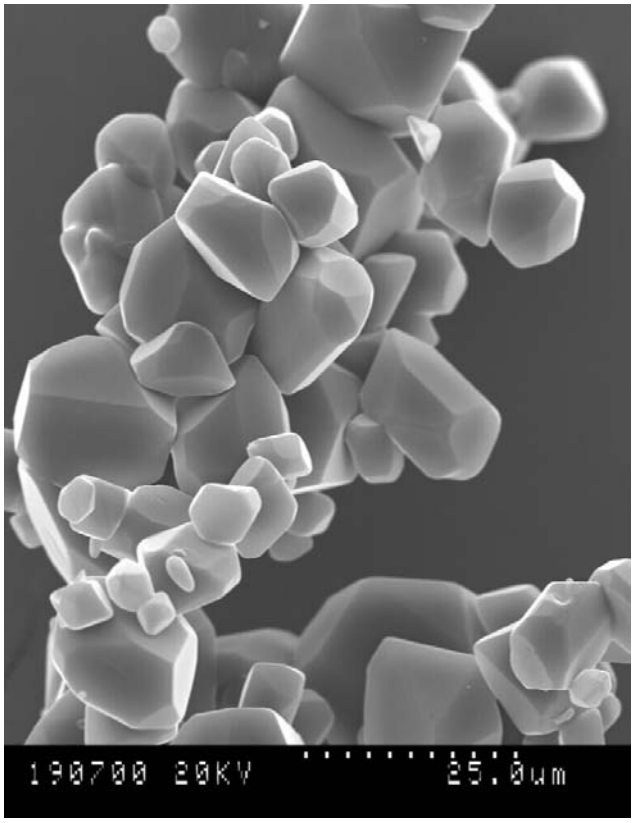

Figure 8

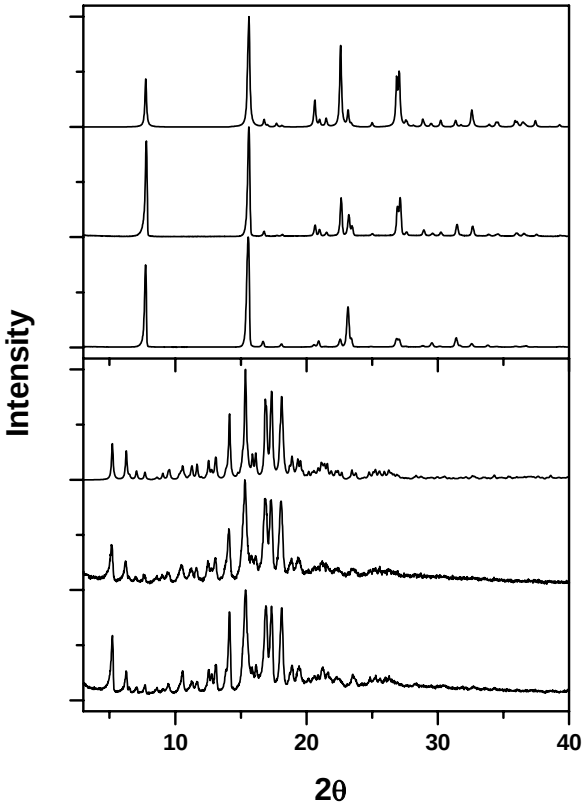

Figure 9

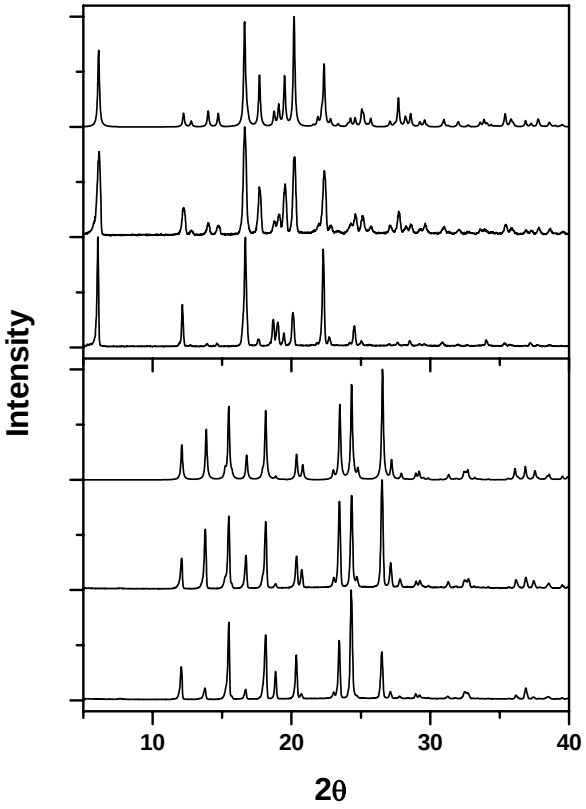

Figure 10

Figure Captions

Fig. 1. Different steps of a DELOS process.

Fig. 2. Scheme of the equipment used for DELOS experiments. P: pump; S: heat exchanger; V: valve; F: filter; R: high-pressure vessel; RC: recycling collector.

Fig. 3. Solubility curves (continuous line) fitted through the experimental solubility data (■) of aspirin (found in literature, (25)) and cholesterol (measured in this work by the static gravimetric method) in CO_2-expanded acetone, at P_W =7MPa and T_W=295K and at P_W=10MPa and T_W=308K, respectively. Working lines (dotted lines) depicts the evolution of the solute concentration by the addition of pure CO2 in a DELOS experiment performed over initial solutions with a supersaturation ratio of β_I = 0.8 and β_I = 0.6.

Fig. 4. Solubility versus temperature evolution of aspirin and cholesterol in acetone solutions. Experimental measurements (■) obtained through a static gravimetric method were fitted to linear and exponential functions respectively. Degrees of supersaturation $\Delta C=C_I-C^S_F$ obtained in each experiment are also represented.

Fig. 5. SEM image of aspirin DELOS particles.

Fig. 6. SEM image of cholesterol DELOS particles.

Fig. 7. SEM image of ibuprofen DELOS particles.

Fig. 8. SEM image of acetaminophen DELOS particles.

Fig. 9. X-ray powder diffraction spectra of a) aspirin and b)cholesterol. For each product the lower trace corresponds to the pattern of the starting material, the middle one to DELOS

particles and the upper to the simulated diffractograms of the only reported aspirin crystalline structure and the cholesterol most stable crystalline structure at room temperature.

Fig. 10. X-ray powder diffraction spectra of a)acetaminophen and b)ibuprofen. For each product the lower trace corresponds to the pattern of the starting material, the central to DELOS particles and the upper to the simulated diffractograms of acetaminophen polymorph I and the only reported ibuprofen crystalline structure.

ARTICLE D:

Títol: Crystallization of Pure Polymorphic Phases from CO_2-Expanded Solutions in the DELOS Process

Autors: Santiago Sala, Nora Ventosa, Jaume Veciana

Publicació: En preparació

(No presentat a la comissió de doctorat)

Crystallization of Pure Polymorphic Phases from CO_2-Expanded Solutions in the DELOS® Process

*Santiago Sala, Nora Ventosa and Jaume Veciana**

Institut de Ciència de Materials de Barcelona (CSIC), Campus Universitari de Bellaterra, 08193-Cerdanyola (Spain)

E-mail: vecianaj@icmab.es.; Tel: 34-93-580 18 53; Fax: 34-93-580 57 29

RECEIVED DATE (to be automatically inserted after your manuscript is accepted if required according to the journal that you are submitting your paper to)

The *DELOS*® process is a crystallization method for the straightforward production of nano and micron sized particles of organic compounds with a narrow particle size distribution. The driving force of this crystallization method is the high and extremely homogeneous temperature decrease experimented by a CO_2-expanded solution of the compound to crystallize when it is depressurized to atmospheric pressure. In the present work we have studied the influence of the magnitude of the temperature decrease, experimented in a *DELOS*® process, on the polymorphic purity of the solids produced. The polymorphic nature of the *DELOS*® crystalline solids is compared to the one achieved by *GAS* crystallization and to the one reached by conventional cooling techniques.

KEYWORDS (Word Style "BG_Keywords"). If you are submitting your paper to a journal that requires keywords, provide significant keywords to aid the reader in literature retrieval.

INTRODUCTION

In recent years, several crystallization techniques based upon the utilization of compressed fluids (CF) as crystallization media have been developed.[1] Some of the most usual compressed fluids employed in these methods are supercritical CO_2 (RESS method)[2] and CO_2-expanded solvents (GAS method)[3], both considered as cleaner solvents and good substitutes to conventional ones. Their main advantage in terms of crystallization efficiency arises from the introduction of the pressure as a new degree of freedom to take into account when controlling the crystallization phenomena. Pressure is specially influent on the control of the supersaturation ratio (β) during crystallization phenomenon and hence it has strong incidence on the evolution of nucleation and crystal growth steps of crystals formed. In CF methods, abrupt changes in pressure usually lead to attain equally abrupt changes in β which produce a dominance of nucleation phenomenon in the process. In this case, the solute precipitates as monodisperse small particles, which is the main goal of most of the CF crystallization techniques. However, not only the influence of pressure on the kinetics and the thermodynamics of the process is observed on the particle size obtained, but also it is shown in the occurrence of different polymorphic forms of the compound crystallized.[4]

A polymorph can be defined as a solid crystalline phase of a given compound resulting from the possibility of at least two different arrangements of the molecules of that compound in the solid state.[5] In order to obtain a certain polymorph of a certain compound, it becomes necessary to know what is called the occurrence domain,[6] which consist of the collection of conditions under which this polymorph would crystallize, such as the solvent employed, the temperature range, the rate of evaporation or cooling, as well as the pressure in case of CF techniques. The control over the polymorph obtained as a result of the crystallization process, is very crucial for those industries that produce sugars, amino acids, pharmaceuticals and fatty acids.

The *DELOS*® crystallization technique is an efficient process, which uses a compressed fluid for the straightforward production of nano- or micron-sized crystalline particles.[7] Like in the *GAS* process, the *DELOS*® technique consist of a crystallization performed over CO_2-expanded solutions. In the *DELOS*®

process the precipitation is caused by the high and greatly homogeneous temperature decrease ($\Delta T = T_F - T_W$) experienced by the CO_2-expanded solution when it is depressurized (see Figure 1). This temperature decrease is provoked by the evaporation of CO_2, which is acting as co-solvent of the solute to crystallize, from the expanded solution during the depressurization step. The higher is the CO_2 content, the higher is the heat required for its vaporization, and a higher temperature decrease is produced.[8] Contrarily, the driving force of the crystallization in a GAS process is the anti-solvent effect of CO_2 manifested during the expansion of the solution –solute in an organic solvent-. In this method, the addition of CO_2 provokes a reduction of the solvating power of the solvent up to produce the precipitation of the solute. Therefore, in the GAS and *DELOS*® crystallization techniques, the supersaturation which lead the solute to crystallize is differently generated. This fact is very important when studying the balance between thermodynamics and kinetics responsible for the occurrence of one polymorph instead of others.

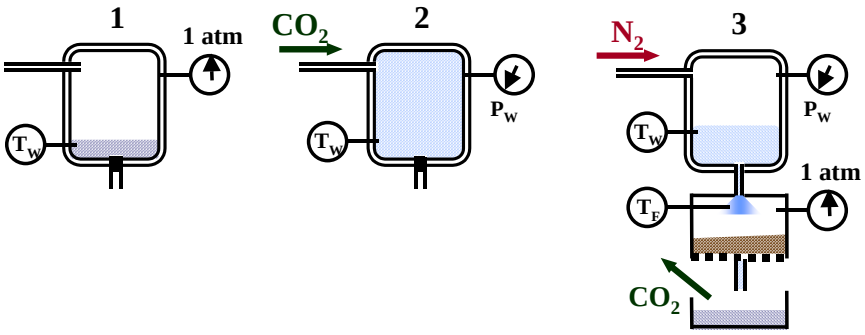

Figure 1. Different steps of a *DELOS*® process: (1) A liquid solution of the compound to be crystallized is added to the autoclave. (2) Addition of CO_2 that produces a new expanded liquid solution, which fills all the autoclave volume at a given pressure, P_W, temperature, T_W, and molar fraction of CO_2, X_W. (3) The solution is depressurized through a valve leading to the precipitation of monodispersed nano- or micron-sized particles.

In the present work we use stearic acid as a probe molecule for studying the influence of the temperature decrease magnitude experimented during a *DELOS*® process on the polymorphic nature and purity of the crystalline solids produced. Stearic acid, like other lipids and related long-chain compounds, may crystallize into different polymorphic forms depending on the conditions in which the crystallization is performed. Up to now, there are described five polymorphic phases of stearic acid:[9] two triclinic forms A_2 i A_3, belonging to what is called A-form, and three monoclinic forms called B, C

and E having an orthorhombic subcell. Two of these forms, B and E, show the phenomenon called polytypism, corresponding to a higher order structural difference caused by a different stacking sequence of the layers. In both B and E forms there are two polytypes: a single-layered structure with monoclinic space symmetry and a double-layered structure with orthorhombic space symmetry. With regards to stability of these different polymorphs, it is known that B and C forms are stable below and above 30ºC, respectively. A and E-forms are considered as metastable phases in the whole temperature region.[6] The A, B and E forms occur only by solution crystallization, whereas C form can be obtained by both solution and melt crystallization.[10]

In this work, we study the nature and polymorphic purity of the stearic acid crystals produced by *DELOS*® crystallization from "CO_2-expanded ethyl acetate" with different contents of CO_2. The polymorphic purity and nature of the *DELOS*® crystallized stearic acid has been compared to the one shown by the crystalline solids produced by a *GAS* like process, when employing the same CO_2-expanded solvent. Finally, we have contrasted the results reached through the *DELOS*® method with those achieved by conventional cooling crystallization, in which the cooling rate is much slower and less homogeneous over all the solution than the one experimented in a *DELOS*® process.

EXPERIMENTAL SECTION

Chemicals. Stearic acid (purity 99%) was purchased from SIGMA-ALDRICH (Steinheim, Germany), ethyl acetate (purity 99%) from SDS (Peypin, France) and CO_2 (purity 99.995%) was supplied by Carburos Metálicos S.A. (Barcelona, Spain). All chemicals were employed without further purification.

***DELOS*® Crystallizations.** The crystallization of stearic acid through a *DELOS*® process was realized using "CO_2-expanded ethyl acetate" as solvent. The crystallization experiments either by *GAS* or *DELOS*® have been performed using the same equipment described in previous works.[7, 8] The operational procedure and experimental conditions employed were as follows. A known volume of a solution of stearic acid in ethyl acetate, with a known initial supersaturation ratio ($\beta_I = C_I/C_S$), $\beta_I = 0.8$, was loaded in a high-pressure vessel. In all experiments the temperature (T_W) was kept constant at

298K. The initial solution was then pressurised up to the desired working pressure, P_W=10MPa, by the addition of a given amount of CO_2, which is represented as a CO_2 molar ratio, X_W. After leaving the system under the same conditions for 30-60 minutes, in order to achieve a complete homogenization and its thermal equilibration, the solution was depressurized over a non-return valve from P_W to atmospheric pressure. When the solution depressurization started, the temperature registered after the depressurization valve decreased suddenly till reaching a constant value. This temperature value was taken as T_F and enabled to calculate $\Delta T = T_F - T_W$.

The crystals produced through a *GAS* process during the CO_2 addition, were collected at P_W on a filter plate placed inside the high-pressure vessel, whereas the precipitate produced through a *DELOS*® process during the depressurization, was collected at atmospheric pressure on a filter placed after the depressurization valve. After the filtration, the cleaning of the precipitates was carried out with CO_2 at 3MPa and 293K during 60min.

Several *DELOS*® crystallization experiments of stearic acid from "CO_2-expanded ethyl acetate", at 10MPa and 298K, were carried out using different values of CO_2 content, X_W=0.3, 0.5, 0.7 and 0.8, leading, respectively, to the following values of temperature decrease ΔT=-20, -38, -68 and -80. Only in the case of X_W=0.8 experiment, *GAS* particles were also obtained inside the high-pressure vessel.

Samples obtained through conventional crystallization methods. A precipitate of stearic acid obtained from conventional cooling crystallization was also prepared. A solution of stearic acid in ethyl acetate at 298K and β_i=0.8 was introduced in an acetonitrile/CO_2 bath at 231K (ΔT=-68). The precipitate was filtered and dried under vacuum. In addition, a sample of solid stearic acid crystallized from a melt was also obtained. In order to obtain this solid a certain amount of stearic acid was immersed in a 80ºC bath until melting down. Afterwards, the melt was slightly cooled up to solidify.

FT-IR spectroscopy. IR spectra of KBr disks from all the samples produced were recorded by a Perkin-Elmer Spectrum One Spectrometer (PerkinElmer España, Madrid, Spain). Number of scans were 10 and resolution was 4 cm^{-1}. The samples were scanned from 4000 to 400 cm^{-1}. In order to compare the

spectra from different samples, they were normalized in relation to the lower % transmittance value contained in the represented range (1250-500 cm^{-1}).

Powder X-ray Diffractrometry (PXRD). Powder X-ray Diffraction patterns were obtained from a Rigaku DS5000 diffractometer using Cu anode (λ=1.540598 Å). Step size was 0.02º in a 2θ interval from 3.0º to 40.0º. Powder X-ray diffractogram simulations of the different stearic acid polymorphs were obtained using the program CRYSTALLOGRAPHICA v1.22a, Oxford Cryosystems Ltd., 1995-1997. In order to facilitate diffractogram comparison, spectra were normalized in relation to the maximum of the represented range (3º to 18º).

Scanning Electron Microscopy (SEM). SEM images of DELOS particles produced were recorded using a Hitachi scanning electron microscopy model S-570. Dry powder samples were sputtered and coated with a conducting gold layer.

Differential Scanning Calorimetry (DSC). DSC profiles were measured by a DSC7 Perkin-Elmer calorimeter (PerkinElmer España, Madrid, Spain). The apparatus was calibrated using a pure indium standard (T_m=156.6 ºC and ΔH_m=28.42 $J \cdot g^{-1}$). Samples (typically between 0.8-1.2 mg) were accurately weighed by a precision balance (±0.001 mg) into crimped aluminum pans. All samples were heated at 5ºC/min from 25ºC to 80ºC.

RESULTS AND DISCUSSION

In Figure 2 and Figure 3 are plotted, respectively, the FT-IR spectra and PXR diffractograms of the stearic acid obtained by melt crystallization, and those of the crystalline solids obtained in the different *DELOS®* experiments. As it was mentioned above, melt crystallization can only lead to C polymorphic form. The IR spectrum of the C-form, and hence that of the solid crystallized from the melt, shows a strong band at 941cm^{-1} (profile (a) of Figure 2), which corresponds to the OH bending vibration band of carboxyl group (δ_{OH}).[11] Concerning the IR spectrum of the *DELOS®* processed stearic acid at X_W=0.8 (profile (e) of Figure 2), it is observed that the δ_{OH} band appears shifted to 892cm^{-1}. This position of the δ_{OH} band and the thin plate morphology observed in the SEM images of Figure 4, attributes the possible

polymorphic forms for this *DELOS®* processed material to B- and E-forms. The clear distinction between B and E polymorphs is provided by another vibrational mode. The OCO in-plane deformation band (δ_{OCO}) has a band maximum at 648cm^{-1} for the B-form and at 688cm^{-1} for the E-form.[12] In the IR spectra of the *DELOS®* processed material (profile (e) of Figure 2) this weak intense band appears at 685cm^{-1}. This fact allows to assign to that sample an E-form crystalline structure. When specifying which E-form polytype we are dealing with, the PXR diffractogram (see profile (e) of Figure 3) lead to conclude that the crystalline stearic acid produced through a *DELOS®* process from "CO_2-expanded ethyl acetate" at X_W=0.8 has an orthorhombic polytype crystalline structure of polymorph E, consisting of a double-layered structure. The simulated powder X-ray diffractograms corresponding to E-form orthorhombic polytype and C- form are also represented in Figure 3.[13]

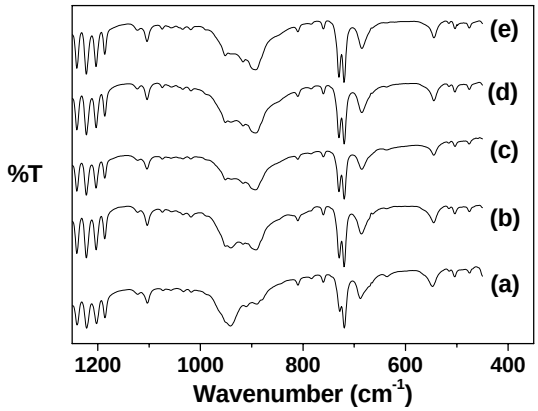

Fig. 2*:* IR spectra of: (a) crystallized from melt C-form; *DELOS®* processed stearic acid at: (b) X_W=0.3, ΔT=-20ºC; (c) X_W=0.5, ΔT=-38ºC; (d) X_W=0.7, ΔT=-68ºC; (e) X_W=0.8, ΔT=-80ºC.

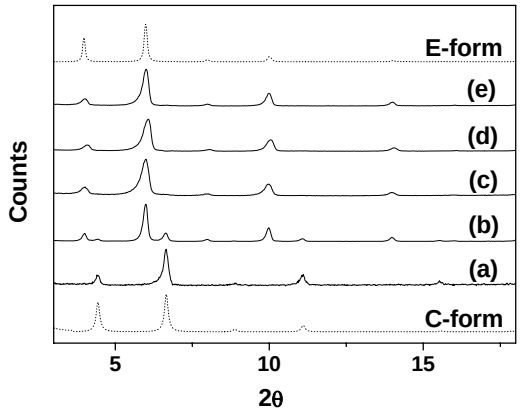

Fig. 3*:* PXR diffractograms of: (a) crystallized from melt C-form; *DELOS®* processed stearic acid at (b) X_W=0.3, ΔT=-20ºC; (c) X_W=0.5, ΔT=-38ºC; (d) X_W=0.7, ΔT=-68ºC; (e) X_W=0.8, ΔT=-80ºC. Dotted lines correspond to PXR simulated diffractograms obtained from monoclinic crystal structure of C-form and the orthorhombic polytype crystal structure of E-form.

The FT-IR spectra and the PXR diffractograms of the different crystalline stearic acid solids obtained by *DELOS®* crystallization at different values of X_W are also represented, respectively, in Figure 2 and Figure 3 (profiles (b) to (e)). As it can be observed, when the absolute value of ΔT is higher or equal to 38ºC, the crystalline solids of stearic acid produced by *DELOS®* crystallization show a pure

orthorhombic polytype E-form (profiles (c), (d), and (e)). However, for ΔT values lower than 38ºC, even though the orthorhombic E-form is the most present, small quantities of the stearic acid C-form were also detected (profile (b) of Figure 2 and Figure 3), since the peak corresponding to (003) reflection is weakly observed. Therefore, it has been defined the occurrence domain, in relation to ΔT, of pure E orthorhombic phases of stearic acid crystallized in "CO_2-expanded ethyl acetate" by the *DELOS®* process. This domain includes those ΔT values equal or higher than 38ºC and corresponds to those conditions where higher supersaturation levels, β_{max}, are attained during crystallization. The higher is β_{max}, the more is enhanced the crystallization of E-form instead of C-form. Below this ΔT, E and C forms concomitantly crystallize.[14]

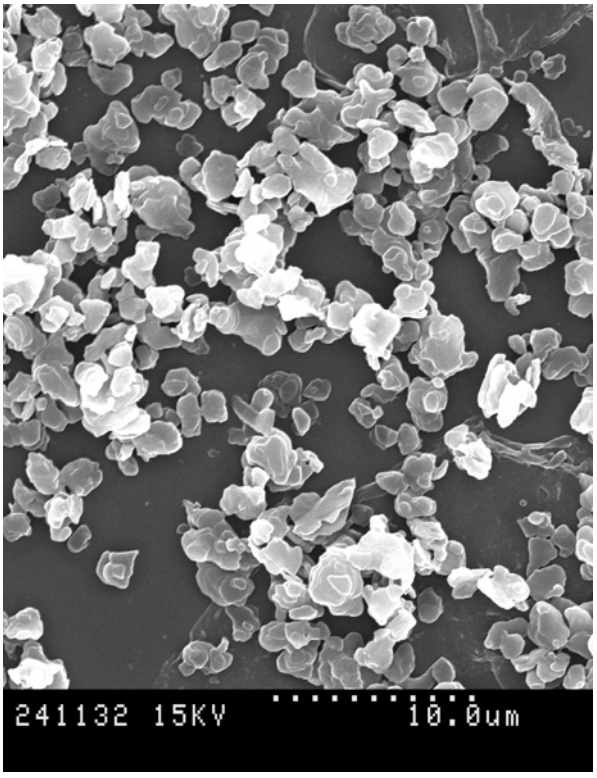

Figure 4. Stearic acid micro-particles obtained from a *DELOS* experiment where X_W=0.8 and ΔT=-80

In Figure 5 and Figure 6, the FT-IR spectra and the PXR diffractograms of the crystalline solids obtained by conventional cooling crystallization and by *DELOS®* process are represented together with those corresponding to the solid crystallized from the melt (C-form). The conventional cooling crystallization and the *DELOS®* experiment had been performed with the same ΔT magnitude. As it can

be observed, a mixture of orthorhombic E-form and C-form constitutes the crystalline structure of the stearic acid conventionally crystallized, whereas pure orthorhombic E-form of stearic acid is produced through the *DELOS®* process. This different result of the crystallization process has taken place because the solution cooling rate and the supersaturation generation rate, caused by the former, are much slower and less homogeneous over all the solution in the conventional cooling process than those experienced in the *DELOS®* crystallization. As a consequence, the E-form promoted at high β_{max} values is only partially obtained. The sudden CO_2 evaporation experienced during the depressurization of the CO_2-expanded solution in a *DELOS®* process causes an internal and identical sub-cooling effect in all the points of that solution, which is not possible to be achieved by conventional cooling techniques.

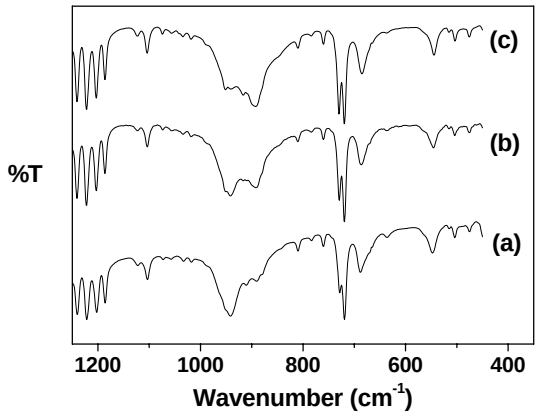

Fig. 5*:* IR spectra of stearic acid: (a) crystallized from melt C-form; (b) crystallized by a conventional cooling technique; (c) *DELOS®* processed at X_W=0.7, ΔT=-68ºC.

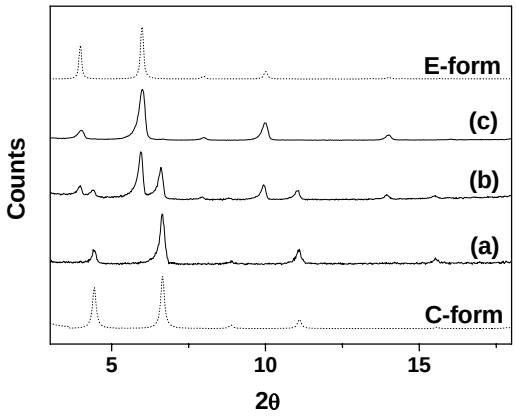

Fig. 6*:* PXR diffractograms of stearic acid: (a) crystallized from melt C-form; (b) crystallized by a conventional cooling technique; (c) *DELOS®* processed at X_W=0.7, ΔT=-68ºC. Dotted lines correspond to PXR simulated diffractograms obtained from monoclinic crystal structure of C-form and the orthorhombic polytype crystal structure of E-form.

Finally, the FT-IR spectra and the PXR diffractograms of the crystalline solids produced in a *GAS* and in a *DELOS®* experiment, using in both cases "CO_2-expanded ethyl acetate" with the same CO_2 content (X_W=0.8), are compared in Figure 7 and Figure 8. Both the spectrum and the diffractogram of *GAS* processed stearic acid are very similar to those corresponding to the solid crystallized from the melt, composed of C-form. Only a few amount of E-form is detected in the PXR trace of the GAS precipitate,

because of the presence of a weak peak corresponding to (006) reflection of E-form. The different polymorphic nature of GAS precipitates in relation to that obtained by *DELOS®* is a consequence of the weak CO_2 anti-solvent character over the system "stearic acid/ethyl acetate/CO_2", which is inferred from the high X_W values required for the GAS precipitation of stearic acid. This weakness of the GAS driving force causes that, even at high concentrations of CO_2, the values of maximum supersaturation reached by a *GAS* process are remarkably smaller than those achieved for the same ternary system in a *DELOS®* crystallization. For that reason the formation of C-form is promoted by the GAS process, whereas the formation of E orthorhombic form, favored by high supersaturation levels, is promoted by the *DELOS®* process.

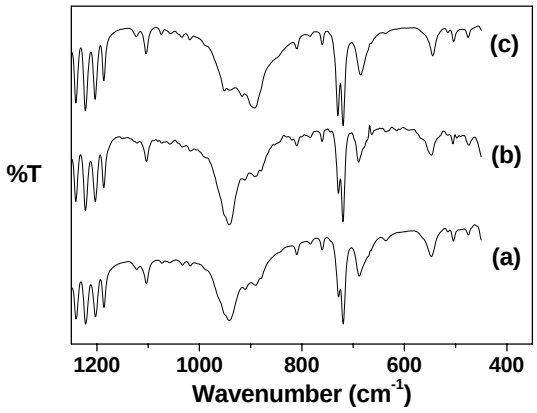

Fig. 7*:* IR spectra of stearic acid: (a) crystallized from melt C-form; (b) *GAS* processed at X_W=0.8; (c) *DELOS®* processed at X_W=0.8, ΔT=-80ºC.

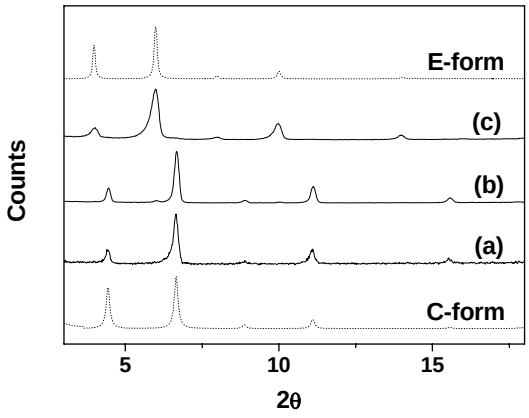

Fig. 8*:* PXR diffractograms of stearic acid: (a) crystallized from melt C-form; (b) *GAS* processed at X_W=0.8; (c) *DELOS®* processed at X_W=0.8, ΔT=-80ºC. Dotted lines correspond to PXR simulated diffractograms obtained from monoclinic crystal structure of C-form and the orthorhombic polytype crystal structure of E-form.

From the results obtained in the FTIR and PXRD analysis of the different samples prepared, it is shown a competition between E orthorhombic form and C form to crystallize both in pure ethyl acetate and in "CO_2-expanded ethyl acetate". It has been demonstrated that this competition is driven to E-form when increasing supersaturation. The thermodynamic relationship between these two polymorphs has been studied by Differential Scanning Calorimetry (DSC) analysis of the precipitate obtained from

X_W=0.8 *DELOS®* experiment, which presented a crystalline structure only based on E orthorhombic form. This analysis is shown in Figure 9 together with that corresponding to stearic acid crystallized from the melt. The DSC trace corresponding to *DELOS®* precipitate heated at 5ºC/min locates, at 53ºC, a solid-solid transition of E orthorhombic phase to C monoclinic phase by an endothermic peak. After this transition the new phase obtained melts at the same temperature as the solid crystallized from the melt (C-form). The transition endothermic nature points out that both polymorphs are enantiotropically related and hence their corresponding Gibbs Free Energy versus temperature diagrams crosses at a certain thermodynamic transition point. This result involves that E-form becomes thermodynamically more stable than C-form at a temperature lower than 53ºC. [15] In previous literature, it has been reported that other experimental techniques observe this transition at 45ºC when heating.[9] However, Kaneko et al. expose that the Gibbs Energy crossing point is far below the experimental transition temperature owing to kinetic aspects related with the high potential barrier at the initiation of the structural changes which lead from one polymorph to the other.[16] Therefore, C-form has probably lower energy than E-form until a temperature far below ambient temperature. Anyway, it has to be taken into account that below the E-C thermodynamic transition point, E-form is still a metastable polymorph in relation to B-form.

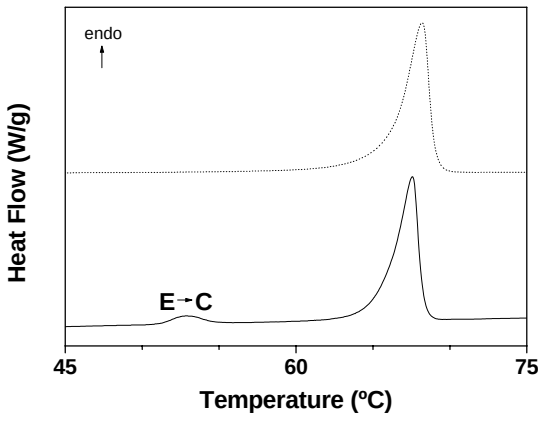

Figure 9: DSC traces for a DELOS precipitate obtained when X_W=0.8 (lower trace) and for the solid obtained from melt crystallization (upper trace). The scan rate has been fixed at 5ºC/min.

C-form is hence thermodynamically enhanced at room temperature over E-form. At lower temperatures such as the ones reached in DELOS process, E-form may become thermodynamically enhanced in relation to C-form. However, in the DELOS process, the thermodynamic balance is less determinant in polymorphic production than the kinetic control owing to the high supersaturation generation rates that this method is able to produce. Its driving force is the high, fast and extremely homogeneous temperature decrease experienced by the depressurized solution which produces an equally high, fast and homogeneous supersaturation increase. The high value of the maximum supersaturations attained lead to a kinetic control of the process with dominance of nucleation over crystal growth. A first outcome of this control is observed in Figure 4 and consists of the production of stearic acid monodisperse microparticulate materials. Another consequence has been manifested in the present work through the occurrence, in most of the experiments, of pure metastable E orthorhombic form. Therefore, E-form is a kinetically enhanced polymorph in all the range of temperatures studied, since its nucleation is able to relieve the high supersaturations reached in the DELOS process.

With regards to the conventional crystallization cooling technique examined, the characterization of its precipitates points out that this technique is not able to generate the supersaturation and nucleation rates provided by the *DELOS®* process, since the competition between of C and E forms lead them to be crystallized as concomitant polymorphs. This fact is produced because, at these conditions, the generated supersaturation leads to similar nucleation rates for the two polymorphs. Concerning GAS precipitate, the crystallization is governed by the low values of supersaturation attained. The driving force of the process is the weak CO_2 anti-solvent effect over the system "stearic acid/ethyl acetate/CO_2" which gives low nucleation rates and dominance of crystal growth over nucleation. In addition, C-form is probably much more stable than E-form at the temperature employed in GAS crystallization. Consequently, the thermodynamically enhanced C-form has been obtained.

CONCLUSION

From the results presented in this work it can be inferred that the stearic acid orthorhombic E-form is more favoured when using those crystallization techniques kinetically controlled, like the *DELOS®*

process, in which high supersaturation levels are rapidly achieved. On the contrary, the stearic acid C-form seems to be preferentially obtained by those crystallization techniques thermodynamically controlled, in which the increase of the solution supersaturation is slow and/or low supersaturation levels are attained.

Acknowledgment. This work was supported by grants from DGI, Spain (project MAT2000-1388-C03-01), and DGR, Catalunya (project 2000 SGR 00114). We thank J. Fraile for and R. Solanes (ICMAB) for particle size measurements and the operation of high-pressure facilities at the ICMAB as well as to D. Amabilino (ICMAB) for correcting the manuscript. We also thank to Servei de Microscòpia de la UAB.

REFERENCES

1. Jung, J.; Perrut, M. *J. Supercrit. Fluids* **2001**, *20*, 179-219.
2. Matson, D. W.; Fulton, J. L.; Petersen, R. C.; Smith, R. D. *Ind. Eng. Chem. Res.* **1987**, *26*, 2298-2306; b) Tom, J. W.; Debenedetti, P. G.; *J. Aerosol Sci.* **1991**, *22*, 555-584.
3. Gallagher, P. M.; Coffey, M. P.; Krukonis, V. J.; Klasutis, N. *ACS Symp. Ser.* **1989**, *406*, 334-354.
4. Tong, H. Y. H.; Shekunov, B.Y.; York, P.; Chow, A. H. L. *Pharm. Res.* **2001**, *18*, 852-858.
5. Mc Crone, W. C.; In *Physics and Chemistry of the Organic Solid State*; Fox, D., Labes, M. M., Weissberger, A., Eds.; Wiley Interscience: New York, 1965.
6. Sato, K.; Boistelle, R. *J. Cryst. Growth* **1984**, *66*, 441-450.
7. Ventosa, N.; Sala, S.; Torres, J.; Llibre, J.; Veciana, J. *Cryst. Growth & Design* **2001**, *1*, 299-303.
8. Ventosa, N.; Sala, S.; Veciana J., *J. Supercrit. Fluids* **2003**, *26*, 33-45.

9. Kaneko, F.; Kobayashi, M.; Kitagawa, Y.; Matsuura, Y. *J. Phys. Chem.* **1992**, *96*, 7104-7107.

10. Kaneko, F.; Sakashita, H.; Kobayashi, M. *J. Phys. Chem.* **1994**, *98*, 3801-3808.

11. Holland, R. F.; Rud Nielsen, J. *J. Molec. Spectroscopy* **1962**, *9*, 436-460.

12. Kaneko, F.; Tashiro, K.; Kobayashi, M. *J. Cryst. Growth* **1999**, *198/199*, 1352-1359.

13. E-form orthorhombic polytype crystalline structure coordinates: Kaneko, F.; Sakashita, H.; Kobayashi, M.; Kitagawa, Y.; Matsuura, Y.; Suzuki, M. *Acta Cryst. C* **1994**, *50*, 247-250; C-form crystalline structure coordinates: Malta V.; Celotti, G.; Zannetti, R.; Martelli, A. F. *J. Chem. Soc. B* **1971**, 548-

14. Bernstein, J.; Davey, J.D.; Henck, J.- O. *Angew. Chem. Int. Ed.* **1999**, *38*, 3440-3461.

15. Bernstein, J. *Polymorphism in Molecular Crystals*, Clarendon Press: Oxford, 2002.

16. Kaneko, F.; Shirai, O.; Miyamoto, H.; Kobayashi, M.; Suzuki, M. *J. Phys. Chem.* **1994**, *98*, 2185-2191.

Annex 3 – Articles relacionats amb el Capítol 3

ARTICLE E:

Títol: Molecular Insight, through IR Spectroscopy, on Solvating Phenomena Occurring in CO_2-Expanded Solutions

Autors: Santiago Sala, Thierry Tassaing, Nora Ventosa, Yann Danten, Marcel Besnard, Jaume Veciana

Publicació: ChemPhysChem **2004**, *5*, 243-245

(Presentat a la comissió de doctorat)

Molecular Insight, through IR Spectroscopy, on Solvating Phenomena Occurring in CO_2-Expanded Solutions

Santiago Sala,[a] Thierry Tassaing,[b] Nora Ventosa,[a] Yann Danten,[b] Marcel Besnard,*[b] and Jaume Veciana*[a]

The use of compressed CO_2, either in its liquid or its supercritical state, as a "green" substitute for organic solvents is a subject of major interest in both academic and industrial processing.[1] However, in those processes in which polar organic compounds are involved, the complete substitution of organic solvents by compressed CO_2 is limited by the low capacity of CO_2 to dissolve such compounds, which is often faced by high-pressure conditions. Carbon dioxide-expanded solvents, composed of subcritical CO_2 condensed into an organic solvent, have a much higher capacity to dissolve polar compounds than pure CO_2, and thus chemical processes can be performed under milder and hence more cost-efficient conditions.[2] In these subcritical mixtures, the organic solvent is substantially, but not totally, replaced (up to 80 vol.%) by CO_2. CO_2-expanded solvents can be used to generate a continuum of solvent media, as a function of either its composition or expansion degree, offering endless opportunities in material processing (such as micro- and nanoparticle formation),[3] as well as in reaction and separation schemes.[2b, 4]

Up to now, most of the investigations concerning the solvation power of CO_2-expanded solvents have been based on the measurement of macroscopic properties (phase changes, thermodynamic parameters, etc.).[5] However, studies at the molecular-microscopic level of the nonideal behaviour of CO_2-expanded solutions are scarce. Herein, mid-IR spectroscopy has been used to explore and understand at molecular level the differential solvating power of "CO_2-expanded acetone" and "CO_2-expanded ethanol" to dissolve *N*-(4-hydroxyphenyl)acetamide (**1**), an analgesic drug commercially known as acetaminophen (paracetamol).[6] Vibrational spectroscopy is particularly useful in this context because the vibrations of a solvent or solute molecule are usually quite sensitive to the environment of that molecule and the spectrum is able to highlight the presence of interactions between solute and solvent functional groups, which would govern the solubility behaviour.[7]

[a] *Drs. S. Sala, Dr. N. Ventosa, Prof. J. Veciana*
Institut de Ciència de Materials de Barcelona (CSIC)
Campus Universitari, 08193 Bellaterra, Catalonia (Spain)
Fax: (+34) 93-5805729
E-mail: vecianaj@icmab.es

[b] *Dr. T. Tassaing, Dr. Y. Danten, Dr. M. Besnard*
Laboratoire de Physico-Chimie Moléculaire, CNRS (UMR 5803)
Université Bordeaux I, 351 Cours de la Libération
33405 Talence Cedex (France)

Supporting information for this article is available on the WWW under http://www.chemphyschem.org or from the author.

Mid-IR spectroscopy has been used before to analyse preferential solvation in various solvent media.[8] However, as far as we know, this is the first time where this technique is used to study solute – solvent molecular interactions in CO_2-expanded solutions.

In Figure 1 the solubility variation of acetaminophen in "CO_2-expanded ethanol" and "CO_2-expanded acetone" is depicted, at 10 MPa and 315 K, with the CO_2 content measured as a mole

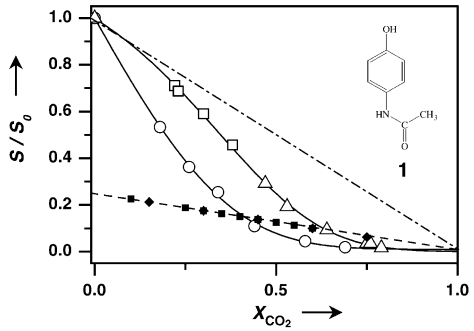

Figure 1. *Acetaminophen solubility ratio(S/S_0) at 315 K and 10 MPa (S_0 = solubility in pure solvent): in "CO_2-expanded ethanol" (data from literature (△),[9] measured by the vanishing point method, data measured in this work (□) by a static gravimetric method (see Supporting Information)); in "CO_2-expanded acetone" (data from literature (○),[9] measured by the vanishing point method). •-•-•- = ideal dilution line, - - - - = working line at which the mid-IR measurements were performed: (◆) acetaminophen in CO_2-expanded ethanol, (■) acetaminophen in CO_2-expanded acetone. Inset, molecular structure of* N*-(4-hydroxyphenyl)acetamide.*

fraction, X_{CO_2}. The difference between both solubility curves indicates that the nature of the CO_2-expanded solvent has a strong influence on the acetaminophen solubility. The increase of X_{CO_2} causes a more pronounced solubility decrease when the CO_2-expanded solvent is acetone, a non-hydrogen bond donor (non-HBD) solvent, than when it is ethanol, an HBD solvent. Thus, in the **1**/acetone/CO_2 system the CO_2 behaves as an antisolvent from very low CO_2 concentrations, whereas in the **1**/ethanol/CO_2 system, the solubility curve follows ideal dilution behaviour up to $X_{CO_2} = 0.2$, which indicates an ideal co-solvent behaviour of CO_2. At higher values of X_{CO_2}, the CO_2 antisolvent character is manifested in a softer way than in the former system.

To investigate which "solute – solvent" molecular interactions are responsible for this differential solvation behaviour, mid-IR spectra of acetaminophen from $\tilde{\nu} = 400$ to $3700\ cm^{-1}$ were obtained in CO_2-expanded ethanol and in CO_2-expanded acetone, at 315 K and 10 mPa, at different CO_2 concentrations from $X_{CO_2} = 0$ to 0.75 (see Figure 1). Herein, the IR spectroscopic data were acquired using a high-pressure optical cell attached to a high-pressure 6 mL agitation vessel which was attached to an infrared absorption spectrometer (see Supporting Information for details).

The IR spectra of acetaminophen in both CO_2-expanded solvents show one isolated band around $\tilde{\nu} = 1650 - 1700\ cm^{-1}$, associated with the ν_{CO} stretching mode, and two overlapping bands around $\tilde{\nu} = 3300 - 3500\ cm^{-1}$, the ν_{OH} and the ν_{NH} stretch-

 DOI: 10.1002/cphc.200300921

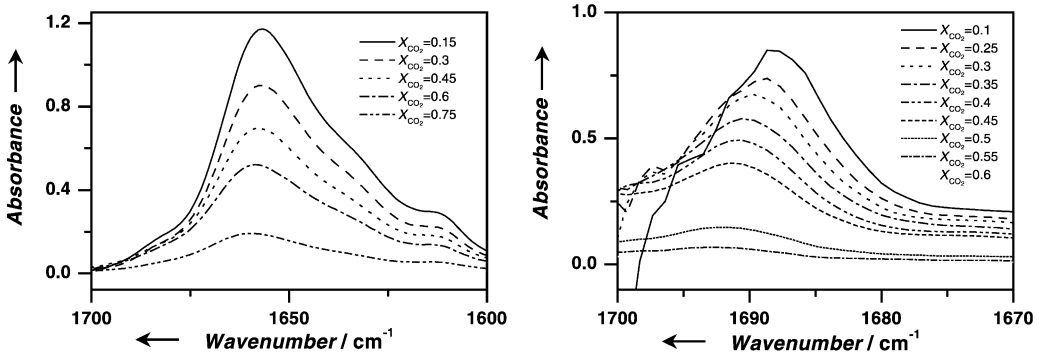

Figure 2. *Evolution of the IR absorption spectra of acetaminophen in the ν_{CO} stretching mode region when X_{CO_2} is increased from $X_{CO_2} = 0$ to $X_{CO_2} = 0.75$ in CO_2-expanded ethanol (left) and in CO_2-expanded acetone (right).*

ing modes. As the CO_2 content of the solvent changes, each mode experiences frequency shifts, $\Delta\tilde{\nu}$. The shift of the overlapping ν_{OH} and ν_{NH} bands is not sensitive to the nature of the organic solvent. In contrast, as the concentration of CO_2 increases, the evolution of the ν_{CO} band shift is markedly different in CO_2-expanded acetone from that observed in CO_2-expanded ethanol.

The vibrational mode ν_{CO} of **1** is very sensitive to its solvent environment and the position of the corresponding IR band provides information on the solute–solvent interactions existing in the solvation shell of the solute.[10] In Figure 2, we report the evolution of the IR ν_{CO} band of acetaminophen with increasing CO_2 content in both CO_2-expanded solvents according to the working line depicted in Figure 1 from $X_{CO_2} = 0$ to 0.75.

The shift experienced by the band ν_{CO} ($\Delta\tilde{\nu}_{CO}$) for the systems **1**/ethanol/CO_2 and **1**/acetone/CO_2 is reported in Figure 3.[11] In both cases, a nonlinear evolution of the blue shift is observed as the CO_2 content of the CO_2-expanded solvent increases. However, we notice that the ν_{CO} band shift of **1** is smoother and reaches lower values when ethanol—an HBD solvent—is present in the system than when acetone—a non-HBD solvent—is used.

The IR spectroscopic data indicate that the increase of CO_2 concentration in the system **1**/acetone/CO_2 produces a steeper and greater perturbation of the cybotactic region of acetaminophen molecules than in the system **1**/ethanol/CO_2.[12] This can explain the stronger "anti-solvent" character exhibited by CO_2 in the former system. The nonlinearity between $\Delta\tilde{\nu}_{CO}$ and X_{CO_2} observed in both systems points out the existence of preferential solvation of acetaminophen molecules by organic solvent molecules.[13] The smoother blue shift, together with the lower absolute values observed for the ν_{CO} of **1** dissolved in CO_2-expanded ethanol, suggests a stronger preferential solvation effect (see Figure 4) in this system. The greater strength of the preferential solvation effect in the **1**/ethanol/CO_2 system can be related to the greater co-solvent behaviour of CO_2 at lower values of X_{CO_2}.

To compare the IR spectroscopic data with phase behaviour measurements, we have plotted in Figure 5, for different values of X_{CO_2}, the acetaminophen free energy of solvation, calculated from the solubilities ($\Delta\mathbf{G} = -RT\ln S$), versus the ν_{CO} shift of acetaminophen.

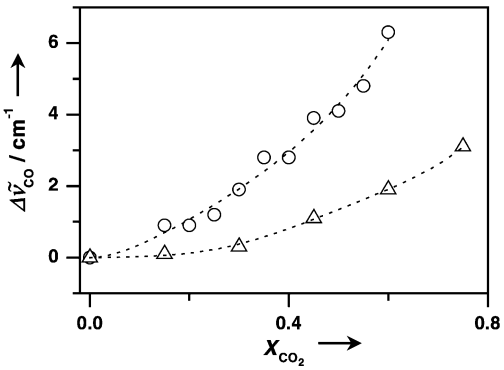

Figure 3. *Evolution of acetaminophen $\Delta\tilde{\nu}_{CO}$ (see text) versus X_{CO_2} of the CO_2-expanded solvent (CO_2-expanded ethanol (△), CO_2-expanded acetone (○)). Dotted lines are for guiding eyes.*

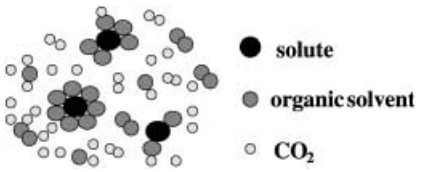

Figure 4. *Schematic representation of the preferential solvation phenomenon.*

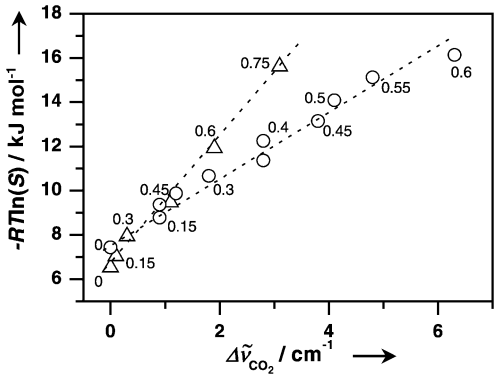

Figure 5. *Correlation between the free energy of solvation and $\Delta\nu_{CO}$ shift (CO_2-expanded ethanol (△), CO_2-expanded acetone (○)). Numbers over the graph point out the CO_2 molar fraction corresponding to each point. - - - - = linear regression fit obtained from experimental data (**1**/acetone/CO_2 system r = 0.990, **1**/ethanol/CO_2 system r = 0.997).*

We can see in Figure 5 that the free energy of solvation is linearly related to the shift of the ν_{CO} vibration of acetaminophen for both expanded solvents. This linear behaviour between IR spectroscopic data and the free energy of solvation has been previously reported.[14] This result shows that the ν_{CO} mode is a well-adapted probe to check the acetaminophen solubility sensitivity to CO_2-expanded solvent changes.

To conclude, our results show that high-pressure IR spectroscopy is a valuable tool to investigate, at the molecular-microscopic level, macroscopic phenomena occurring in CO_2-expanded solutions, such as the solubility behaviour of suitable solutes such as **1**.

Acknowledgements

This work was supported by a grant from the contract HPMT-CT-2000 – 00143 between the European Community and the Université de Bordeaux I and also by grants from DGI, Spain (project MAT2003 – 04699) and DGR, Catalunya (project 2001 SGR 00362). Financial support from "Fundación Domingo Martínez" (Spain) and from Catalunya Innovació (CIDEM) is gratefully acknowledged. Santiago Sala is enrolled in the Chemistry Ph.D. Program from the Universitat Autònoma de Barcelona (Spain).

Keywords: acetaminophen · carbon dioxide · IR spectroscopy · solute-solvent interactions · solvent effects

[1] a) E. J. Beckman, *J. Supercrit. Fluids* **2003** (published on the web) DOI: 10.1016/50896-8446(03)00029-9; b) W. Leitner, *Nature* **2003**, *423*, 930; c) L. A. Blanchard, D. Hancu, E. J. Beckman, J. F. Brennecke, *Nature* **1999**, *399*, 28; d) J. M. DeSimone, Z. Guan, C. S. Elsbemd, *Science* **1992**, *257*, 945.

[2] a) P. M. Gallagher, M. P. Coffey, V. J. Krukonis, N. Klasutis, *ACS Symp. Ser.* **1989**, *406*, 334; b) M. Wei, G. T. Musie, D. H. Busch, B. Subramaniam, *J. Am. Chem. Soc.* **2002**, *124*, 2513.

[3] a) N. Ventosa, S. Sala, J. Torres, J. Llibre, J. Veciana, *Crystal Growth & Design* **2001**, *1*, 299; b) P. M. Gallagher, V. Krukonis, G. D. Botsaris, *AIChE Symp. Ser.* **1991**, *87*, 96.

[4] C. A. Eckert, D. Bush, J. S. Brown, C. L. Liotta, *Ind. Eng. Chem. Res.* **2000**, *39*, 4615.

[5] a) J. C. De la Fuente Badilla, C. J. Peters, J. de Swaan Arons, *J. Supercrit. Fluids* **2000**, *17*, 13; b) F. W. Giacobbe, *Fluid Phase Equilib.* **1992**, *72*, 277; c) X. Zhang, B. Han, Z. Hou, J. Zhang, Z. Liu, T. Jiang, J. He, H. Li, *Chem. Eur. J.* **2002**, *8*, 5107.

[6] *The Merck Index*, 12th ed, (Ed.: S. Budavari), Merck & Co. Inc., Whitehouse Station, New Jersey, **1996**, p. 9.

[7] a) M. Poliakoff, S. M. Howdle, S. G. Kazarian, *Angew. Chem.* **1995**, *107*, 1409; *Angew. Chem. Int. Ed.* **1995**, *34*, 1275; b) S. G. Kazarian, M. F. Vincent, F. V. Bright, C. L. Liotta, C. A. Eckert, *J. Am. Chem. Soc.* **1996**, *118*, 1729; c) S. Akimoto, O. Kajimoto, *Chem. Phys. Lett.* **1993**, *209*, 263.

[8] a) T. Tassaing, P. Lalanne, S. Rey, F. Cansell, M. Besnard, *Ind. Eng. Chem. Res.* **2000**, *39*, 4470; b) S. G. Kazarian, R. B. Gupta, M. J. Clarke, K. P. Johnston, M. Poliakoff, *J. Am. Chem. Soc.* **1993**, *115*, 11099; c) Y. Iwai, D. Tanabe, M. Yamamoto, T. Nakajima, M. Uno, Y. Arai, *Fluid Phase Equilib.* **2002**, *193*, 203.

[9] F. E. Wubbolts, Ph. D. Thesis, University of Delft (Netherlands), **2000**.

[10] a) M. Yamamoto, Y. Iwai, T. Nakajima, Y. Arai, *J. Phys. Chem. A* **1999**, *103*, 3525; b) M. A. Blatchford, P. Raveendran, S. L. Wallen, *J. Am. Chem. Soc.* **2002**, *124*, 14818.

[11] $\Delta\tilde{\nu}_{CO}$ corresponds to $\tilde{\nu}_{CO}(X_{CO_2}) - \tilde{\nu}(X_{CO_2} = 0)$.

[12] The cybotactic region is the zone around the solute where the structural order of the solvent molecules has been influenced by the solute: C. R. Yonker, J. C. Linehan, J. L. Fulton in *Chemical Synthesis Using Supercritical Fluids*, chapter 3, (Eds.: P. G. Jessop, W. Leitner), Wiley-VCH, Weinheim, **1999**, p. 195.

[13] J. F. Brennecke, J. E. Chateauneuf, *Chem. Rev.* **1999**, *99*, 433.

[14] a) P. R. Wells, *Linear Free-Energy Relationships.* Academic Press, London, **1968**; b) C. Reichardt, *Solvent Effects in Organic Chemistry*, Verlag Chemie, Weinheim, **1979**.

Received: July 25, 2003 [Z921]

Modelling of the Adsorption of C_{60} on the Au(110) Surface

Richard J. Baxter,[a, b] Petra Rudolf,[c] Gilberto Teobaldi,[a] and Francesco Zerbetto*[a]

The adsorption of organic molecules on inorganic surfaces is a thriving field with applications that range from adhesion, lubrication and chromatographic separation to the modification of the properties of plasticized polymeric materials (e.g., varying the surface and interior concentration of reinforcing fillers), and even to the biocompatibility of artificial internal organs.

Gold surfaces are a prime example of "well-behaved" inorganic surfaces because their reactivity and reconstruction patterns are usually well-understood. While the Au(111) surface is the most studied and exploited because of its high stability, probably second is the more reactive Au(110), which reconstructs into a (1×2) missing row motif, in which alternate rows of atoms along $[1\bar{1}0]$ are removed to produce stable (111) microfacets with 8.16 Å periodicity and 1.4 Å height.[1] In recent years, C_{60} has become one of the most investigated molecules both because of its highly symmetrical shape and because of its properties, foremost among them its electron-accepting capacity. The interaction of C_{60} with gold surfaces has attracted much interest and the structural properties of the C_{60}/metal interface have been studied for Au(111),[2] Au(110),[3] Au(001),[4] and also for polycrystalline Au substrates.[5] The Au(110) missing row (1×2) reconstructed surface provides a corrugated surface, which places more stringent geometric constraints than Au(111) on the

[a] *Dr. R. J. Baxter, Dr. G. Teobaldi, Prof. F. Zerbetto*
Dipartimento di Chimica "G. Ciamician"
Università di Bologna
Via F. Selmi 2, 40126 Bologna (Italy)
Fax: (+39) 051 – 2099456
E-mail: gatto@ciam.unibo.it

[b] *Dr. R. J. Baxter*
Department of Materials, University of Oxford
Parks Road, Oxford, OX1 3PH (UK)

[c] *Prof. P. Rudolf*
Materials Science Centre, University of Groningen
Nijenborgh 4, 9747 AG Groningen (The Netherlands)

ARTICLE F:

Títol: Solute-solvent interactions governing preferential solvation phenomena of acetaminophen in CO_2-expanded organic solutions. A spectroscopic and theoretical study.

Autors: Santiago Sala, Yann Danten, Nora Ventosa, Thierry Tassaing, Marcel Besnard, Jaume Veciana

Publicació: Enviat a “The Journal of Supercritical Fluids”

(No presentat a la comissió de doctorat)

Solute-solvent interactions governing preferential solvation phenomena of acetaminophen in CO_2-expanded organic solutions. A spectroscopic and theoretical study.

Santiago Sala,[†] Yann Danten,[§] Nora Ventosa,[†]* Thierry Tassaing,[§] Marcel Besnard,[§]* Jaume Veciana[†]*

[†] Institut de Ciència de Materials de Barcelona (CSIC), Campus Universitari de Bellaterra; 08193-Cerdanyola (Spain)

[§] Laboratoire de Physico-Chimie Moléculaire, UMR 5803 CNRS-Université de Bordeaux I, 351 Cours de la Libération, 33405 Talence Cedex (France).

Corresponding author. Tel.: +34-93-5801853; fax: +34-93-5805729

E-mail address:

ventosa@icmab.es, vecianaj@icmab.es and m.besnard@lpcm.u-bordeaux1.fr

Solute-solvent interactions governing preferential solvation phenomena of acetaminophen in CO_2-expanded organic solutions. A spectroscopic and theoretical study.

S. Sala,[†] Y. Danten,[§] N. Ventosa,[†]* T. Tassaing,[§] M. Besnard,[§]* J. Veciana[†]*

[†] Institut de Ciència de Materials de Barcelona (CSIC), Campus Universitari de Bellaterra; 08193-Cerdanyola (Spain)

[§] Laboratoire de Physico-Chimie Moléculaire, UMR 5803 CNRS-Université de Bordeaux I, 351 Cours de la Libération, 33405 Talence Cedex (France).

Abstract

The present work aims to characterize the nature and intensity of the specific and non-specific solute-solvent interactions responsible for the different solvating behaviour of "CO_2-expanded ethanol" and "CO_2-expanded acetone" towards acetaminophen(**1**), an analgesic drug commercially known as paracetamol. The intermolecular interactions between acetaminophen and solvent molecules involved in these expanded media and its sensitivity to solvent composition changes, have been analyzed by high-pressure IR spectroscopy, Linear Solvation Energy Relationships, and theoretical ab-initio calculations performed with acetaminophen-$(ethanol)_n$ and acetaminophen-$(acetone)_n$ complexes. It comes out that the distinct perturbation experienced by the cybotactic region of acetaminophen in "CO_2-expanded ethanol" and "CO_2-expanded acetone" when CO_2 content increases is basically a consequence of the higher sensitivity to solvent composition changes of the dipole-dipole interactions, established between the acetaminophen carbonyl group and acetone solvent molecules, in relation to that of the hydrogen bond interactions existing between this group and ethanol solvent molecules.

Keywords

Solute-solvent interactions, CO_2-expanded solvents, IR spectroscopy, ab-initio calculations, acetaminophen, LSER.

1. Introduction

In contrast with liquid solvents, the solvation power of compressed fluids (e.g. CO_2) can be tuned by pressure changes, which propagate much more quickly than temperature and composition solvent changes. Therefore, using compressed solvent media it is often possible to synthesize materials with unique physico-chemical characteristics (size, porosity, polymorphic nature, morphology, etc..) unachievable with classical liquid media [1,2]. Moreover, during the past few years, compressed CO_2 has gained considerable attention as a green substitute for organic solvents because of its non-toxicity, the ease of its removal, its abundance, low cost, and tunability of solvation power [3]. Nevertheless, the low solubility of the majority of polar and ionic materials seriously limits the possibilities of using such solvent media. By contrast, carbon dioxide expanded solvents, composed of sub-critical CO_2 condensed into an organic solvent, have a much higher capacity to dissolve polar compounds than pure CO_2 [4,5]. In these sub-critical mixtures, the organic solvent is substantially replaced (up to 80 vol.%) by CO_2. Consequently CO_2-expanded solvents can be used to generate a continuum of solvent media with tunable solvation power, as a function of either its composition or expansion degree, offering endless opportunities in material processing, such as micro- and nanoparticle formation [6], and in reaction and separation schemes [5,7]. In order to maximize the miscibility and dissolution of materials, and make possible all kinds of chemical processes in CO_2-expanded solvents, a deep knowledge

of intermolecular solute-solvent interactions in this media is essential. However, up to now most of the investigations concerning the solvation power of CO_2-expanded solvents have been based on the measurement of macroscopic properties (phase changes, thermodynamic parameters, etc…) [8] being studies at molecular level very scarce.

Insert Figure 1 about here

The nature and contents of the organic solvent determines strongly the solvation behavior of a "CO_2-expanded solvent" over a given compound [9]. In a recent communication [10], we have analyzed at the molecular level, through high pressure infrared (IR) spectroscopy, the origin of differential solvating power of "CO_2-expanded acetone" and "CO_2-expanded ethanol" of N-(4-hydroxyphenyl)acetamide (**1**); an analgesic drug commercially known as acetaminophen or paracetamol [11]. As shown in Figure 1, the increase in CO_2 content causes a more pronounced acetaminophen solubility decrease in "CO_2-expanded acetone" than in "CO_2-expanded ethanol". Thus, in the "**1**/acetone/CO2" system, CO_2 behaves as an anti-solvent from the very low CO_2 concentrations [4], whereas in the "**1**/ethanol/CO2" system, the solubility curve follows the ideal dilution behavior up to a molar fraction of X_{CO2}=0.2 indicating an ideal co-solvent behavior of CO_2 up to this concentration [12,13]. In addition, at higher values of X_{CO2}, the CO_2 anti-solvent character is manifested in a softer way than in the former system. As schematically represented in Figure 2, we have demonstrated that this differential solubility behavior is related to the different perturbation of the cybotactic region of acetaminophen in both "CO_2-expanded solvents" as the CO_2 content increases [10,14].

Insert Figure 2 about here

Several studies have been carried out to find out specific and non-specific solute-solvent intermolecular interactions in supercritical solvents, mainly in pure supercritical CO_2 or modified by small amounts of polar co-solvents [15,16]. CO_2-expanded solutions and their solvent power have been mainly analyzed by UV-Vis spectroscopy [17,18]. Recently, we have used IR spectroscopy to analyze solvent effects in these expanded media [10,19]. In the present work, by using experimental IR spectroscopic measurements along with its Linear Solvation Energy Relationship (LSER) [20] analysis and theoretical calculations, we investigate the fundamental nature of the solute-solvent intermolecular interactions which cause the differential clustering phenomena that experience acetaminophen molecules in "CO_2-expanded acetone" and in "CO_2-expanded ethanol". We also analyze how the relative contribution of these intermolecular forces are affected by the increase of CO_2 solvent content. This study provides a molecular insight on the role of some molecular functional groups in the solubilization process of a molecular material in "CO_2-expanded solvents".

2. Experimental

2.1. Materials and solvents.

Acetaminophen (purity 99%), N-(4-ethoxyphenyl)acetamide (purity 97%) and all liquid solvents (spectroscopic grade) were purchased from SIGMA-ALDRICH (Steinheim, Germany) and employed without further purification. CO_2 (purity 99.995%) was supplied by Carburos Metálicos S.A. (Barcelona, Spain).

2.2. IR spectroscopic measurements in "CO_2-expanded solvents".

IR spectroscopic data under high pressure was acquired using a home-made experimental set-up which allows to modify the CO_2 content of the sample without changing its pressure and temperature. As shown in Figure 3, this device was composed of a 6 mL stainless steel agitated vessel (R), an optical cell (C) [21] and a fluid separator (S, 'Top Industrie' S. A.) which controls the total volume, V_T, of the device and enables system composition modifications while keeping pressure constant. The optical cell windows were made of Zinc Selenide or Silicon and a cooper spacer was placed between them to fix the path-length. In order to control the system temperature, the whole device was coated with a heating resistance connected to a temperature controller PID ('T C' S.A.). The CO_2 supply to this device was done through a manual pump (PU1, 'Top Industrie' S. A.) connected to a CO_2 bottle. This configuration was assembled to an infrared spectrometer Bio-Rad (type FTS-60A). The optical path-length employed was 90 μm, the spectral resolution was 2 cm^{-1} and the number of accumulated spectra was 50.

Prior loading, the cell was evacuated by connecting a pump to the purge valve (V3). A known initial volume, V_I, of either pure organic solvent or acetaminophen solution in pure organic solvent, with an initial supersaturation ratio β_I=0.25, was injected into the cell. The working temperature, T_W, was selected in the temperature controller, and the initial liquid solvent or solution was pressurized up to the working pressure, P_W, by moving the piston of the fluid separator. Then, CO_2 was slowly added until the CO_2 molar fraction, X_{CO2}, of the solvent mixture reached the desired value. During the CO_2 addition the P_W was kept constant by increasing V_T. After recording the IR spectrum,

CO_2 was added to the system to reach a higher system X_{CO2} value and to proceed to a new measurement.

Insert Figure 3 about here

In "ethanol/CO_2" experiments, the difficulty in mixing both components [22] leads to a long equilibrium time and we could not use the device and procedures described above. In that case, the fluid separator (S) was removed and the experiments were performed at constant V_T. The CO_2 was slowly added to an initial volume, V_I, of either pure ethanol or acetaminophen solution in ethanol, with β_I=0.25, until reaching P_W. With this working procedure, it was necessary to load different amounts of V_I into the cell in order to perform IR measurements at different values of X_{CO2}.

To ensure that the system has reached the equilibrium, measurements were repeated until no spectral changes were observed. The spectra of acetaminophen were obtained by removing from the spectra of the ternary mixtures "**1**/organic solvent/CO_2" the spectra of the corresponding "organic solvent/CO_2"mixture with the same CO_2 content. For "CO_2-expanded acetone" mixture, the ν_{CO} band of acetaminophen was partially overlapped by the ν_{CO} band of acetone, nevertheless the former was successfully isolated after spectral subtraction. To measure the IR spectra of acetaminophen in "CO_2-expanded ethanol" in the spectral region of NH and OH stretching modes, deuterated ethanol was used. Spectra of acetaminophen solutions with different values of β_I ranging from 0.25 to 1, at P_W=10MPa, T_W=315 K and constant solvent composition, were measured. The lack of any observed spectral variations with different values of β_I ensures that solute-solute interactions can be ruled out under these acetaminophen concentrations.

2.3. IR spectroscopic measurements in liquid solvents at atmospheric pressure.

The infrared spectra used for the Linear Solvation Energy Relationship (LSER) analysis were obtained after averaging 50 spectra measured on a Perkin Elmer spectrometer at 2 cm^{-1} resolution. We used a commercial (Perkin Elmer) IR liquid cell equipped with ZnSe windows and teflon spacers of thicknesses ranging between 25 and 500μm for the measurements of diluted solutions of **1** and N-(4-ethoxyphenyl)acetamide (**2**) [23], with a solute concentration ≤ 0.35mol/l. Spectra of compound **1** and **2** have been obtained by removing from the solution spectra, those corresponding to pure solvents recorded under the same conditions.

3. Results and Discussion

3.1. IR spectroscopic studies.

Vibrations of a solute or solvent molecule are usually quite sensitive to the environment of that molecule [14,24]. In this work, high-pressure mid-IR vibrational spectroscopy has been used to probe solute-solvent intermolecular interactions existing in acetaminophen CO_2-expanded solutions, and to study how they are affected by CO_2 solvent content changes. The mid-IR spectra of acetaminophen were measured in the spectral range 400 to 3700 cm^{-1} for "CO_2-expanded ethanol" and "CO_2-expanded acetone" at 315 K, 10 MPa and CO_2 molar fraction ranging from 0 to 0.75, using the equipment and procedures detailed in the experimental section.

Insert Figure 4 about here

As displayed in Figure 4, the spectra of **1** in both expanded solvents show an isolated asymmetric band in the spectral range 1650-1700cm^{-1}, which can be unambiguously

assigned to the acetaminophen carbonyl ν_{CO} stretching mode. The assignment of the NH and OH stretching modes which should be observed in the 3100 to 3600 cm^{-1} spectral range is less obvious as two overlapping bands are observed in the "CO_2-expanded acetone" system whereas a single asymmetric band is noticeable for "CO_2-expanded ethanol" (Figure 5).

Insert Figure 5 about here

In order to assign properly these two modes, we have proceeded in two steps. Firstly, we have compared the spectra of a model compound, the 4-(ethoxyphenyl)acetamide (**2**), with that of acetaminophen in acetone (see Figure 6). Since in **2** the hydroxyl group of acetaminophen is replaced by an ethoxy group, the comparison of the spectra of the two molecules should allow distinguishing between the ν_{OH} and ν_{NH} modes. Indeed, the examination of Figure 7 (top) shows that the ν_{NH} stretching mode can be assigned to the intense component observed at lower frequency in the region of the two overlapping bands of acetaminophen in "CO_2-expanded acetone", as represented in Figure 5 (top).

Insert Figure 6 about here

In a second step, the IR spectra of **1** and **2** in deuterated ethanol were measured. In the spectral range of interest, a single asymmetric band is observed for both molecules with bandshapes and band center frequencies almost identical (Figure 7 (bottom)). It is well known that in hydrogenated/deuterated alcohol isotopic mixtures, the hydroxyl proton easily exchange with deuterium [25,26]. It comes out that the observed bands in Figure 7 (bottom) and Figure 5 (bottom) can be assigned to the ν_{NH} mode. This assignment is

supported by ^{1}H-RMN spectroscopic measurements, which show a total replacement of the phenolic proton of acetaminophen by deuterium, and only a partial isotopic substitution of the amide proton.

Insert Figure 7 about here

As the CO_2 concentration increases, the shape of ν_{CO} carbonyl, ν_{NH} amino and ν_{OH} hydroxy bands of the acetaminophen, shown in Figures 4 and 5, do not change although all of them experience blue frequency shifts. These shifts suggest that the clustering of the organic solvent around acetaminophen molecules, arising from specific and non-specific interactions between solvent molecules and acetaminophen functional groups (carbonyl, amino and hydroxyl), became weaker as X_{CO2} increases in the ternary mixture.

The evolution of the frequency shifts of the ν_{CO} carbonyl band ($\Delta\nu_{CO}$) and the ν_{NH} amino band ($\Delta\nu_{NH}$) with X_{CO2} changes in "CO_2-expanded ethanol" and "CO_2-expanded acetone" [27], are reported in Figure 8. We also report on this figure the frequency shifts expected for an ideal mixture. They are obtained by assuming a linear evolution of the shift between the values corresponding to acetaminophen in pure CO_2 and in the pure organic solvents. Because of the measurement of the IR spectra of acetaminophen in pure CO_2 is not possible due to its extremely low solubility, we have assumed that these values are very close to $\tilde{\nu}_{CO}$ and $\tilde{\nu}_{NH}$ in a non-interactive solvent, which were obtained from the independent term of the solvent-induced LSER acetaminophen ν_{CO} and ν_{NH} frequency shift models reported in Table 1 (*vide infra*) [28].

Insert Figure 8 about here

A non-linear evolution of the blue-shift, as the CO_2 content of the solvent increases, is observed for both bands in the two CO_2-expanded solvents. We also notice that the evolution of $\Delta\nu_{CO}$ is markedly different in "CO_2-expanded acetone" than in "CO_2-expanded ethanol". In contrast, the evolution of the ν_{NH} frequency shift is almost independent on the nature of the organic solvent. The departure from the linear ideal evolution of the ν_{NH} and ν_{CO} band-center shifts with the CO_2 concentration, observed in both expanded solvents, put in evidence a preferential solvation of acetaminophen molecules by organic solvent molecules due to specific and/or non-specific interactions between the organic solvent (ethanol or acetone) and acetaminophen functional groups [29]. As observed in Figure 8 (top), the blue shift evolution experienced by ν_{CO} band is clearly different in both "CO_2-expanded solvents". The evolution of $\Delta\nu_{CO}$ in "CO_2-expanded ethanol" is smoother and reaches lower values than in "CO_2-expanded acetone". This result indicates that the interactions between ethanol, a hydrogen-bond donor (HBD) solvent, and the carbonyl group of **1** are less sensitive towards CO_2 solvent content increase than those established between acetone, a non-HBD, and the carbonyl group. In contrast, Figure 8 (bottom) shows a similar evolution of $\Delta\nu_{NH}$ with X_{CO2} in both "CO_2-expanded solvents", indicating that the interactions between the HBD ethanol molecules and the amino group of acetaminophen have a similar sensitivity towards a X_{CO2} increase than those between the non-HBD acetone and the amino group. In order to get insights on the molecular interactions at the origin of the previous observations, we have determined the nature and the relative importance of the specific and non-specific interactions between acetaminophen functional groups and, acetone and ethanol solvent molecules. This study has been done through a Linear Solvation Energy Relationship (LSER) analysis of acetaminophen solvent-induced IR

frequency shifts, and the analysis of the energetically favored acetaminophen-ethanol and acetaminophen-acetone interaction geometries calculated by an ab initio method.

3.2. Linear Solvation Energy Relationship Analysis.

One of the most ambitious, and successful, quantitative multi-parameteric treatment of solvent effects is that introduced by Taft et al, called Linear Solvation Energy Relationship [30-32]. The LSER theory relates the free energy changes of a given molecular process that takes place in solution with several specific and non-specific properties of the solvents in which the process is carried on. LSER assumes linear free energy or electronic energy relationships for each of the contributing terms to the observed solvent effects, and presumes that each term is independent and additive. Such a multiparametric treatment has been used for correlating molecular vibrational frequencies in several systems [20,33]. The generalized LSER equation for correlation of solvent effects on a given IR vibrational mode (i) frequency shift ($\Delta\tilde{\nu}_i^{solv}$) adopts the form of Equation 1.

$$\Delta\tilde{\nu}_i^{solv} = \Delta\tilde{\nu}_i^{0} + s(\pi^* + d\delta) + a\alpha + b\beta + e\xi \qquad (1)$$

In this expression π^*, δ, α, β and ξ are descriptive solvatochromic parameters describing the solvent: π^* corresponds to a measure of the solvent polarity-polarizability [34], δ is a discontinuous "polarizability correction" term for certain solvent types [35], α is a measure of the solvent hydrogen-bond donor acidity and describes the ability of a solvent to accept an electron pair in a solvent-solute interaction [36], β parameter refers to the hydrogen-bond acceptor (HBA) basicity of the solvent and describes the ability of a solvent to donate an electron pair in a solvent-solute interaction [37], and ξ is a coordinate covalency parameter useful in correlating certain

types of basicity properties [20,38]. The independent term $\Delta\tilde{\nu}_i^0$ represents the difference between ν_i band frequency measured in an "ideal" non-interactive solvent, in which all the solvatochromic parameters are null, and in the gaseous state. Coefficients *s*, *d*, *a*, *b* and *e* are characteristic of the vibrational mode (i) of the molecule under study being independent of the solvent. These coefficients are indicative of the vibrational mode sensitivity towards each solvent property (π^*, δ, α, β and ξ) variation. Coefficients with a negative sign, point out that an increase of the associated solvent-solute interaction strength causes a vibrational energy decrease of the vibrational mode under study and therefore a red frequency shift. On the contrary, coefficients with positive sign indicate that an increase of the associated solvent-solute interaction strength provokes a vibrational energy increase of the vibrational mode and consequently a blue frequency shift.

The solvent-induced IR frequency shift measured for the C=O stretching vibration of acetaminophen and of 4-(ethoxyphenyl)acetamide varies 64cm^{-1} in going from toluene ($\tilde{\nu}$ = 1697) to water ($\tilde{\nu}$ = 1633) as solvent, while the solvent-induced IR frequency shift observed for the N-H stretching vibration of 4-(ethoxyphenyl)acetamide changes 166 cm^{-1} in going from chloroform ($\tilde{\nu}$ = 3439) to pyridine ($\tilde{\nu}$ = 3273).

Table 1 summarizes the resulting solvent-induced IR frequency shift LSER models, calculated for the C=O stretching vibrational mode of molecules **1** and **2**, and for the N-H stretching vibrational mode of compound **2**. Due to overlapping between the ν_{NH} and ν_{OH} bands it is not possible to calculate the solvent-induced frequency shifts LSER models for the N-H and the O-H stretching vibrational modes of acetaminophen. The LSER models were calculated from the C=O stretching vibrational mode frequency shifts of **1** ($\Delta\tilde{\nu}_{CO}^{solv}$(**1**)) and **2** ($\Delta\tilde{\nu}_{CO}^{solv}$(**2**)), and the N-H stretching vibrational mode

frequency shifts of **2** ($\Delta\tilde{\nu}_{NH}^{solv}$ (**2**)), measured in different liquid solvents with known π^*, δ, α, β and ξ parameters [39]. In order to guarantee a complete representation of all types of solute/solvent interactions, the selected solvents were taken from the eleven groups of a classification of the most common organic solvents published elsewhere [40]. Coefficients *s*, *d*, *a*, *b* and *e* and the independent term $\Delta\tilde{\nu}_i^0$ for each LSER model, were calculated by fitting, through a multivariable linear regression, the frequency shifts of the band under study together with the corresponding solvent parameters to Equation 1 [41]. By mean of a statistical analysis those coefficients with a low significance level were removed from the calculated models. The final LSER models described in Table 1 are those which only include the solute/solvent interaction terms that contribute significantly to the solvent induced IR frequency shifts experimented by each of the vibrational modes studied.

LSER models summarized in Table 1 show that the nature and strength of solvent-solute interactions that influence the ν_{CO} frequency shifts of compounds **1** and **2** are identical. By contrast, such solvent-solute interactions are very different to those governing the ν_{NH} frequency shifts of **2**. Indeed, the LSER models describing the ν_{CO} frequency shifts of compounds **1** and **2**, show that $\Delta\tilde{\nu}_{CO}^{solv}$ is firstly sensitive to changes of the HBD acidity of the surrounding media ($a\alpha$) [42], secondly to polarity/polarizability variations of the solvent media ($s\pi^*$) and, finally, to changes of the HBA basicity of the solvent ($b\beta$) [42]. However, the LSER model describing the ν_{NH} solvent induced frequency shifts, show that changes of the HBA basicity of the surrounding media ($b\beta$ and $e\xi$) strongly influence the $\Delta\tilde{\nu}_{NH}^{solv}$ of acetaminophen, meanwhile variations of the HBD acidity of the solvent media only provokes small modifications of ν_{NH} vibrational frequency. In this work we have used the LSER model

describing the solvent-induced IR frequency shift of ν_{NH} (**2**) to describe in a first approximation the solvent effects over the ν_{NH} (**1**) of acetaminophen molecule. In support of this approximation is the fact that solvent effects over ν_{CO} frequency shifts are exactly the same for compounds **1** and **2**.

Insert Table 1 about here

Using the solvatochromic parameters ($\pi*$, α, β and ξ) corresponding to acetone and ethanol [43,44], we have calculated through the LSER models of Table 1 the influence of the different solvent/solute interactions to the solvent-induced IR frequency red shift experimented by the C=O and by the N-H stretching vibrational modes of acetaminophen in both solvents. As it is shown in Figure 9 (top), the solvent-induced frequency shift experimented by ν_{CO} in acetone is mainly due to dipole-dipole solvent-solute interactions ($s\pi^*$), whereas the solvent-induced $\Delta\tilde{\nu}_{CO}^{solv}$ in ethanol is principally caused by stronger H-bond solute-solvent interactions in which the ethanol acts as H-bond donor ($a\alpha$). However, as it is observed in Figure 9 (bottom) the solvent-induced frequency shifts experimented by ν_{NH}, in both solvents, are caused essentially by H-bond solute-solvent interactions in which the solvent acts as H-bond acceptor ($b\beta$) and acetaminophen acts as H-bond donor.

Insert Figure 9 about here

In brief, the LSER analysis of $\Delta\tilde{\nu}_{CO}^{solv}$(**1**) in ethanol and acetone points out the presence of specific and non-specific interactions between the carbonyl group of acetaminophen and solvent molecules. The large difference between $a\alpha$ terms, observed in ethanol and

acetone, indicates the existence of a strong hydrogen bond interaction between the C=O group and HBD ethanol molecules, which is non-existent with acetone molecules. This analysis also reveals the presence of dipole-dipole interactions between the carbonyl group and the solvent molecules of similar strength for acetone and for ethanol, measured by the $s\pi^*$ term, and interactions between the C=O group and the solvent molecules behaving as Lewis bases, as measured by the $b\beta$ term, which are weaker than the other types of interactions in both solvents. In contrast, the LSER analysis of $\Delta\tilde{\nu}_{NH}^{solv}$(**1**), indicates that the strongest interaction between the amino group of acetaminophen and the solvent molecules is a hydrogen bond type interaction, as measured by the $b\beta$ term, in which the amino group is the HBD in the case of acetone as well as in the case of ethanol. This analysis also reveals a very similar relative strength of the different types of solvent-solute interactions, for ethanol and for acetone.

In order confirm the fundamental nature of the specific and non-specific interactions and to quantify the strengths of interactions between acetaminophen and both solvent molecules, derived from experimental LSER analysis, solute-solvent interactions between acetaminophen and ethanol (or acetone) solvent molecules, were determined by ab initio calculations.

3.3. Theoretical calculations.

Ab initio calculations have been carried out using the Gaussian-98 program [45]. Structures have been fully optimized at the RHF/6-31G level for dimeric complexes composed by one molecule of acetaminophen and one ethanol (or acetone) molecule interacting with one of the three distinct chemical groups of acetaminophen, namely hydroxyl, amino and carbonyl groups. Structures were also fully optimized for

acetaminophen·(ethanol)$_3$ and acetaminophen·(acetone)$_3$ complexes in which each of the three chemical groups interact with a solvent molecule. The relevant computed internal bonds lengths of the C=O, O-H and N-H groups of acetaminophen, the intermolecular distances and relative angles are reported in Tables 2 and 3 with binding energy values. For all calculated complexes, the acetaminophen structure interacting with ethanol or acetone species was allowed to vary but always found close to that of the most stable conformer of acetaminophen found by Binev et al [46]. For dimeric complexes, the calculated interaction energies (ΔE_{int}) have been corrected using the basis set superposition error (BSSE) by the full counterpoise (CP) technique [47]. For oligomeric complexes of higher size, the BSSE corrected binding energy has been obtained according to the site-site function counterpoise method (SSFC) [48].

Insert Figure 10 about here

For dimeric complexes formed between acetaminophen and ethanol (or acetone), the most stable structure is found with the solvent molecule interacting with the OH group of acetaminophen. In that case, a quasi-linear hydrogen O-H¨¨O intermolecular bonding is formed between OH group of acetaminophen and the O-atom of ethanol (structure **D1** in Table 2) or acetone (structure **D'1** in Table 3). The BSSE corrected binding energy values $\Delta E_{int}^{(CP)}$ are -8.9 kcal/mol and -8.1 kcal/mol, respectively (Tables 2 and 3). As the solvent molecule interacts with the NH group of acetaminophen, a quasi-linear N-H¨¨O intermolecular bonding is formed between the proton of the NH group of acetaminophen and the O atom of solvent leading to structures **D2** (Table 2) and **D'2** (Table 3) or ethanol and acetone respectively. Binding energies $\Delta E_{int}^{(CP)}$ are -7.0 kcal/mol (ethanol) and -6.8 kcal/mol (acetone) (Tables 2 and 3). When the solvent

molecule interacts with the CO group, the nature of the intermolecular interactions differs according whether ethanol or acetone is concerned. With ethanol, acetaminophen forms a hydrogen bond with the O-atom of the CO group which plays the role of proton acceptor centre. In this structure (**D3** in Table 2), the BSSE corrected binding energy $\Delta Eint^{(CP)}$ is -6.8 kcal/mol. In contrast, with acetone, the intermolecular interaction results from dipole-dipole interactions and lead to the formation of a complex with a structure (**D'3** in Table 3) in which the CO group of acetone interacts in a head to tail configuration with the CO group of acetaminophen. The corresponding BSSE corrected binding energy $\Delta Eint^{(CP)}$ is -4.8 kcal/mol (Tables 2 and 3).

Insert Table 2 about here

Finally, we have considered complexes of acetaminophen in which the CO, OH and NH groups interacts with a solvent molecule. Optimized structures of the tetrameric complexes are displayed on Figures 10A (ethanol) and 10B (acetone). For ethanol and acetone, it is found that the structure of the tetrameric complex is a quasi superposition of the three dimeric complex structures. The BSSE corrected total binding energy $\Delta Eint^{(CP)}$ and the separate solvent-acetaminophen pair interaction energy values have also been gathered in Tables 2 and 3.

Insert Table 3 about here

To summarize, it comes out from ab initio calculations that OH and NH functional groups of acetaminophen act as proton donor centers in their interaction with acetone and ethanol molecules. From the comparison of the pair interaction energies of the OH and NH functional groups interacting with acetone or ethanol, we conclude that the

interactions are stronger with ethanol than with acetone. It is also noteworthy that the CO acetaminophen group interacts with ethanol through an intermolecular H-bond whereas for acetone dipole-dipole interactions are involved. All these conclusions validate the results obtained from LSER analysis of band frequency shifts.

4. Conclusions

From the knowledge about the interactions between acetaminophen functional groups with acetone and ethanol solvent molecules, derived from LSER analysis and ab initio calculations, and from the variation of $\Delta\nu_{CO}$ and $\Delta\nu_{NH}$ with CO_2 solvent content in "CO_2-expanded ethanol" and in "CO_2-expanded acetone", valuable information about intermolecular solute-solvent interactions can be withdrawn. Remarkable are the informations dealing with the sensitivity, towards the CO_2 content increase, of the specific and non-specific interactions established between acetone and ethanol solvent molecules with the CO and NH functional groups of acetaminophen. Indeed the smoother blue shift for ν_{CO} of acetaminophen in "CO_2-expanded ethanol" than in "CO_2-expanded acetone", observed in Figure 8 (top), as CO_2 content increases, points out that the dipole-dipole interactions established between the carbonyl group of **1** and acetone molecules are more easily perturbed by CO_2 than the H-bond interactions between the C=O group and ethanol molecules. On the other hand, the similar evolution of $\Delta\nu_{NH}$ with X_{CO2} increase, in both expanded solvents, indicates that the H-bond interactions between the acetaminophen NH group and the organic solvent molecules, in which the N-H group behaves as H-bond donor, are equally sensitive to the CO_2 solvent content increase in "CO_2-expanded ethanol" than in "CO_2-expanded acetone" even though the strength of this interaction is higher with ethanol than with acetone molecules. Due to

band overlapping, it was not possible to study the perturbation produced by the CO_2 solvent content changes of the interactions established between the OH group of acetaminophen with acetone and ethanol solvent molecules. However, taking into account that the OH group interacts equally with ethanol and acetone through an H-bond interaction, in which the OH acetaminophen group behaves as H-bond donor, we expect an equal sensitivity of both interactions towards CO_2 solvent content changes, as it was experimentally observed for the NH group.

These results point out that the more abrupt perturbation experienced by the cybotactic region of acetaminophen in "CO_2-expanded acetone" than in "CO_2-expanded ethanol", when the CO_2 solvent content increases, is mainly due to the markedly higher sensitivity, towards CO_2 solvent content changes, of the dipole-dipole interactions between C=O and acetone than of the H-bond interactions between the carbonyl group and ethanol. Thus, the evolution of the microscopic observable ν_{CO} when CO_2 concentration increases in both CO_2-expanded solvents can be used as a molecular probe to interpret the differential solubility behavior of acetaminophen in "CO_2-expanded ethanol" and in "CO_2-expanded acetone". Indeed, as we have shown in a previous work [10], there exist a good linearity between the $\Delta\nu_{CO}$ shift and the free energy of solvation of **1,** a macroscopic observable, in both systems.

Summarizing, the effect of CO_2 content over the intermolecular interactions between the C=O and N-H groups of acetaminophen with ethanol and acetone solvent molecules, in "CO_2-expanded ethanol" and in "CO_2-expanded acetone", were deeply studied in the present work. We have demonstrated that the dipole-dipole interactions between the carbonyl acetaminophen group and acetone molecules suffer a more effective disruption by a CO_2 content increase than the H-bond interactions between the C=O group and

ethanol, where the ethanol behaves as H-bond donor. We have proved that the H-bond type interactions established between the acetaminophen amino group and the organic solvent molecules, where the N–H group behaves as H-bond donor, are equally perturbed by the CO_2 solvent content increase in both CO_2-expanded solvents. This information can be highly useful for the interpretation and prediction of the solubility behavior, in "CO_2-expanded ethanol" and in "CO_2-expanded acetone", of other organic compounds with N-aryl amide and phenol groups in their molecular structure.

Finally, we have proved that the methodology used in the present study is a good procedure for the analysis at the molecular level of preferential solvation phenomena in "CO_2-expanded solvents" and it can be used as a general methodology for the interpretation of solvation phenomena in such new compressed solvent media.

Acknowledgments

This work was supported by a grant from the contract HPMT-CT-2000-00143 between the European Community and the Université de Bordeaux I, and also by grants from DGI, Spain (project MAT2003-04699) and DGR, Catalunya (project 2001 SGR 00362). Dr. Nora Ventosa thanks to the "Ramon y Cajal" Program of the Ministerio de Educiación y Ciencia (Spain) for her contract.

References

[1] Y.-P. Sun (Ed.), Supercritical Fluid Technology in Material Science and Engineering, Marcel Dekker, New York, 2002.

[2] P. G. Jessop, W. Leitner (Eds.), Chemical Synthesis Using Supercritical Fluids, Wiley-VCH, Weinheim, 1999.

[3] E.J. Beckman, Supercritical and near-critical CO_2 in green chemical synthesis and processing, J. Supercrit. Fluids, 28 (2004) 121.

[4] P.M. Gallagher, M.P. Coffey, V.J. Krukonis, N. Klasutis, Gas Antisolvent Recrystallization: New process to recrystallize compounds insoluble in SCF, in: K.P. Johnston, J.M. Penninger (Eds.), ACS Symposium Series 406, American Chemical Society, Washington, DC, 1989, p. 334.

[5] M. Wei, G.T. Musie, D.H. Busch, B. Subramaniam, CO_2-expanded solvents: Unique and versatile media for performing homogeneous catalytic oxidations, J. Am. Chem. Soc., 124 (2002) 2513.

[6] N. Ventosa, S. Sala, J. Veciana, DELOS process: a crystallization technique using compressed fluids - 1. Comparison to the GAS crystallization method, J. Supercrit. Fluids, 26 (2003) 33.

[7] C.A. Eckert, C.L. Liotta, D. Bush, J.S. Brown, J.P. Hallett, Sustainable reactions in Tunable solvents, J. Phys. Chem. B,. 108 (2004), 18108.

[8] J. de la Fuente Badilla, C.J. Peters, J. de Swaan Arons, Volume expansion in relation to the gas-antisolvent process, J. Supercrit. Fluids, 17 (2000) 13.

[9] Wubbolts, F. E. PhD Thesis, University of Delft, Netherlands, 2000.

[10] S. Sala, T. Tassaing, N. Ventosa, Y. Danten, M. Besnard, J. Veciana, Molecular insight, through IR spectroscopy, on solvating phenomena occurring in CO2-expanded solutions, ChemPhysChem, 5 (2004) 243.

[11] The Merck Index, Twelfth Edition, (Ed.: S. Budavari), Merck & CO INC., Whitehouse Station, New Jersey, 1996, p. 9.

[12] N. Ventosa, S. Sala, J. Veciana, J. Torres, J. Llibre, Depressurization of an expanded liquid organic solution (DELOS): A new procedure for obtaining submicron- or micron-sized crystalline particles, Cryst. Growth Des., 1 (2001) 299.

[13] A. Shariati, C.J. Peters, Measurements and modeling of the phase behavior of ternary systems of interest for the GAS process: I. The system carbon dioxide plus 1-propanol plus salicylic acid, J. Supercrit. Fluids, 23 (2002) 195.

[14] The cybotactic region is the zone around the solute where the structural order of the solvent molecules has been influenced by the solute: C. Reichardt, Solvents and Solvent Effects in Organic Chemistry, Wiley-VCH, Weinheim 2003.

[15] J.L. Fulton, G.G. Yee, R.D. Smith, Hydrogen-bonding of methyl alcohol-d in supercritical carbon-dioxide and supercritical ethane solutions, J. Am. Chem. Soc., 113 (1991) 8327.

[16] D.L. Tomasko, B.L. Knutson, F. Pouillot, C.L. Liotta, C.A. Eckert, Spectroscopic study of structure and interactions in cosolvent-modified supercritical fluids, J. Phys. Chem., 97 (1993) 11823.

[17] S.P. Kelley, R.M. Lemert, Solvatochromic Characterization of the liquid-phase in liquid-supercritical CO_2 mixtures, 42 (1996) 2047.

[18] A. Striolo, N. Elvassore, T. Parton, A. Bertucco, Relationship between volume expansion, solvent-power, and precipitation in GAS processes, 49 (2003) 2671.

[19] S. Sala, N. Ventosa, T. Tassaing, M. Cano, Y. Danten, M. Besnard, J. Veciana, Infrared spectroscopic investigation of the synergistic enhancement of the solubility of hexamethylenetetramine in sub-critical CO_2-ethanol mixtures, ChemPhysChem, submitted.

[20] M.J. Kamlet, J.L.M. Abboud, M.H. Abraham, R.W. Taft, Linear Solvation Energy Relationships .23. A comprehensive collection of the solvatochromic parameters, pi-star, alpha and beta, and some methods for simplifying the generalized solvatochromic equation, J. Org. Chem., 48 (1983) 2877.

[21] V. Bergeot, T. Tassaing, M. Besnard, F. Cansell, A.F. Mingotaud, Anionic ring-opening polymerization of epsilon-caprolactone in supercritical carbon dioxide: parameters influencing the reactivity, J. Supercrit. Fluids, 28 (2004) 249.

[22] A. Weber, L.V. Yelash, T. Kraska, Effect of the phase behaviour of the solvent-antisolvent systems on the gas-antisolvent-crystallisation of paracetamol, J. Supercrit. Fluids, 33 (2005) 107.

[23] The Merck Index, Twelfth Edition, (Ed.: S. Budavari), Merck & CO INC., Whitehouse Station, New Jersey, 1996, p. 1239.

[24] M.M. Wohar, J.K. Seehra, P.W. Jagodzinski, Correlation between solvent-induced vibrational frequency-shifts of the C=O moiety and solvent electron-acceptor numbers - tetramethylurea, Spectroc. Acta Pt. A-Molec. Biomolec. Spectr., 44 (1988) 999.

[25] J.K.M. Sanders, B.K. Hunter, NMR Spectroscopy, Oxford University Press, Oxford 1993.

[26] H. Friebolin, Basic One- and Two-dimensional Spectroscopy, Wiley-VCH, Weinheim 1991.

[27] For each vibrational mode studied, $\Delta\nu$ corresponds to $\tilde{\nu}$ (X_{CO2})- $\tilde{\nu}$ (X_{CO2}=0), $\tilde{\nu}$ being the frequency at the band-center.

[28] $\tilde{\nu}_{CO}$ and $\tilde{\nu}_{NH}$ in a non-interactive solvent are respectively 1707 and 3443 cm^{-1}.

[29] J.F. Brennecke, J.E. Chateauneuf, Homogeneous organic reactions as mechanistic probes in supercritical fluids, Chem. Rev., 99 (1999) 433.

[30] R.W. Taft, J.L.M. Abboud, M.J. Kamlet, M.H. Abraham, Linear solvation energy relations, J. Solut. Chem., 14 (1985) 153.

[31] M.J. Kamlet, R.W. Taft, Linear solvation energy relationships. 1. Solvent polarity - polarizability effects on infrared-spectra, J. Chem. Soc.-Perkin Trans. 2, (1979) 337.

[32] M.J. Kamlet, R.M. Doherty, P.W. Carr, D. Mackay, M.H. Abraham, R.W. Taft, Linear solvation energy relationships .44. Parameter-estimation rules that allow accurate prediction of octanol water partition-coefficients and other solubility and toxicity properties of polychlorinated-biphenyls and polycyclic aromatic-hydrocarbons, Environ. Sci. Technol., 22 (1988) 503.

[33] Q. Liu, X.M. Xu, W.Q. Sang, Solvent effects on infrared spectra of 2-acetylthiophene in organic solvents, Spectroc. Acta Pt. A-Molec. Biomolec. Spectr., 59 (2003) 471.

[34] C. Laurence, P. Nicolet, M.T. Dalati, J.L.M. Abboud, R. Notario, The Empirical-Treatment of Solvent Solute Interactions - 15 Years of Pi, J. Phys. Chem., 98 (1994) 5807.

[35] R.W. Taft, J.L.M. Abboud, M.J. Kamlet, Solvatochromic comparison method .20. Linear solvation energy relationships .12. The d-delta-term in the solvatochromic equations, J. Am. Chem. Soc., 103 (1981) 1080.

[36] R.W. Taft, M.J. Kamlet, Solvatochromic comparison method .2. Alpha-scale of solvent hydrogen-bond donor (Hbd) acidities, J. Am. Chem. Soc., 98 (1976) 2886..

[37] M.J. Kamlet, R.W. Taft, Solvatochromic comparison method. 1. Beta-scale of solvent hydrogen-bond acceptor (Hba) basicities, J. Am. Chem. Soc., 98 (1976) 377.

[38] M.J. Kamlet, J.F. Gal, P.C. Maria, R.W. Taft, Linear solvation energy relationships. 32. A coordinate covalency parameter, Xi, which, in combination with the hydrogen-bond acceptor basicity parameter, Beta, Permits Correlation of Many Properties of Neutral Oxygen and Nitrogen Bases (Including Aqueous Pka), J. Chem. Soc.-Perkin Trans. 2, (1985) 1583.

[39] For each vibrational mode (i) studied, $\Delta\tilde{\nu}^{solv}$ corresponds to $\tilde{\nu}$(in a given solvent)-$\tilde{\nu}$(gas state).

[40] N. Ventosa, D. Ruiz-Molina, J. Sedo, C. Rovira, X. Tomas, J.J. Andre, A. Bieber, J. Veciana, Influence of the molecular surface characteristics of the diastereoisomers of a quartet molecule on their physicochemical properties: A linear solvation free-energy study, Chem.-Eur. J., 5 (1999) 3533.

[41] SYSTAT for windows 10.2, SYSTAT software Inc.: Point Richmond (California), 2002.

[42] Q. Liu, W.Q. Sang, X.M. Xu, Solvent effects on infrared spectra of 5-methyl-7-methoxy-iso-flavone in single solvent systems, J. Mol. Struct., 608 (2002) 253.

[43] Taken from Refs. [19], [33] and [43]. Ethanol solvatochromic parameters : α=0.86; β=0.75; π^*=0.54 and ξ=0.2. Acetone solvatochromic parameters: α=0.08; β=0.43; π*=0.62 and ξ=0.0.

[44] Y. Marcus, The Properties of Organic Liquids That Are Relevant to Their Use as Solvating Solvents, Chem. Soc. Rev., 22 (1993) 409.

[45] M.J. Frisch, G.W. Trucks, H.B. Schlegel, P.M.W. Gill, B.G. Johnson, M.A. Robb, J.R. Cheeseman, T. Keith, G.A. Peterson, J.A. Montgomery, K. Raghavachari, M.A. Al-Laham, V.G.

Zakrewski, J.V. Ortiz, J.B. Foresman, J. Ciolowski, B.B. Stefanov, A. Nannayakkara, M. Challacombe, C.U. Peng, P.Y. Ayala, W. Chen, M.W. Wong, J.L. Andres, E.S. Replogle, R. Comperts, R.L. Martin, D.J. Fox, J.S. Binkley, D.J. DeFrees, J. Baker, J.J.P. Steward, M. Head-Gordon, C. Gonzalez, J.A. Pople, Gaussian 99 Program, Gaussian, Inc., Pittsburgh, PA 1998.

[46] I.G. Binev, P. Vassileva-Boyadjieva, Y.I. Binev, Experimental and ab initio MO studies on the IR spectra and structure of 4-hydroxyacetanilide (paracetamol), its oxyanion and dianion, J. Mol. Struct., 447 (1998) 235.

[47] S.F. Boys, F. Bernardi, Calculation of Small Molecular Interactions by Differences of Separate Total Energies - Some Procedures with Reduced Errors, Mol. Phys., 19 (1970) 553.

[48] K. Mierzwicki, Z. Latajka, Basis set superposition error in N-body clusters, Chem. Phys. Lett., 380 (2003) 654.

Table 1.

LSER models describing the solvent-induced IR frequency shifts for the C=O stretching vibrational modes of compounds **1** and **2**, and for the N-H stretching vibrational mode of compound **2**.

				Statistics				
ν_i [a]	n[b]	N[c]	*IR frequency band shift LSER model*[d]	R[e]	s [f]	R^2_a [g]	F[h]	F_{99} [i]
ν_{CO} (**1**)	18	14	$\Delta\tilde{\nu}_{CO}^{solv}$ (**1**) = -15(2) - 19(3)(π^*) -38(2)α -12(3)β	0.993	3	0.991	324	9.73
ν_{CO} (**2**)	17	13	$\Delta\tilde{\nu}_{CO}^{solv}$ (**2**) = -15(2) - 18(2)(π^*) -38(2)α - 11(2)β	0.993	2	0.991	313	10.2
ν_{NH} (**2**)	17	13	$\Delta\tilde{\nu}_{NH}^{solv}$ (**2**) = -22(8) + 55(13)α - 201(17)β – 74(27)ξ	0.964	16	0.956	57	10.2

[a] IR vibrational mode under study. [b] Number of studied solvents. [c] Degrees of freedom. [d] Numbers in parentheses are coefficient standard errors. [e] Coefficient of multiple correlation. [f] Standard error of the estimate. [g] Adjusted coefficient of multiple determination. [h] *F*-test value for derived equation. [i] *F*-test value from statistical tables appropriate for the 99% confidence level.

Table 2.

Calculated geometrical parameters and interaction energies of the optimized structures of the acetaminophen-(ethanol)$_n$ complexes at the HF/6-31G level.[a]

Acetaminophen-(ethanol)$_1$						**Acetaminophen-(ethanol)$_3$**	
Structure D1		**Structure D2**		**Structure D3**			
Eth…HO(**1**)		Eth…HN(**1**)		Eth…OC(**1**)		Eth…HO(**1**) Eth…HN(**1**) Eth…OC(**1**)	
Structural Parameters[b]							
d_{OH} (Å)	0.96 (+1.10^{-2})	d_{OH} (Å)	0.95	d_{OH} (Å)	0.95	d_{OH} (Å)	0.96 (+1.10^{-2})
d_{NH} (Å)	0.99	d_{NH} (Å)	1.00 (+1.10^{-2})	d_{NH} (Å)	0.99	d_{NH} (Å)	1.00 (+1.10^{-2})
d_{CO} (Å)	1.23	d_{CO} (Å)	1.23	d_{CO} (Å)	1.24 (+1.10^{-2})	d_{CO} (Å)	1.24 (+1.10^{-2})
$R_{O...HO}$ (Å)	1.81					$R^{(1)}_{O...HO}$ (Å)	1.82
$\alpha_{O\cdots HO}$	177.5					$\alpha_{O\cdots HO}$	177.0
		$R_{O...HN}$ (Å)	2.01			$R^{(2)}_{O...HN}$ (Å)	1.99
		$\alpha_{O\cdots HN}$	178.4			$\alpha_{O\cdots HN}$	178.0
				$R_{H...OC}$ (Å)	1.93	$R^{(3)}_{H...OC}$ (Å)	1.90
				$\alpha_{H\cdots OC}$	117.6	$\alpha_{H\cdots OC}$	118.0
Binding Energy [c,d]							
$\Delta E_{int}^{(cor)}$	-8.9	$\Delta E_{int}^{(cor)}$	-7.0	$\Delta E_{int}^{(cor)}$	-6.8	$\Delta E_{int}^{(CP)}$	-22.8
						$\varepsilon^{(2)}_{Eth...HO}$	-8.8
						$\varepsilon^{(2)}_{Eth...NH}$	-7.1
						$\varepsilon^{(2)}_{Eth...CO}$	-6.8

[a] Eth: ethanol solvent molecule; OH(**1**): acetaminophen hydroxyl group; NH(**1**): acetaminophen amino group; OC(**1**): acetaminophen carbonyl group. [b] Significant bond length deviations of OH, NH, CO functional groups from isolated acetaminophen monomer have been reported in parentheses. [c] The binding energy $\Delta Eint(^{cor})$ values in this table are corrected from BSSE according to the generalized Boys-Bernardy scheme. [d] Energy unit (kcal/mol).

Table 3.

Calculated geometrical parameters and interaction energies of the optimized structures of the acetaminophen-(acetone)$_n$ complexes at the HF/6-31G level.[a]

Acetaminophen-(acetone)$_1$						**Acetaminophen-(acetone)$_3$**	
Structure D'1		**Structure D'2**		**Structure D'3**			
Acet…HO(**1**)		Acet…HN(**1**)		Acet…OC(**1**)		Acet…HO(**1**) Acet…HN(**1**) Acet…OC(**1**)	
Structural Parameters [b]							
d_{OH} (Å)	0.96 (+1.10^{-2})	d_{OH} (Å)	0.95	d_{OH} (Å)	0.95	d_{OH} (Å)	0.96 (+1.10^{-2})
d_{NH} (Å)	0.99	d_{NH} (Å)	0.99	d_{NH} (Å)	0.99	d_{NH} (Å)	0.99(+4.10^{-3})
d_{CO} (Å)	1.23	d_{CO} (Å)	1.23	d_{CO} (Å)	1.23	d_{CO} (Å)	1.24 (+1.10^{-2})
$R_{O...HO}$ (Å)	1.88					$R^{(1)}_{O...HO}$ (Å)	1.89
$\alpha_{O\cdots HO}$	166.2					$\alpha_{O\cdots HO}$	164.9
		$R_{O...HN}$ (Å)	2.07			$R^{(2)}_{O...HN}$ (Å)	2.10
		$\alpha_{O\cdots HN}$	179.4			$\alpha_{O\cdots HN}$	147.0
				$R_{C...OC}$ (Å)	3.16	$R^{(3)}_{C...OC}$ (Å)	3.30
				$\alpha_{C\cdots OC}$	98.1	$\alpha_{C\cdots OC}$	89.9
Binding Energy [c,d]							
$\Delta E_{int}^{(cor)}$	-8.1	$\Delta E_{int}^{(cor)}$	-6.8	$\Delta E_{int}^{(cor)}$	-4.8	$\Delta E_{int}^{(CP)}$	-21.3
						$\varepsilon^{(2)}_{Acet...HO}$	-8.0
						$\varepsilon^{(2)}_{Acet...NH}$	-5.2
						$\varepsilon^{(2)}_{Acet...CO}$	-4.4

[a] Acet: acetone solvent molecule; OH(**1**): acetaminophen hydroxyl group; NH(**1**): acetaminophen amino group; OC(**1**): acetaminophen carbonyl group. [b] Significant bond length deviations of OH, NH, CO functional groups from isolated acetaminophen monomer have been reported in parentheses. [c] The binding energy $\Delta E_{int}^{(cor)}$ values in this table are corrected from BSSE according to the generalized Boys-Bernardy scheme. [d] Energy unit (kcal/mol).

Figure Captions

Fig. 1. Relative solubility (S/S_0) of acetaminophen at 315 K and 10 MPa in "CO_2-expanded ethanol" (△) and in "CO_2-expanded acetone" (○) as function of CO_2 molar fraction; where S_0 is the solubility in the pure organic solvent. Straight dotted line depicts the ideal dilution line.

Fig. 2. Schematic representation of the perturbation of the cybotactic region of acetaminophen (●) in ethanol (upper drawing) and in acetone (bottom drawing) as compressed CO_2 is added.

Fig. 3. High-pressure IR spectroscopic set-up.

Fig. 4. Evolution of the IR absorption spectra of acetaminophen in the ν_{CO} stretching mode region with the molar fraction of CO_2 in "CO_2-expanded acetone" (top) and in "CO_2-expanded ethanol" (bottom).

Fig. 5. Evolution of the IR absorption spectra of acetaminophen in the region of the ν_{OH} and ν_{NH} stretching modes with the molar fraction of CO_2 in "CO_2-expanded acetone" (top) and "CO_2-expanded ethanol" (bottom).

Fig. 6. Chemical structures of acetaminophen (**1**) and 4-(ethoxyphenyl)acetamide (**2**)

Fig. 7. IR absorption spectra, in the ν_{OH}/ν_{NH} stretching modes region, of **1** (dashed line) and **2** (continuous line) in acetone (top) and in deutherated ethanol (bottom). Spectra are scaled at their maximum absorbance.

Fig. 8. Evolution of $\Delta\nu_{CO}$ (top) and $\Delta\nu_{NH}$ (bottom) versus X_{CO2} for "CO_2-expanded ethanol" (Δ) and "CO_2-expanded acetone" (○). Dotted lines are given to guide the eyes. Continuous and dash lines depict an ideal linear evolution of $\Delta\nu_{CO}$ and $\Delta\nu_{NH}$ with CO_2 content in "CO_2-expanded ethanol" and "CO_2-expanded acetone" mixtures, respectively. Double headed arrows provide an indication of the deviation from ideality

of the ν_{NH} and ν_{CO} band shifts evolution with increasing CO_2 in both CO_2-expanded solvents.

Fig. 9. Contributions of the different types of solvent-solute interactions to the frequency shift observed for ν_{CO} (top) and for ν_{NH} (bottom) of acetaminophen in acetone (filled columns) and in ethanol (empty columns).

Fig. 10. Optimized structures (HF/6-31G) for acetaminophen-$(ethanol)_3$ (A) and acetaminophen-$(acetone)_3$ (B) tetrameric complexes. The pair interaction energies and intermolecular distances are displayed over each 'acetaminophen functional group-solvent' interaction.

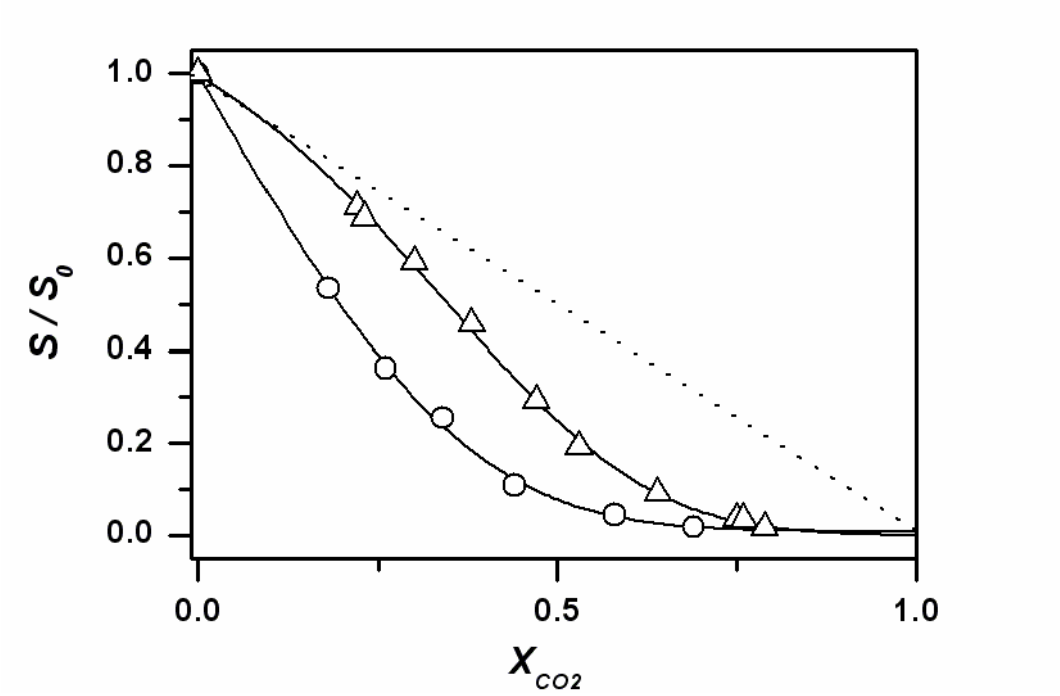

Figure 1

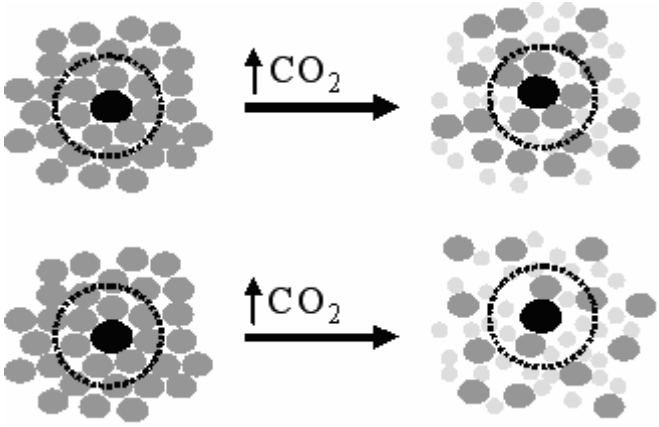

Figure 2

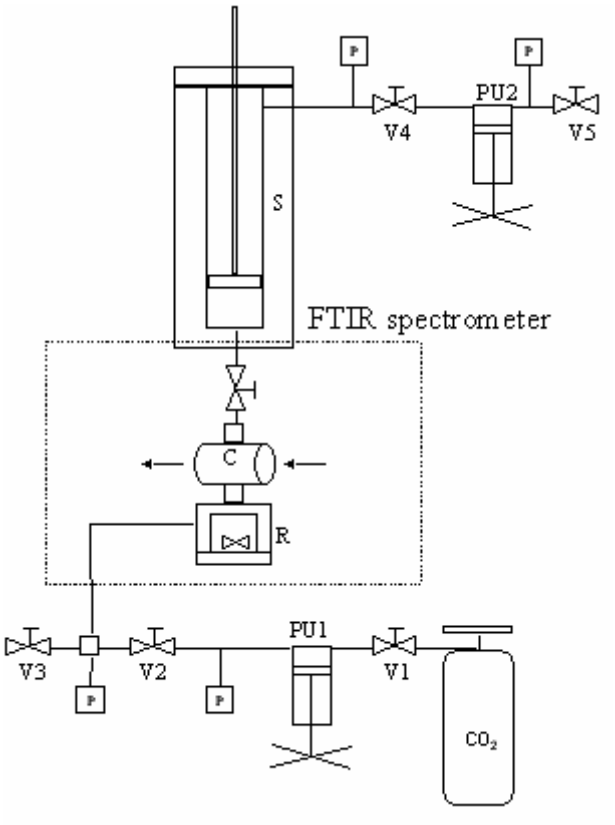

Figure 3

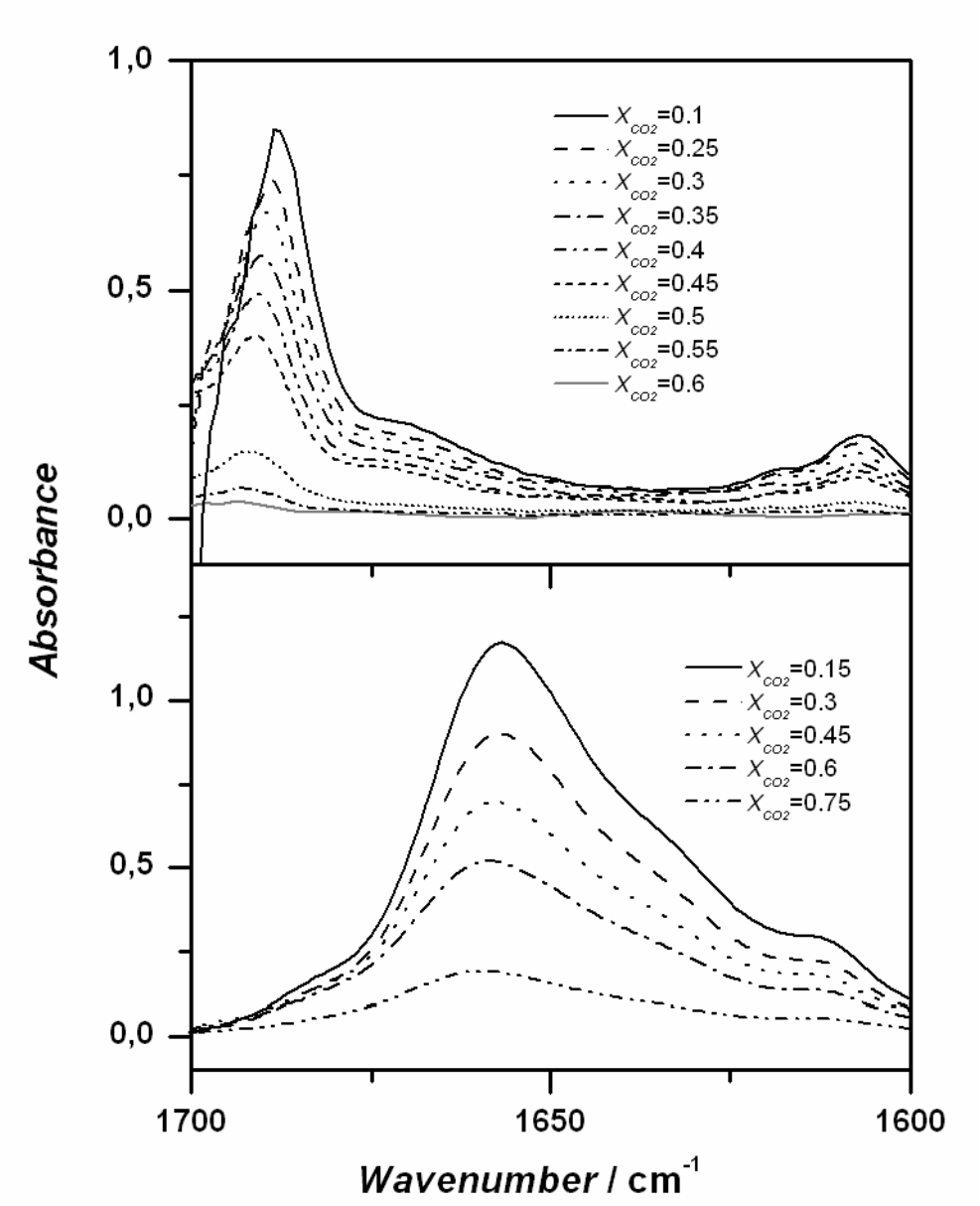
1,0
0,5
0,0
Absorbance
X_{CO2}=0.1
X_{CO2}=0.25
X_{CO2}=0.3
X_{CO2}=0.35
X_{CO2}=0.4
X_{CO2}=0.45
X_{CO2}=0.5
X_{CO2}=0.55
X_{CO2}=0.6
1,0
0,5
0,0
X_{CO2}=0.15
X_{CO2}=0.3
X_{CO2}=0.45
X_{CO2}=0.6
X_{CO2}=0.75
1700
1650
1600
Wavenumber / cm^{-1}

Figure 4

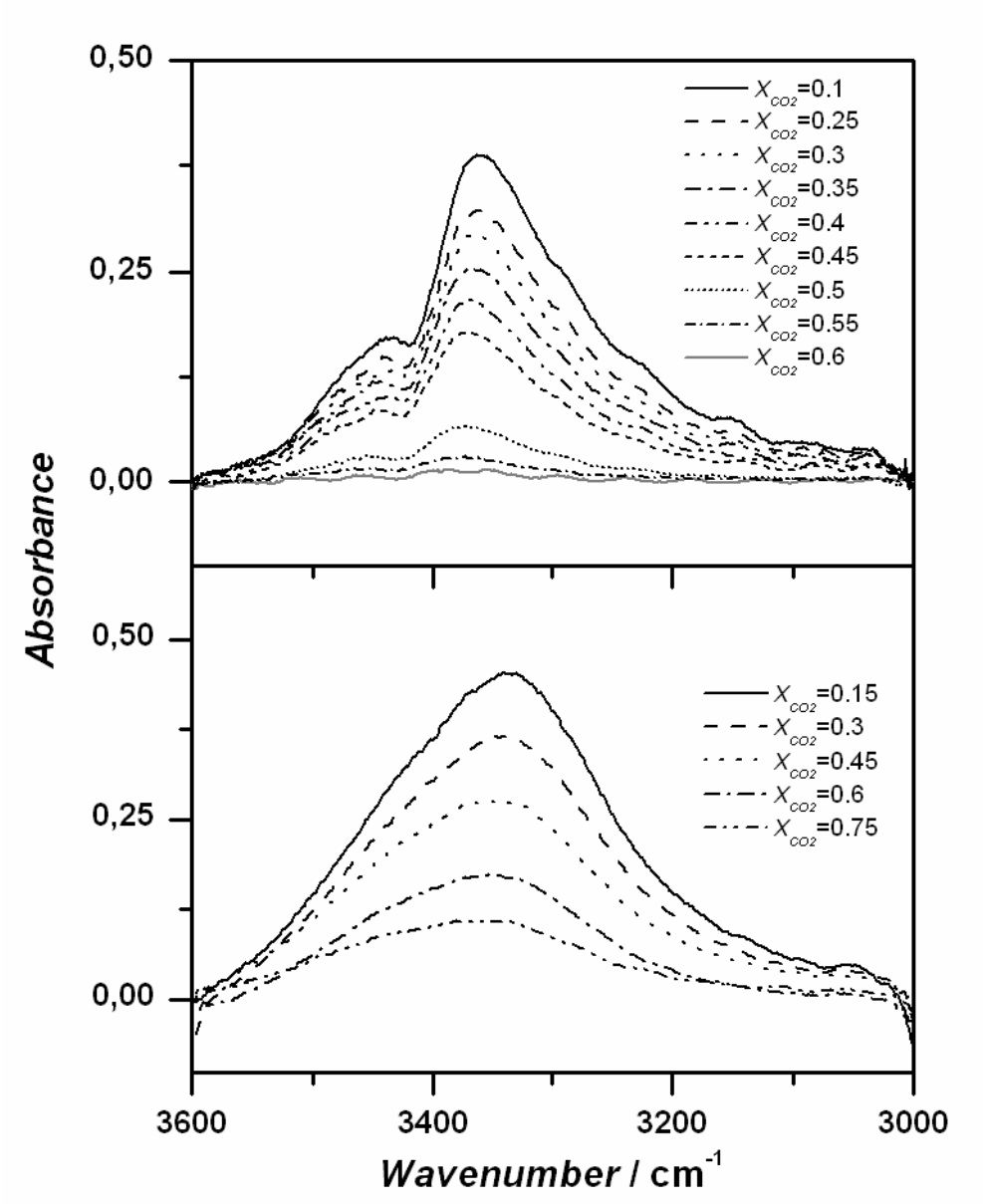
0,50
0,25
0,00
Absorbance
X_{CO2}=0.1
X_{CO2}=0.25
X_{CO2}=0.3
X_{CO2}=0.35
X_{CO2}=0.4
X_{CO2}=0.45
X_{CO2}=0.5
X_{CO2}=0.55
X_{CO2}=0.6
0,50
0,25
0,00
X_{CO2}=0.15
X_{CO2}=0.3
X_{CO2}=0.45
X_{CO2}=0.6
X_{CO2}=0.75
3600
3400
3200
3000
Wavenumber / cm^{-1}

Figure 5

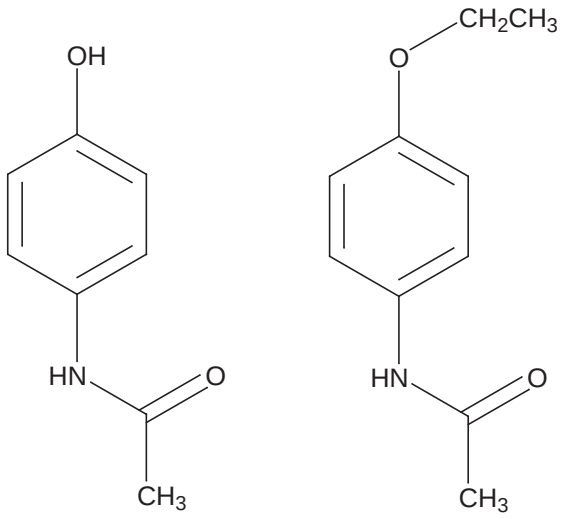

1 **2**

Figure 6

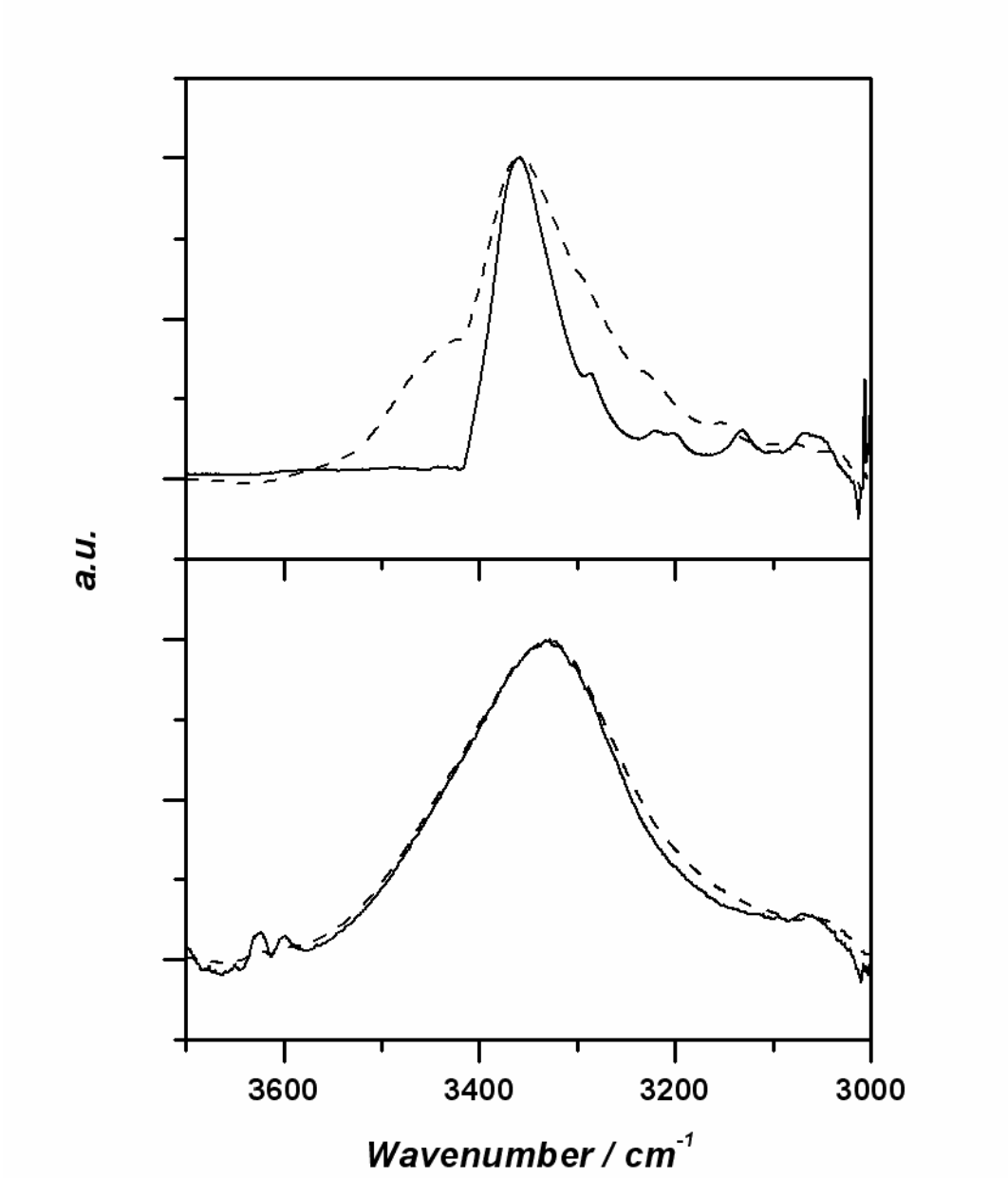

Figure 7

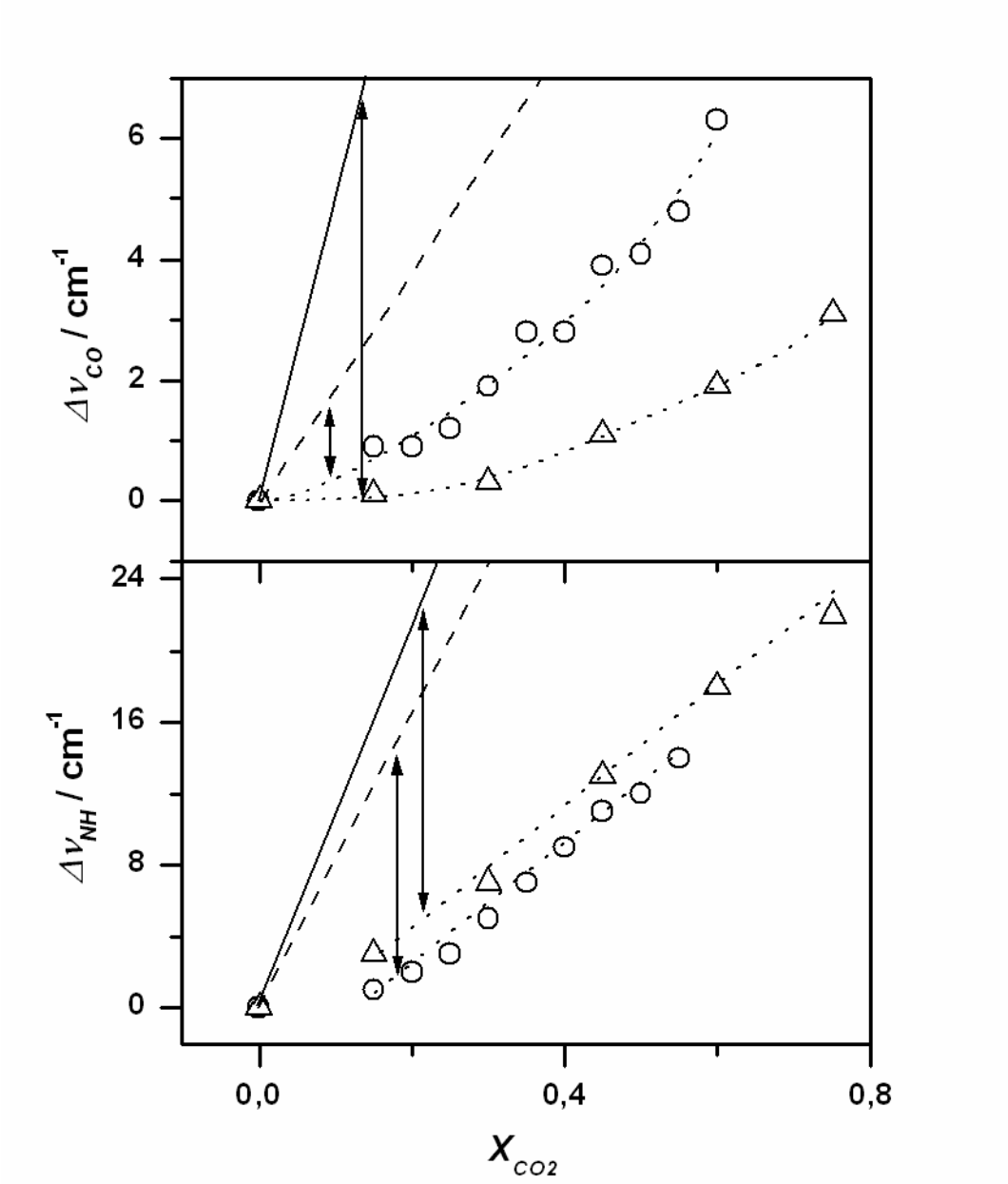

Figure 8

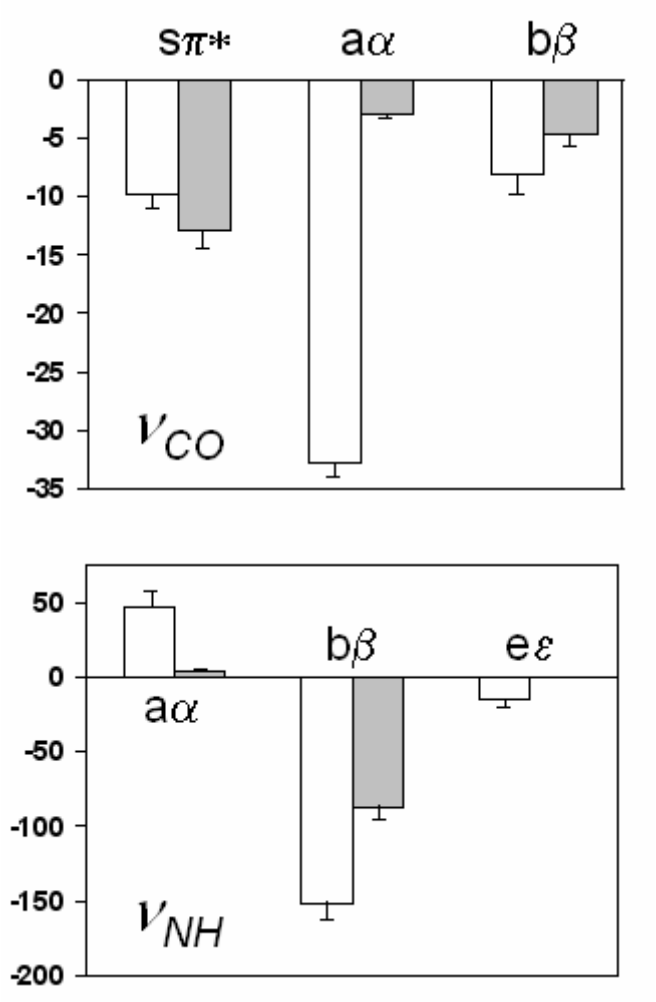

Figure 9

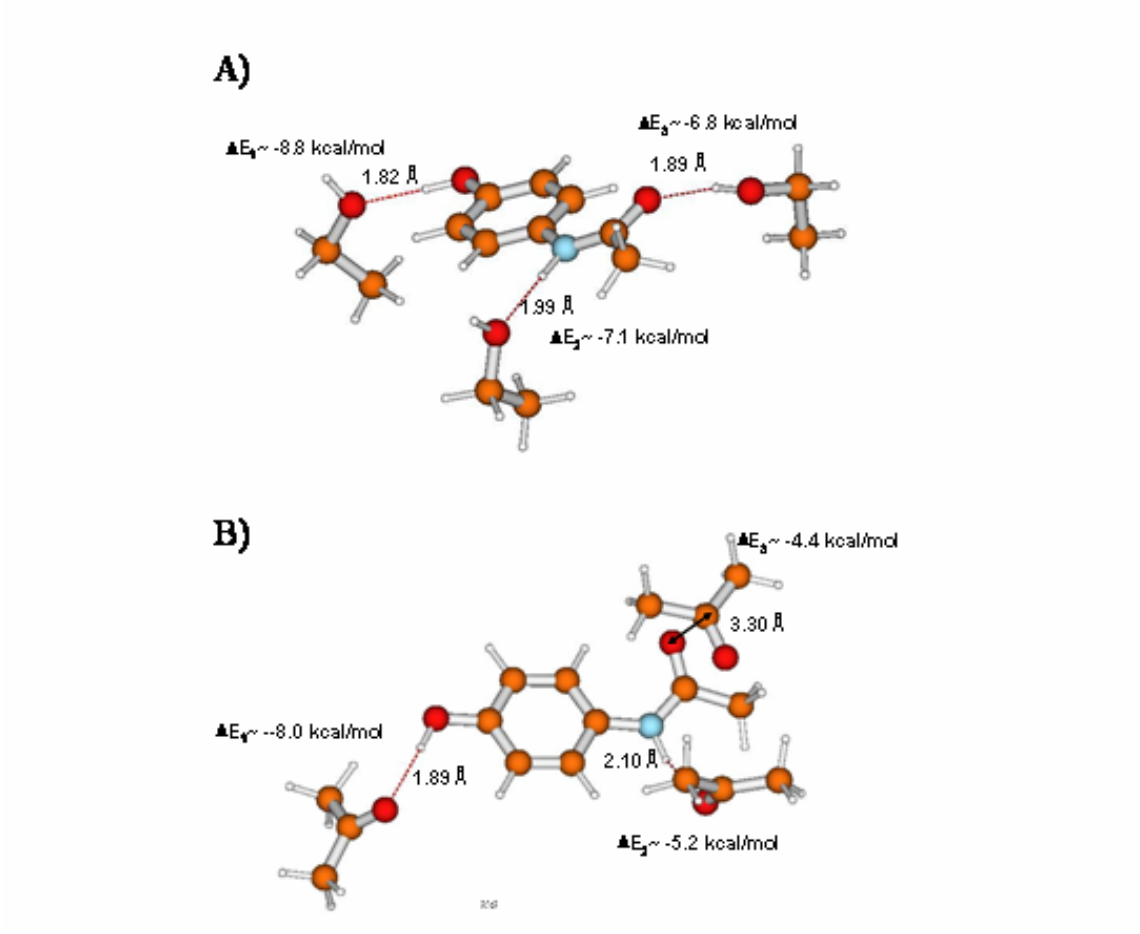
A)
ΔE1~ -8.8 kcal/mol
1.82 Å
ΔE3~ -6.8 kcal/mol
1.89 Å
1.99 Å
ΔE2~ -7.1 kcal/mol
B)
ΔE3~ -4.4 kcal/mol
3.30 Å
ΔE1~ --8.0 kcal/mol
1.89 Å
2.10 Å
ΔE2~ -5.2 kcal/mol

Figure 10

ARTICLE G:

Títol: Synergistic Enhancement of the Solubility of Hexamethylenetetramine in Subcritical CO_2-Ethanol Mixtures Studied by Infrared Spectroscopy

Autors: Santiago Sala, Nora Ventosa, Thierry Tassaing, Mary Cano, Yann Danten, Marcel Besnard, Jaume Veciana

Publicació: ChemPhysChem, en premsa

(No presentat a la comissió de doctorat)

Synergistic Enhancement of the Solubility of Hexamethylenetetramine in Subcritical CO_2–Ethanol Mixtures Studied by Infrared Spectroscopy

Santiago Sala,[a] Nora Ventosa,*[a] Thierry Tassaing,[b] Mary Cano,[a] Yann Danten,[b] Marcel Besnard,*[b] and Jaume Veciana*[a]

Carbon dioxide is widely considered as an environmentally acceptable alternative to organic solvents in chemical processes, due to its non-toxicity, non-flammability, low cost and plentiful supply.[1] It is well-known that CO_2-based processing technologies are limited by the low solubility of the majority of polar and ionic compounds in liquid and supercritical CO_2.[1] To overcome this limitation different ways to enhance the CO_2 solvent power are proposed such as the design of CO_2-philic surfactants,[2] or the addition of few amounts of conventional polar solvents.[3] A promising third choice, also based on polar solvent–CO_2 binary mixtures, are solvents expanded with compressed CO_2. These mixtures are composed of subcritical CO_2 (up to 80 vol%) condensed into an organic solvent and generally show a much higher capacity to dissolve polar compounds than pure CO_2.[4] The study of solvating phenomena in such compressed fluids is an area of active research, since it is crucial for understanding and promoting compound solubility in these solvent media.[5] Solubility enhancement observed in binary systems involving CO_2 and polar solvents, with respect to neat CO_2, are attributed to local density augmentation and local composition enhancements of the polar solvent around dissolved solutes.[6] The analysis of this phenomenon, generally called solvent clustering, is mainly interpreted from UV/Vis solvatochromic shifts and fluorescence spectroscopy.[7] Vibrational spectroscopic techniques are also used to characterize clustering phenomena with compressed fluids as they are well-adapted for the detection of specific molecular interactions in solution.[8,9] In the majority of these studies, the solvent structure around the solute is indirectly deduced from the observed solvent effects on the absorption spectrum of the probe. Thus, from solute spectroscopic band frequency shifts it is possible to gain insight on the first solute solvation shell. However, information on the large-scale organization of solvent molecules in the cybotactic region directly inferred from solvent spectroscopic observables is still lacking.[10]

Herein, the structure of the first solvation shell, as well as the organization of solvent molecules at larger distances, around the solute molecules of hexamethylenetetramine (**1**)[11] in CO_2-expanded ethanol solutions his characterized by infrared (IR) spectroscopic measurements of solute and solvent spectra. This structural information allows to rationalize the unprecedented synergistic enhancement of the solubility of **1** produced by the simultaneous presence of CO_2 and ethanol solvent molecules. Solutions of hexamethylenetetramine in CO_2-expanded ethanol (CO_2-exp EtOH) are chosen due to the ability of **1** to interact, through its four nitrogen basic sites, either by hydrogen bonding (HB) with a HB-donor molecule such as ethanol or by electron donation to a Lewis acid molecule such as CO_2. As shown in Figure 1, the solubility of **1** in

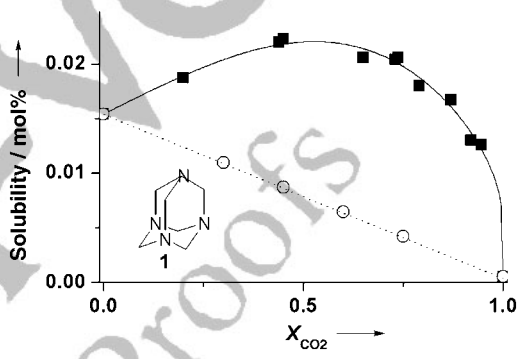

Figure 1. *Experimental solubility (■) of hexamethylenetetramine measured at 313 K and 10 MPa in CO_2-expanded ethanol. (Solubility measurements were performed by the vanishing point method; see Supporting Information). Solute concentrations (○) used in the spectroscopic measurements are located over the ideal dilution line of a saturated solution of **1** in ethanol (dotted line).*

CO_2-exp EtOH, at 313 K and 10 MPa, is highly enhanced compared with those measured in pure CO_2 and neat EtOH. The solubility of **1** in CO_2-exp EtOH, at a CO_2 molar fraction $X_{CO2} = 0.75$, is greater by more than one order of magnitude than that measured in pure CO_2 under the same pressure and temperature conditions. The solubility is 30% greater than in pure ethanol. Since a long time, solubility enhancement upon solvent mixing was always under considerations due to important implications in industrial chemical processing.[12,13] Up to now, studies on synergistic solvent effects in CO_2-expanded solvents are rather scarce and devoted to polymer dissolution for which entropic factors play a key role.[14]

To understand at molecular level the solubility enhancement of hexamethylenetetramine in CO_2-exp EtOH in relation to pure CO_2 and neat EtOH, we analyzed by IR spectroscopy how EtOH and CO_2 solvent molecules are organized around the tetramine **1**. For this purpose, we recorded the spectra of hexamethylenetetramine solutions in CO_2-exp EtOH at 313 K and 10 MPa for different CO_2 molar fractions (see Figure 2). The spectra of the corresponding solute-free CO_2-exp EtOH mixtures with the same CO_2 content were also measured and sub-

[a] *S. Sala, Dr. N. Ventosa, M. Cano, Prof. J. Veciana*
Institut de Ciència de Materials de Barcelona (CSIC)
Campus Universitari, 08193 Bellaterra, Catalonia (Spain)
Fax: (+34) 93-580-5729
E-mail: ventosa@icmab.es
vecianaj@icmab.es

[b] *Dr. T. Tassaing, Dr. Y. Danten, Dr. M. Besnard*
Laboratoire de Physico-Chimie Moléculaire, CNRS (UMR 5803)
Université Bordeaux I, 351 Cours de la Libération
33405 Talence Cedex (France)
Fax: (+33) 556-848-402
E-mail: m.besnard@lpcm.u-bordeaux1.fr

Supporting information for this article is available on the WWW under http://www.chemphyschem.org or from the author.

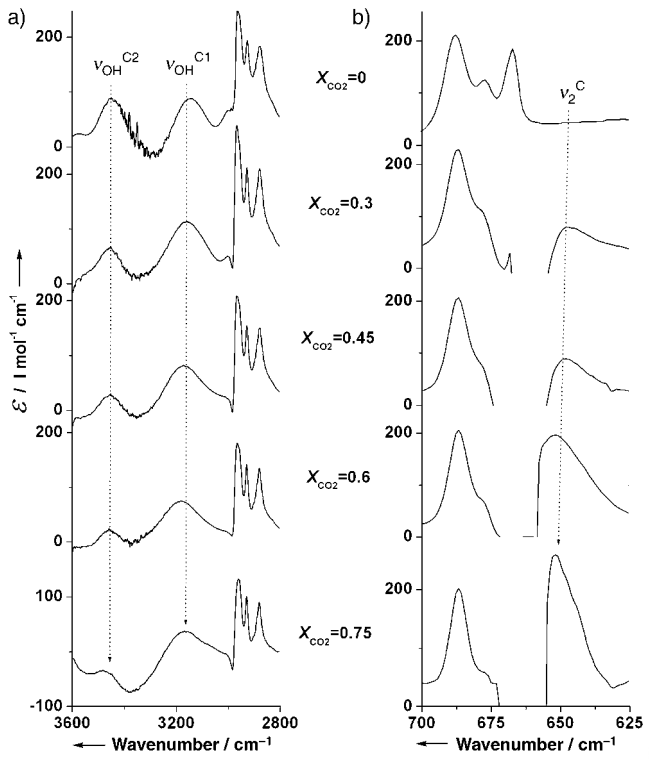

Figure 2. *Evolution of the IR absorption spectra of hexamethylenetetramine in the 2800–3600 cm^{-1} region (a) and the 625–700 cm^{-1} region (b), with the molar fraction of CO_2, X_{CO2}. Normalized spectra (in l mol^{-1} cm^{-1} units) are displayed after subtraction of the solvent contribution.*

stracted from the spectra of the solution. These difference spectra in hexamethylenetetramine molar absorptivity units, are displayed in Figure 2a in the 3600 to 2800 cm^{-1} region. As shown, solute and solvent vibrational bands are well detected and resolved. The two CH_2-stretching vibrational bands (the ν_{18} symmetric band at 2880 cm^{-1}, and the ν_{17} asymmetric band at 2965 cm^{-1}) as well as the combination $\nu_2+\nu_9$ band and the $2\nu_{19}$ overtone situated at 2929 cm^{-1} corresponding to hexamethylenetetramine are clearly observed.[15] In this spectral region, we assign the two broad bands, namely ν_{OH}^{c1} and ν_{OH}^{c2} positioned at about 3180 cm^{-1} and 3456 cm^{-1}, respectively, to the OH-stretching modes of the EtOH molecule interacting in two different environments. Indeed, the band center frequency of these two bands are found different from the ν_{OH}^{b} band associated with the OH-stretching vibration of EtOH molecules observed at 3365 cm^{-1} in the solute-free CO_2-exp EtOH. The ν_{OH}^{c1} band and the ν_{OH}^{c2} band are found shifted towards lower (red-shifted) and higher (blue-shifted) frequencies, respectively, compared with ν_{OH}^{b} for all compositions investigated. Therefore, it can be assessed that the ν_{OH}^{c1} mode corresponds to EtOH molecules in a first solvating shell of hexamethylenetetramine interacting specifically through HB to the N atoms of hexamethylenetetramine.[16] The extent of the red shift of the ν_{OH}^{c1} band with respect to the ν_{OH}^{b} mode indicates that the strength of the N···H–O interactions is higher than the O···H–O interactions of EtOH in the solute-free CO_2-exp EtOH. In contrast, the ν_{OH}^{c2} band can be assigned to EtOH molecules belonging to the second solvating shell of hexamethylenetetramine. These EtOH molecules do not interact directly with hexamethylenetetramine, but more likely are hydrogen-bonded with other EtOH molecules. The extent of the blue-shift of the ν_{OH}^{c2} band with respect to the ν_{OH}^{b} mode indicates that the strength of the O···H–O interactions between the EtOH molecules of the primary and secondary solvation shells are weaker than the HB interactions established between EtOH molecules in the solute-free CO_2-exp EtOH. The evolution of the normalized spectra presented in Figure 2a also shows that the relative absorbance of the ν_{OH}^{c1} and ν_{OH}^{c2} bands is not constant with the X_{CO2} variation. It is observed that the absorbance of the ν_{OH}^{c2} band decreases progressively whilst the absorbance of ν_{OH}^{c1} is not affected by the CO_2 content changes. Therefore, increasing the CO_2 concentration of the mixture affects differently the structure of the two solvation shells around methenamine.

The spectral region (625–700 cm^{-1}) containing the CO_2-bending vibrational mode (ν_2) was also analyzed to assess the role of CO_2 in the structural organization around hexamethylenetetramine in CO_2-exp EtOH solutions (Figure 2b). The normalized spectra obtained after removing the spectra of solute-free solvent mixture, exhibit, in addition to a hexamethylenetetramine composite band (ν_{24}),[15] a new band (ν_2^c) found at lower frequency than that corresponding to the bending mode (ν_2^b) of CO_2 in CO_2-exp EtOH mixtures. We emphasize that the ν_2^b mode is not visible in Figure 2b as we subtracted the contribution of the solute-free solvent mixture. To assign this band, let us remind that previous experimental work performed on solutions of CO_2 diluted in organic solvent and in CO_2-swollen polymers,[17] as well as theoretical calculations[18] showed that CO_2 interacts through a Lewis acid–base specific interaction. In this interaction, molecules possessing lone electron pairs, such as R_2O, R_3N, R_2CO, etc., act as an electron donor center whilst C atoms of CO_2 play the role of Lewis acid site. As a consequence, a doublet structure of the IR spectrum associated with the bending of CO_2 is expected. Moreover, the degeneracy removing is also accompanied by a redistribution of the intensity in the infrared doublet. Usually, the high-frequency component of the doublet is only slightly shifted from the frequency of the free mode of CO_2 whereas the low-frequency component is more strongly shifted. In addition, the intensity of the low-frequency component is usually greater than that of the high one. By removing the spectrum of CO_2 from the spectrum of CO_2 interacting with a Lewis base, the difference spectrum should exhibit a band at lower frequency which corresponds to the low-frequency component of the doublet. Applied to the ternary mixtures hexamethylenetetramine/ethanol/CO_2, these considerations provide the reason for not observing directly a doublet structure in the spectra obtained by removing the spectra of CO_2-exp EtOH but allow an assignment of the band (ν_2^c) which is found at lower frequencies than that of the ν_2^b band and can be attributed to the bending mode of CO_2 molecules with stronger Lewis acid–base interactions with surrounding electron pair donor (EPD) molecules than those established between CO_2 and EtOH in the bulk. The EPD molecules can be either methenamine or EtOH in the cybotatic region of methenamine. To discriminate

between these two possibilities, the evolution of ν_2^c with the CO_2 content of the solution is considered. A progressive increase of the ν_2^c band absorbance is observed with increasing CO_2 concentration in the mixture. In contrast, the ν_{OH}^{c2} band absorbance decreases whereas the absorbance and shape of the ν_{OH}^{c1} band remain almost unaffected by the progressive replacement of EtOH molecules of the second solvation shell by CO_2 molecules.

Therefore, in the cybotactic region of **1**, CO_2 molecules do not interact directly with hexamethylenetetramine, but form Lewis acid–base interactions with EtOH molecules of the first solvation shell (Scheme 1). Moreover, the interaction between

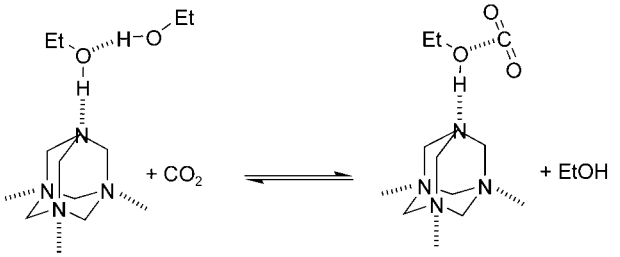

Scheme 1. *Hexamethylenetetramine **1** interacting with CO_2 and EtOH.*

CO_2 and EtOH molecules in the cybotactic region of tetramine **1** is enhanced compared to bulk ethanol. Indeed, ethanol molecules forming strong hydrogen bonds to **1** have a greater electron donor character than in pure ethanol, leading to a stronger Lewis acid–base interaction with CO_2 molecules. Finally, this co-operative/many body effect explains the presence of the ν_2^c band, and its red-shift compared to ν_2^b.

To get more insight in the structural information provided by this spectroscopic study, we also studied the evolution of relevant vibrational bands of hexamethylenetetramine with the evolution of the CO_2 concentration in the mixture.[6,7] The spectral region of 1220–1255 cm^{-1}, which contains the most sensitive hexamethylenetetramine band to solvent composition changes, is displayed in Figure 3 for three different CO_2 concentrations. This band, assigned to the (ν_{21}) C–N-stretching vibration of hexamethylenetetramine, is a degenerate triple with F_2 symmetry.[15] At all solvent compositions investigated, this degeneracy is partially removed due to interactions of hexamethylenetetramine with surrounding molecules. A bandshape analysis reveals that the band is a composite band involving at least a doublet structure whereas this band is unique in pure CO_2. This finding confirms that CO_2 does not directly interact with hexamethylenetetramine. Therefore, as the amount of CO_2 increases in the CO_2-exp EtOH solutions, the evolution of the hexamethylenetetramine band reveals the existence of a first solvating shell around hexamethylenetetramine which is mainly composed of EtOH molecules strongly interacting with the N sites of **1** and a second solvating shell in which the EtOH molecules are progressively replaced by CO_2.

We emphasize that on going from a situation in which hexamethylenetetramine is only surrounded by EtOH molecules to that observed in pure CO_2, the drastic narrowing of the ν_{21}

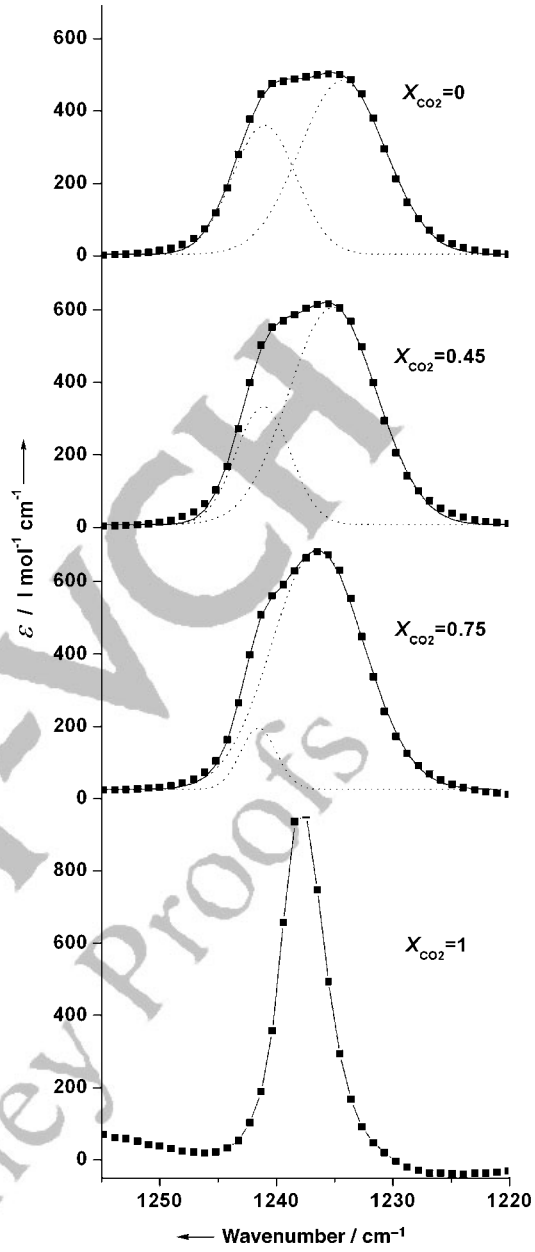

Figure 3. *Experimental (■) and fitted (solid line) IR absorption spectra of hexamethylenetetramine in the region of ν_{21} CN stretching mode at different solvent compositions. Normalised Spectra (in l mol^{-1} cm^{-1} units) are displayed after subtraction of the solvent contribution. The ν_{21} CN-stretching bands were fitted using two Gaussian functions (dashed lines).*

profile is due to the vanishing removal of the degeneracy degree of the mode. With increasing concentration of CO_2 in the mixture, the variation of the broadening (from 6.7 cm^{-1} for $X_{CO2}=0$ to 5.1 cm^{-1} for $X_{CO2}=0.75$) indicates that the splitting degree progressively decreases. Thus, replacing EtOH by CO_2 molecules in the second solvation shell by increasing the CO_2 concentration, induces a variation of the strength of the H bond interactions existing between hexamethylenetetramine and ethanol molecules in the first shell. Thus, we conclude that co-operative Lewis acid–base interactions between the

CO_2 and these EtOH molecules are also involved in these solutions.

The co-operative interactions hexamethylenetetramine–EtOH and EtOH–CO_2 occurring at the cybotactic region of **1** would explain, at the molecular level, the synergistic enhancement of hexamethylenetetramine solubility in CO_2-exp EtOH, compared to both pure solvents.

This study provides structural insight in the solvent organization around hexamethylenetetramine molecules in CO_2-exp EtOH solutions showing that the formation of hexamethylenetetramine–EtOH–CO_2 clusters due to specific molecular interactions are evidenced by vibrational spectroscopy. The present investigation also shows that the occurrence of co-operative solute–polar solvent and polar solvent–CO_2 interactions is a promising way to enhance the solubility of solute molecules in CO_2-based media offering large potentialities in industrial CO_2-based processing technologies.

Acknowledgements

This work was supported by a grant from the contract HPMT-CT-2000-00143 between the European Community and the Université de Bordeaux I, and also by grants from DGI (Spain), project MAT2003-04699 and DGR (Catalunya), project 2001SGR00362. Nora Ventosa thanks to the Ramon y Cajal Program of Ministerio de Ciencia y Tecnología (Spain) for her contract.

Keywords: carbon dioxide · hexamethylenetetramine · IR spectroscopy · solute–solvent interactions · solvent effects

[1] a) *Chemical Synthesis Using Supercritical Fluids*, (Eds.: P. G. Jessop, W. Leitner), Wiley-VCH, Weinheim, **1999**; b) G. Brunner, *Gas Extraction: An Introduction to Fundamentals of Supercritical Fluids and the Application to Separation Processes*, Steinkopff, Darmstadt, Springer, New York, **1994**.

[2] J. L. Panza, E. J. Beckman in *Supercritical Fluid Technology in Materials Science and Engineering, chapter 6* (Ed.: Y.-P. Sun), Marcel Dekker, Inc., New York, **2002**, p. 255.

[3] T. Clifford, *Fundamentals of Supercritical Fluids*, Oxford Science Publications, Oxford, **1999**, p. 26.

[4] M. Wei, G. T. Musie, D. H. Busch, B. Subramaniam, *J. Am. Chem. Soc.* **2002**, *124*, 2513.

[5] C. A. Eckert, D. Bush, J. S. Brown, C. L. Liotta, *Ind. Eng. Chem. Res.* **2000**, *39*, 4615.

[6] J. F. Brennecke, J. E. Chateauneuf, *Chem. Rev.* **1999**, *99*, 433.

[7] a) S. Kim, K. P. Johnston, *AICHE J.* **1987**, *33*, 1603; b) D. L. Tomasko, B. L. Knutson, F. Pouillot, C. L. Liotta, C. A. Eckert, *J. Phys. Chem.* **1993**, *97*, 11 823; c) S. P. Kelley, R. M. Lemert, *AICHE J.* **1996**, *42*, 2047; d) D. S. Bulgarevich, T. Sako, T. Sugeta, K. Otake, M. Sato, *J. Chem. Phys.* **1998**, *108*, 3915; e) D. S. Bulgarevich, T. Sako, T. Sugeta, K. Otake, Y. Takebayashi, C. Kamizawa, Y. Horikawa, M. Kato, *Ind. Eng. Chem. Res.* **2002**, *41*, 2074.

[8] a) M. Poliakoff, S. M. Howdle, S. G. Kazarian, *Angew. Chem.* **1995**, *107*, 1409; *Angew. Chem. Int. Ed. Engl.* **1995**, *34*, 1275; b) S. Akimoto, O. Kajimoto, *Chem. Phys. Lett.* **1993**, *209*, 263.

[9] a) R. B. Gupta, J. R. Combes, K. P. Johnston, *J. Phys. Chem.* **1993**, *97*, 707; b) S. G. Kazarian, R. B. Gupta, M. J. Clarke, K. P. Johnston, M. Poliakoff, *J. Am. Chem. Soc.* **1993**, *115*, 11 099; c) S. Sala, T. Tassaing, N. Ventosa, Y. Danten, M. Besnard, J. Veciana, *ChemPhysChem* **2004**, *5*, 243.

[10] The cybotactic region is the volume around a solute molecule in which the ordering of the solvent molecules is influenced by the solute.

[11] IUPAC name of hexamethylenetetramine (**1**): 1,3,5,7-tetraazatricyclo-[3.3.1.-$1^{3,7}$]decane.

[12] a) L. J. Leonard, R. L. Scott, *J. Am. Chem. Soc.* **1952**, *74*, 4138; b) K. Nakanishi, S. Asakura, *J. Phys. Chem.* **1977**, *81*, 1745.

[13] a) S. Romero, A. Reillo, B. Escalera, P. Bustamante, *Chem. Pharm. Bull.* **1996**, *44*, 1061; b) U. Domanska, *J. Solution Chem.* **1989**, *18*, 1153.

[14] a) T. Tassaing, P. Lalanne, S. Rey, F. Cansell, M. Besnard, *Ind. Eng. Chem. Res.* **2000**, *39*, 4470; b) K. Matsuyama, K. Mishima, H. Umemoto, S. Yamaguchi, *Environ. Sci. Technol.* **2001**, *35*, 4149.

[15] This assignment is taken from previous studies in the solid state; see: J. E. Bertie, M. Solinas, *J. Chem. Phys.* **1974**, *61*, 1666.

[16] H. J. Kim, S. -H. Park, T. S. Chair, S. H. Choh, *J. Mol. Struct.* **1999**, *478*, 275.

[17] a) S. G. Kazarian, M. F. Vincent, F. V. Bright, C. L. Liotta, C. A. Eckert, *J. Am. Chem. Soc.* **1996**, *118*, 1729; b) J. C. Meredith, K. P. Johnston, J. M. Seminario, S. G. Kazarian, C. A. Eckert, *J. Phys. Chem.* **1996**, *100*, 10 837.

[18] a) Y. Danten, T. Tassaing, M. Besnard, *J. Phys. Chem. A* **2002**, *106*, 11 831; b) M. H. Jamroz, J. C. Dobrowolski, K. Bajdor, M. A. Borowiak, *J. Mol. Struct.* **1995**, *349*, 9.

Received: October 18, 2004
Published online on ■■ ■■, 2005

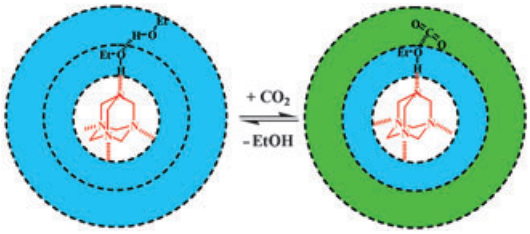

A vibrational spectroscopic survey of CO_2-expanded ethanol solutions of hexamethylenetetramine allows to investigate the organization of solvent molecules in the solute cybotactic region. The synergistic solubility enhancement observed in this system is explained by the occurrence of co-operative interactions of EtOH and CO_2 around hexamethylenetetramine molecules, as schematized in the picture.

S. Sala, N. Ventosa, T. Tassaing, M. Cano, Y. Danten, M. Besnard,* J. Veciana**

■■ – ■■

Synergistic Enhancement of the Solubility of Hexamethylenetetramine in Subcritical CO_2–Ethanol Mixtures Studied by Infrared Spectroscopy

Infrared spectroscopic investigation of the synergistic enhancement of the solubility of hexamethylenetetramine in sub-critical CO_2-ethanol mixtures

Santiago Sala, Nora Ventosa,* Thierry Tassaing, Mary Cano, Yann Danten, Marcel Besnard,* and Jaume Veciana.*

Experimental Section

The experimental set-up and methodology employed in the present work for IR high-pressure measurements on hexamethylenetetramine/ethanol/CO_2 system has already been described in a previous work.[1] The only modifications concerning the previous configuration was the use of ZnSe windows and the method to fix the path-length. ZnSe was employed due to its low absorption in the ν_2 bending mode region (680-600 cm^{-1}). Very short path-lengths were selected to record the spectra and for that no window spacers were used. The cell employed, based on a design described by Fishman et al,[2] allowed to fix the path-length as a function of the internal fluid pressure ant the external tightening of empty cylindrical bodies which joined the two windows before pressurization. The use of the same pressure for all measurements together with the use of Kalrez o-rings to ensure sealing of cell, made possible to work with very reproducible path-lengths. The reproducibility of this system was tested by recording different spectra of CO_2 at constant pressure (10 MPa)

and temperature (313 K). These spectra were also used to measure, approximately, the resulting path-length using the interference fringes method. The absolute path-lenghts used in this work were in the range 16-33 μm. The lower path-lengths allowed to obtain non-saturated solvent bands in most of the compositions studied. All measurements were performed on a Biorad interferometer (type FTS-60A) equipped with a global source, a germanium KBr supported beam splitter, and a DTGS detector. Single-beam spectra recorded in the spectral range 400-6000 cm^{-1} with 2 cm^{-1} resolution were obtained by Fourier transformation of 50 accumulated interferograms. As an example, Figure S1 shows the complete spectra of solute containing and solute free CO_2-expanded ethanol solutions at X_{CO2}=0.45 (top), and the spectrum result of the subtraction between these spectra (bottom).

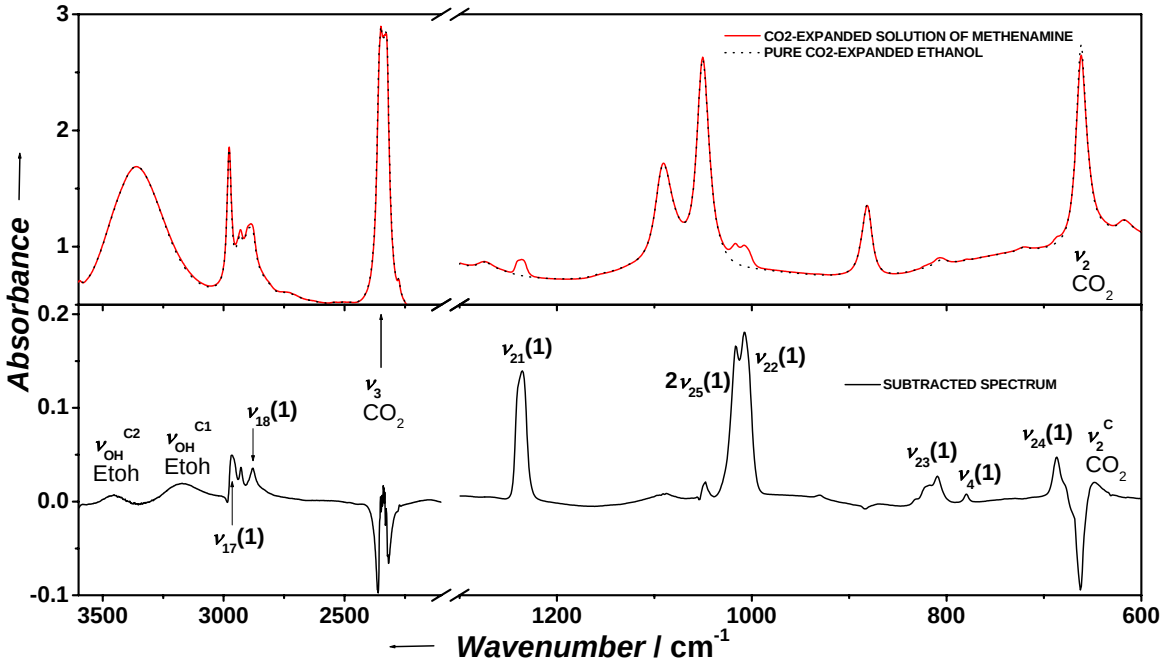

Figure S1: Spectra of a solution of **1** in "CO_2-exp etOH" at X_{CO2}=0.45 and a solute-free "CO_2-exp etOH" mixture at X_{CO2}=0.45 (top) and difference between them (bottom)

Solubility measurements of hexamethylenetetramine in CO_2-expanded ethanol were performed in a home made high pressure phase equilibria analyser. The main components of this configuration are a Jergusson T-40 view cell, a JASCO PU-1580 HPLC pump to introduce liquid solvents or solutions, an ISCO 260D pump to introduce CO_2 and a micropump to re-circulate the internal mixture. The variation of the cell volume is realized by a stainless-steel piston introduced into the view cell and moved by a pneumatic system. In this way, the cell internal volume can be varied from 50 to 75 mL. Solid samples can be introduced into the cell previously to pressurization by a stainless steel cylinder supported in a Teflon base. The vanishing-point method was employed to measure solubility of **1** at 10 MPa, 313K and at different solvent composition, X_{CO2}.[3] The use of this procedure with our equipment has a systematic relative error lower than 1% in the determination of solubilities and lower than 2% in the determination of CO_2 molar fractions. These errors arise from the weighing of the solute and organic solvent components, from the CO_2 volume delivery and from the calculation of CO_2-density in the pump.[4] Solubilities in ethanol and CO_2 neat solvents were measured through a static and a dynamic method respectively. In both methods the systematic relative errors were lower than 1%. Hexamethylenetetramine (Aldrich, 99%), ethanol (Normapur, 99.8%) and CO_2 (Carburos Metalicos, 99.995%) were used as received.

[1] S. Sala, T. Tassaing, N. Ventosa, Y. Danten, M. Besnard, J. Veciana, *ChemPhysChem* **2004**, *5*, 243.

[2] E. Fishman, *J. Phys. Chem.* **1961**, *65*, 2204.

[3] a) F. E. Wubbolts, Ph. D. Thesis, University of Delft (Netherlands), **2000**; b) P. H. Karpinski, J. Nývlt, *Crystal Res. and Technol.* **1983**, *18*, 959.; c) F. E. Wubbolts, O. S. L. Bruinsma, G. M. van Rosmalen, *J. Supercrit. Fluids* **2004**, *32*, 79.

[4] *Carbon Dioxide. Internacional Thermodynamic Tables of the Fluid State – 3.* Compiled by S. Angus, B. Armstrong, K. M. de Reuck. IUPAC Project Centre, Imperial College, London.